Quantum Chemical Calculations of the Spectroscopy of Core Electrons

Frans Augusthinus Asmuruf

Thesis submitted to the University of Nottingham for the degree of Doctor of Philosophy

DECEMBER 2010

Abstract

The near edge X-ray absorption fine structure and infrared spectroscopy of acetylene and benzene adsorbed on C(100)-2x1, Si(100)-2x1 and Ge(100)-2x1 surfaces is studied with density functional theory calculations. Time dependent density functional theory calculations of the near edge X-ray absorption fine structure with a modified exchange-correlation functional agree well with experiment, and show that the spectral features arise from excitation to π^*, $\sigma^*_{\mathrm{C-H}}$ and $\sigma^*_{\mathrm{X-C}}$ orbitals, where X represents C, Si or Ge. The $\sigma^*_{\mathrm{X-C}}$ excitation energies are dependent on the surface, and for acetylene, the location of the π^* band also varies with the surface. Calculations of the vibrational modes show the C-H stretching frequencies for carbon atoms bonded directly to the surface vary significantly between the three surfaces, while those for carbon atoms not bonded to the surface do not change significantly.

The investigation on the near-edge X-ray absorption fine structure of benzene in the gas-phase and adsorbed on the Au(111) and Pt(111) surfaces is also investigated with time dependent density functional theory. Excitation energies computed with hybrid exchange correlation functionals are too low compared with experiment. However, after applying a constant shift the spectra are in good agreement with experiment. For benzene on the Au(111) surface, two bands arising from excitation to the $\mathrm{e}_{2u}(\pi^*)$ and $\mathrm{b}_{2g}(\pi^*)$ orbitals of benzene are observed for photon incidence parallel to the surface. On the Pt(111) surface, a broader band arising from excitation to benzene orbitals that are mixed with the surface that have both σ^*(Pt-C) and π^* character is predicted.

The calculation of near-edge X-ray absorption fine structure with a simple-size consistent doubles correction to single excitation configuration interaction, CIS(D) method, is also performed. Core excitation energies computed with time-dependent density functional theory using standard exchange-correlation functionals are systematically underestimated. CIS(D) predicts core excitation energies that are closer to experiment. However, excitation energies for Rydberg states are too low with respect to valence states, and for some systems spectra that are qualitatively incorrect are obtained. A scaled opposite spin only approach is proposed that reduces the error in the computed core excitation energies, and results in spectra that are in good agreement with experiment.

Lastly I report our recent work on the development of accurate calculations of X-ray emission spectra with time-dependent density functional theory and equations of motion coupled cluster theory. The calculation of the spectra of small molecules is described, and highlights problems with standard exchange-correlation functionals.

Publications

A major portion of the work presented in this thesis has been published in several journals.

1. *Time-dependent density functional theory of the near-edge X-ray absorption fine structure of benzene in the gas-phase and adsorbed on the Au(111) and Pt(111) surfaces*

   F. A. Asmuruf and N. A. Besley, *J. Chem. Phys.*, 129 (2008) 064705.

2. *Density functional theory calculations the near edge X-ray absorption fine structure and infrared spectroscopy of acetylene and benzene adsorbed on C(100)-2x1, Si(100)-2x1 and Ge(100)-2x1 surfaces*

   F. A. Asmuruf and N. A. Besley, *Surface Science*, 603 (2009) 158.

3. *Calculation of near-edge X-ray absorption fine structure with the CIS(D) method*

   F. A. Asmuruf and N. A. Besley, *Chem. Phys. Lett.* 463 (2008) 267.

4. *Time-dependent density functional theory calculations of the core electrons spectroscopy*

   N. A. Besley and F. A. Asmuruf, *Phys. Chem. Chem. Phys.* 12 (2010) 12024.

Author's Declaration

The material contained within this thesis has not previously been submitted for a degree at the University of Nottingham or any other university. The research reported within this thesis has been conducted by the author unless otherwise indicated.

Copyright Notice

For Eslye, Chika and Gibe

This work is dedicated to My Dad and Mom who always pray for me...

Acknowledgements

Being a PhD student in the UK has been the most exciting part of my life. During my studentship, I have had the happiness working with a few talented individuals, who filled me with the valued knowledge, hard-work and good company. Firstly my sincere thanks and gratitude goes to Nick Besley, for his endless excitement and enthusiasm in administering, and giving me opportunity to learn and discover. My special thanks go to Ben Bulheller who introduced me with LATEX, Elena Bichoutskaia for the short quantum chemistry meeting, and also to the Papua Province Government and School of Chemistry for the funding and stipend.

All along of my life time in Nottingham, I have had made a number of very good friends. My thanks goes to all of them. There are few people that I would like to thank, however—Rudi Santoso, I Gusti Made Sanjaya, Hsu-Jui Cheng, Pooja Jain, Mari Chikvaidze, Abrar Hussain, Petros Kountoris, Hainam Do, Mark Oakley and Olga Ershova. A special mention should go to Adriano Santana who has shared a very pleasant moments with me. Finally I wish to thanks to my Dad and Mom, and my wife and children who have been supporting and inspiring me. May God bless you all.

Contents

List of Figures

List of Tables

Chapter 1

Quantum Mechanics

Quantum chemistry applies quantum mechanics to address problems in chemistry. It arises as a consequence of the failure of classical Newtonian mechanics in describing interactions on the atomic scale. Quantum mechanics describes a system by a wavefunction that completely characterizes all of the physical properties of the system.[1] In particular, there are quantum mechanical operators corresponding to each physical observable that, when applied to the wavefunction, allow one to predict the probability of finding the system exhibiting a particular value or range of values for that observable. Computational chemists are concerned with models which mimic real chemical systems or reactions. Any successful model must ultimately find its basis in quantum mechanics. The starting point of any discussion of quantum mechanics is, of course, the Schrödinger equation.

1.1 Schrödinger Equation

In 1926, the Austrian physicist Erwin Schrödinger proposed the concept of the wavefunction and the equation governing its change with time. This equation was then known as the **time–dependent Schrödinger equation** or the **Schrödinger wave equation**.[2] The time-dependent Schrödinger equation

contains the first derivatives of the wavefunction with respect to time, and allows the calculation of the future wavefunction at any time if the wavefunction at time t_0 is known. The Schrödinger wave equation has the form:

$$\hat{H}\Psi = i\hbar\frac{\partial\Psi}{\partial t} \tag{1.1}$$

where Ψ is the wavefunction and $\hat{H}$ is the operator corresponding to the total energy of the system. This operator is called the Hamiltonian and Ψ describes the state of the system. Since the state will, in general, change with time, Ψ is also a function of time. In short, the wavefunction contains all the information we can possibly know about the system it describes. Many applications of quantum mechanics do not use the time–dependent Schrödinger equation and use the **time–independent Schrödinger equation** instead. The time–independent Schrödinger equation can be written as

$$\hat{H}\Psi = E\Psi, \tag{1.2}$$

where the E in equation 1.2 has the dimension of energy.

Quantum chemistry is concerned with describing the behaviour of molecules. For a molecular system, neglecting relativistic effects , the Hamiltonian is

$$\hat{H} = \sum_{A}^{K} -\frac{1}{2M_A}\nabla_A^2 - \frac{1}{2}\sum_{i}^{n}\nabla_i^2 - \sum_{i}^{n}\sum_{A}^{K}\frac{Z_A}{r_{iA}} + \sum_{i>j}^{n}\frac{1}{r_{ij}} + \sum_{A>B}^{K}\frac{Z_A Z_B}{R_{AB}} \tag{1.3}$$

where i and j refer to each of the n electrons, A and B refers to each of the K nuclei, and Z_A is the charge on nuclei A, M_A denotes the mass of the nuclei A, and atomic units are used. The first term of equation 1.3 is the

term for the nuclear kinetic energy. The second term is the description of the electron kinetic energy. The third term Coulombic attraction of electrons to nuclei, and the fourth and fifth terms are electron-electron and nuclear-nuclear repulsions. ∇^2 is the Laplacian operator, which in Cartesian coordinates is defined as

$$\nabla^2 \equiv \frac{\partial^2}{\partial x^2} + \frac{\partial^2}{\partial y^2} + \frac{\partial^2}{\partial z^2} \tag{1.4}$$

The wavefunction is a function of the nuclear positions $\mathbf{R}$ and the electron positions $\mathbf{r}$. The Schrödinger equation can be simplified using the Born-Oppenheimer approximation.[3] This idea suggests separation of the total molecular wavefunction $\Psi_T(\mathbf{R}, \mathbf{r})$ into an electronic wavefunction $\Psi(\mathbf{r})$ and nuclear wavefunction $\Phi(\mathbf{R})$, although $\Psi(\mathbf{r})$ depends parametrically on the position of the nuclei, $\mathbf{R}$. The assumption behind this is that since electrons are much lighter than nuclei, and therefore move much more rapidly, electrons can instantaneously respond to any changes in the relative positions of the nuclei. This allows for the separation of the nuclear variables from the electron variables

$$\Psi_T(\mathbf{R}_1, \mathbf{R}_2 ... \mathbf{R}_N, \mathbf{r}_1, \mathbf{r}_2, ... \mathbf{r}_n) = \Phi(\mathbf{R}_1, \mathbf{R}_2 ... \mathbf{R}_N)\Psi(\mathbf{r}_1, \mathbf{r}_2, ... \mathbf{r}_n) \tag{1.5}$$

The Hamiltonian obtained after applying the Born-Oppenheimer approximation is the electronic Schrödinger equation.

$$\hat{H} = -\frac{1}{2}\sum_{i=1}^{n} \nabla_i^2 - \sum_{i=1}^{n}\sum_{A}^{K} \frac{Z_A}{r_{iA}} + \sum_{i>j}^{n} \frac{1}{r_{ij}} + \sum_{A>B}^{K} \frac{Z_A Z_B}{R_{AB}} \tag{1.6}$$

where the first, second, and third terms of the r.h.s are electron kinetic energy, Coulombic attraction of the electron to the nuclei, and electron-electron repulsion, respectively. In this case, the nuclei-nuclei repulsion term of the equation 1.3 is a constant and is trivial to evaluate. The coordinates $\mathbf{x}_i$ of electron i comprise space coordinates $\mathbf{r}_i$ and spin coordinates s_i. We may rewrite equation 1.6 more compactly as

$$\hat{H} = \hat{T} + \hat{V}_{n,e} + \hat{V}_{e,e} \tag{1.7}$$

where

$$\hat{T} = -\frac{1}{2}\sum_{i}^{n} \nabla_i^2, \tag{1.8}$$

is the kinetic energy operator,

$$\hat{V}_{n,e} = -\sum_{i=1}^{n}\sum_{A}^{K} \frac{Z_A}{r_{iA}} = -\sum_{i=1}^{n} v(\mathbf{r}_i) \tag{1.9}$$

is the electron-nucleus attraction energy operator, and

$$\hat{V}_{e,e} = \sum_{i>j}^{n} \frac{1}{r_{ij}} \tag{1.10}$$

is the electron-electron repulsion energy operator. The $v(\mathbf{r}_i)$ of equation 1.9 is called the external potential which acts on electron i, since it is produced by charges external to the system of electrons. Equation 1.2 must be solved subject to appropriate boundary conditions. Ψ must be well-behaved everywhere and since electrons are fermions, Ψ mus be antisymmetric with respect to interchange of the coordinates (both space and spin) of any two electrons. There are many acceptable solutions for the equation 1.2. Let us say that

the eigenfunctions Ψ_k, with corresponding eigenvalues E_k are acceptable solutions, and the set Ψ_k is also complete. Then Ψ_k may always be taken to be orthogonal and normalized, as in accordance with the probability density of the wavefunction,

$$\int \Psi_k^* \Psi_l d\mathbf{x}^n = \langle \Psi_k | \Psi_l \rangle = \delta_{kl} \tag{1.11}$$

where δ is the Kronecker delta. From here, we can denote the ground state wavefunction and energy by Ψ_0 and E_0. Here $\int d\mathbf{x}^n$ means integration over all spatial and spin coordinates.

Expectation values of observables are given by the formula of

$$\langle \hat{O} \rangle = \frac{\int \Psi^* \hat{O} \Psi d\mathbf{x}}{\Psi^* \Psi d\mathbf{x}} = \frac{\langle \Psi | \hat{O} | \Psi \rangle}{\langle \Psi | \Psi \rangle} \tag{1.12}$$

where $\hat{O}$ is the Hermitian linear operator for the observable O. Many measurements all average to $\langle \hat{O} \rangle$, although particular measurements give particular eigenvalues of $\hat{O}$.

An approximate ground-state energy and wavefunction can be found using the variational method. This method states that the energy expectation value ε is greater than or equal to the true ground-state energy, E_0, system. The equality occurs only when the trial wavefunction is the true ground-state wavefunction of the system.

$$\varepsilon \geq E_0, \text{for any } \psi_{\text{trial}} \tag{1.13}$$

The first step of the method is to choose a group of possible approximate wave functions. The second step is to calculate the expectation value of the energy using the different members of the group of functions. This expectation value,

ε, is called the variation energy. The final step is to find the member of the group that gives a lower (more negative) value of ε than any other member of the group. This value of ε is a better approximation to the ground-state energy than is obtained from any other member of the group of functions. The theorem does not guarantee that this function is a better approximation to the correct wave function than any other member of the group, but it is likely to be so. A typical group of functions is represented by a formula containing one or more variable parameters.

The electronic Schrödinger equation cannot be solved exactly for systems with more than one electron due to the electron-electron interaction. Consequently, approximations have to be introduced. The most prominent approximation is the Hartree-Fock approach[4,5] introduced by D.R. Hartree and V.A. Fock in the 1930's.

1.2 The Hartree-Fock Method

The wavefunction $\Psi(\mathbf{x})$ depends on the coordinates of all of the electrons in the molecule. Hartree proposed the separation of variables whereby the electronic wavefunction can be separated into a product of functions that each depend only on one electron

$$\Psi(\mathbf{x}_1, \mathbf{x}_2, ...\mathbf{x}_n) = \psi_1(\mathbf{x}_1)\psi_2(\mathbf{x}_2)...\psi_n(\mathbf{x}_n) \tag{1.14}$$

By reconsidering the electron-electron repulsion term of the Hamiltonian in equation 1.6, Hartree rewrote this term as an expression that describes the

repulsion an electron feels from the average position of the other electrons, i.e the exact electron-electron repulsion is replaced with an effective field, V_i^{eff}, produced by the average position of the remaining electrons. Hence, the separable functions ψ_i satisfy the Hartree equations

$$\left(-\frac{1}{2}\nabla_i^2 - \sum_A^K \frac{Z_A}{r_{Ai}} + V_i^{eff}\right)\psi_i = E_i\psi_i \tag{1.15}$$

Fock recognized that the wavefunction in equation 1.14 does not satisfy the Pauli Exclusion Principle. He suggested using a Slater determinant instead. Suppose that Ψ is approximated by antisymmetrized product of n orthonormal spin orbitals $\psi_i(\mathbf{x})$, each a product of a spatial orbital $\phi_k(\mathbf{r})$ and a spin function $\sigma(s) = \alpha(s)$ or $\beta(s)$, the Slater determinat

$$\Psi_{HF} = \frac{1}{\sqrt{n!}}\begin{vmatrix} \psi_1(\mathbf{x}_1) & \psi_2(\mathbf{x}_1) & \cdots & \psi_n(\mathbf{x}_1) \\ \psi_1(\mathbf{x}_2) & \psi_2(\mathbf{x}_2) & \cdots & \psi_n(\mathbf{x}_2) \\ \vdots & \vdots & \ddots & \vdots \\ \psi_1(\mathbf{x}_n) & \psi_2(\mathbf{x}_n) & \cdots & \psi_n(\mathbf{x}_n) \end{vmatrix}$$

$$= \frac{1}{\sqrt{n!}} det[\psi_1\psi_2\cdots\psi_n] \tag{1.16}$$

If the normalization integral of equation 1.16 is equal to 1, the energy expectation value is written as

$$E_{HF} = \langle\Psi_{HF}|\hat{H}|\Psi_{HF}\rangle = \sum_{i=1}^{n} h_{ii} + \frac{1}{2}\sum_{i=1}^{n}\sum_{j=1}^{n}(J_{ij} - K_{ij}) \tag{1.17}$$

where

$$h_{ii} = \int \psi_i^*(\mathbf{x}) \left[-\frac{1}{2}\nabla^2 - \sum_A^K \frac{Z_A}{r_{iA}} \right] \psi_i(\mathbf{x}) d\mathbf{x} \tag{1.18}$$

$$J_{ij} = \int \int \psi_i(\mathbf{x}_1)\psi_i^*(\mathbf{x}_1)\frac{1}{r_{12}}\psi_j^*(\mathbf{x}_2)\psi_j(\mathbf{x}_2) d\mathbf{x}_1 d\mathbf{x}_2 \tag{1.19}$$

$$K_{ij} = \int \int \psi_i^*(\mathbf{x}_1)\psi_j(\mathbf{x}_1)\frac{1}{r_{12}}\psi_i(\mathbf{x}_2)\psi_j^*(\mathbf{x}_2) d\mathbf{x}_1 d\mathbf{x}_2 \tag{1.20}$$

J_{ij} and K_{ij} are called the Coulomb and exchange integrals, respectively. The Coulomb energy arises from the interaction of the smeared-out electron potential with an electron density. The exchange energy has no classical interpretation as it takes into account the effects of spin correlation. Minimization the equation 1.17 subject to the orthonormalization conditions

$$\int \psi_i^*(\mathbf{x})\psi_j(\mathbf{x}) d\mathbf{x} = \delta_{ij} \tag{1.21}$$

gives the Hartree-Fock differential equations

$$\hat{F}\psi_i(\mathbf{x}) = \sum_{j=1}^{n} \varepsilon_{ij}\psi_j(\mathbf{x}) \tag{1.22}$$

where

$$\hat{F} = -\frac{1}{2}\nabla^2 + v + \hat{j} - \hat{k} \tag{1.23}$$

Here

$$\hat{j}(\mathbf{x}_1)f(\mathbf{x}_1) \equiv \sum_{k=1}^{n} \int \psi_k^*(\mathbf{x}_2)\psi_k(\mathbf{x}_2)\frac{1}{r_{12}} f(\mathbf{x}_1) d\mathbf{x}_2 \tag{1.24}$$

and

$$\hat{k}(\mathbf{x}_1)f(\mathbf{x}_1) \equiv \sum_{k=1}^{n} \int \psi_k^*(\mathbf{x}_2) f(\mathbf{x}_2)\frac{1}{r_{12}}\psi_k(\mathbf{x}_1) d\mathbf{x}_2 \tag{1.25}$$

with $f(\mathbf{x}_1)$ an arbitrary function. The matrix ε consists of Lagrange multipliers (in general complex) associated with the constraints of the equation 1.21. Also,

$$\varepsilon_{ij}^* = \varepsilon_{ij} \tag{1.26}$$

so that ε is Hermitian . Multiplying equation 1.22 by ψ_i^* and integrating, one obtains the formula for orbital energies,

$$\varepsilon_i \equiv \varepsilon_{ii} = \langle \psi_i | \hat{F} | \psi_i \rangle = h_{ii} + \sum_{j=1}^{n} (J_{ij} - K_{ij}) \tag{1.27}$$

Summing over i and comparing with the equation 1.17, we find

$$E_{HF} = \sum_{i=1}^{n} \varepsilon_i - V_{e,e} \tag{1.28}$$

where the symbol $V_{e,e}$ stand for the total electron-electron repulsion energy

$$V_{e,e} = \int \Psi_{HF}^*(\mathbf{x}^n) \left(\sum_{i<j} \frac{1}{r_{ij}} \right) \Psi_{HF}(\mathbf{x}^n) d\mathbf{x}^n$$

$$= \frac{1}{2} \sum_{i,j=1}^{n} (J_{ij} - K_{ij}) \tag{1.29}$$

Solution of the equation 1.22 must proceed iteratively, since the orbitals ψ_i that solve the problem appear in the operator $\hat{F}$. Consequently, the Hartree-Fock method is a nonlinear "self-consistent" method.

For a system having an even number of electrons, the n orbitals ψ_i are taken to comprise $n/2$ orbitals of form $\phi_k(\mathbf{r})\alpha(s)$ and $n/2$ orbitals of form $\phi_k(\mathbf{r})\beta(s)$.

Thus, the energy of the equation 1.17 become

$$E_{HF} = 2\sum_{k=1}^{n/2} h_{kk} + \sum_{k,l=1}^{n/2} (2J_{kl} - K_{kl}) \tag{1.30}$$

where

$$h_{kk} = \int \phi_k^*(\mathbf{r}) \left[-\frac{1}{2}\nabla^2 + v(\mathbf{r}\right] \phi_k(\mathbf{r}) d\mathbf{r} \tag{1.31}$$

$$J_{kl} = \int \int |\phi_k(\mathbf{r}_1)|^2 \frac{1}{r_{12}} |\phi_l(\mathbf{r}_2)|^2 d\mathbf{r}_1 d\mathbf{r}_2 \tag{1.32}$$

$$K_{kl} = \int \int \phi_k^*(\mathbf{r}_1)\phi_l(\mathbf{r}_1) \frac{1}{r_{12}} \phi_k(\mathbf{r}_2)\phi_l^*(\mathbf{r}_2) d\mathbf{r}_1 d\mathbf{r}_2 \tag{1.33}$$

while Hartree-Fock equation in 1.22 now reads

$$\hat{F}\phi_k(\mathbf{r}) = \sum_{l=1}^{n/2} \varepsilon_{kl}\phi_l(\mathbf{r}) \tag{1.34}$$

Consequently, the operator $\hat{F}$ given in the equations 1.23, 1.24 and 1.25 are replaced by

$$\hat{j}(\mathbf{r}_1)f(\mathbf{r}_1) \equiv 2\sum_{m=1}^{n/2} \int |\phi_m(\mathbf{r}_2)|^2 \frac{1}{r_{12}} d\mathbf{r}_2 f(\mathbf{r}_1) \tag{1.35}$$

$$\hat{k}(\mathbf{r}_1)f(\mathbf{r}_1) \equiv \sum_{m=1}^{n/2} \int \phi_m^*(\mathbf{r}_2) f(\mathbf{r}_2) \frac{1}{r_{12}} d\mathbf{r}_2 \phi_m(\mathbf{r}_1) \tag{1.36}$$

and the determinant wavefunction of the equation 1.16 is also followed for this "even number electrons" or all electrons paired case.

The objective is to minimize the total energy as a function of the molecular orbitals, subject to the orthogonality constraint. To do so, a unitary transformation of the wavefunction is invoked. This important property guarantees that transformation of the occupied orbitals ϕ_k (or ψ_i) to another set

of orbitals θ_m leaves the wavefunction unchanged except possibly by an inconsequential phase factor. The operators $\hat{j}$, $\hat{k}$ and $\hat{F}$ are also invariant to such a transformation. If we let,

$$\theta_m = \sum_k \mathbf{U}_{mk}\psi_k \tag{1.37}$$

where $\mathbf{U}$ is a unitary matrix ,

$$\mathbf{U}^t\mathbf{U} = \mathbf{1} \tag{1.38}$$

then for the even number electron case

$$\hat{F}\theta_m = \sum_{l=1}^{n/2} \varepsilon^{\theta}_{ml}\theta_l \tag{1.39}$$

where

$$\varepsilon^{\theta} = \mathbf{U}\varepsilon\mathbf{U}^t \tag{1.40}$$

Since the matrix ε is Hermitian, one may choose the matrix $\mathbf{U}$ to diagonalize it. The corresponding orbitals ϕ_m, called the canonical Hartree-Fock molecular orbitals which satisfy the canonical Hartree-Fock equations,

$$\hat{F}\phi_m(\mathbf{r}) = \varepsilon^{\phi}_m\phi_m(\mathbf{r}) \tag{1.41}$$

This equation is, for the same case, considerably more convenient for calculation than the equation 1.34. The canonical HF molecular orbitals are convenient for the physical interpretation of the Lagrange multipliers.

For an n-electron system with identical molecular orbitals, the energy differ-

ences by removing one electron from orbital number k

$$E_n - E_{n-1}^k = h_k + \sum_{i=1}^{n}(J_{ki} - K_{ki}) = \varepsilon_k \tag{1.42}$$

which is exactly the orbital energy ε_k in equation 1.27 and is considered as the ionization energy. A principle to produce an orbital energy from ionization energy within frozen molecular orbital approximation is known as *Koopmans' theorem*.[6] Similarly, the electron affinity of a neutral molecule is given as the orbital energy of the corresponding anion as a consequence of attaching additional electron, or as the energy of the kth unoccupied orbital energy in the neutral species.

$$E_{n+1}^k - E_n = \varepsilon_k \tag{1.43}$$

There is more than one possible way to solve the Hartree-Fock equation. For small highly symmetric system, such as atoms and diatomic molecules, the HF equation may be solved by mapping the orbitals on a set of grid points, and referred to as the numerical Hartree-Fock methods.[7] However, the basis set approximation method can be used instead. This approximation, essentially, employs some set of fixed one-electron basis functions and then expanding them to many-electron wave functions. The expansion of each of molecular orbitals, ϕ_i, is through linear combinations of atomic orbitals in term of basis functions $\chi_\alpha(\mathbf{r})$.

$$\phi_i(\mathbf{r}) = \sum_{\alpha=1}^{\eta} c_{\alpha i}\chi_\alpha(\mathbf{r}) \tag{1.44}$$

where $c_{\alpha i}$ are the molecular orbital coefficients and η is the number of basis functions. Thus the Hartree-Fock equation can be written as

$$\hat{F}_i \sum_{\alpha}^{\eta} c_{\alpha i}\chi_\alpha = \varepsilon_i \sum_{\alpha}^{\eta} c_{\alpha i}\chi_\alpha \tag{1.45}$$

These are the Hartree-Fock equations in the atomic orbital basis. Rewriting equation 1.45 through collecting all of the η equations in matrix notation gives

$$\mathbf{FC} = \varepsilon\mathbf{SC} \tag{1.46}$$

where

$$F_{\alpha\beta} = \langle\chi_\alpha|\hat{F}|\chi_\beta\rangle \tag{1.47}$$

$$S_{\alpha\beta} = \langle\chi_\alpha|\chi_\beta\rangle$$

The **S** matrix contains the overlap elements between basis functions, and the **F** matrix contains the Fock matrix elements. Equation 1.46 is called the *Roothaan-Hall* matrix equation.[8] Generalizing to an unrestricted formalism by introducing separate spatial orbitals for α and β spin in equation 1.16 yields the Pople-Nesbet[9] equations.

$$\begin{gathered}\mathbf{F}^\alpha\mathbf{C}^\alpha = \varepsilon^\alpha\mathbf{S}\mathbf{C}^\alpha \\ \\ \mathbf{F}^\beta\mathbf{C}^\beta = \varepsilon^\beta\mathbf{S}\mathbf{C}^\beta\end{gathered} \tag{1.48}$$

Solving equation 1.46 and 1.48 yields the restricted and unrestricted finite basis Hartree-Fock approximation.

If we consider once more the Roothaan-Hall equations or the Pople-Nesbet equations which can be traced back to the integro-differential equation in 1.22, where the effective potential, v^{eff}, depends on the SCF methodology. In the case of an even number electrons or all paired electrons, the effective potential can be written as

$$v^{eff} = \sum_{k}^{n/2}[2\hat{J}_k(\mathbf{r}_1) - \hat{K}_k(\mathbf{r}_1)] - \sum_{A=1}^{K}\frac{Z_A}{r_{1A}} \tag{1.49}$$

where the Coulomb and exchange operators are defined as

$$\hat{J}_k(\mathbf{r}_1) = \int \psi_k^*(\mathbf{r}_2)\frac{1}{r_{12}}\psi_k(\mathbf{r}_2)d\mathbf{r}_2 \tag{1.50}$$

$$\hat{K}_k(\mathbf{r}_1)\psi_l(\mathbf{r}_1) = \left[\int \psi_k^*(\mathbf{r}_2)\frac{1}{r_{12}}\psi_l(\mathbf{r}_2)d\mathbf{r}_2\right]\psi_k(\mathbf{r}_1) \tag{1.51}$$

respectively. From here, we can obtain Fock matrix elements in the atomic orbital basis, $\chi(\mathbf{r})$

$$\hat{F}_{pq} = H_{pq}^{core} + J_{pq} - K_{pq} \tag{1.52}$$

where the core Hamiltonian matrix elements

$$H_{pq}^{core} = T_{pq} + V_{pq} \tag{1.53}$$

consist of kinetic energy elements

$$T_{pq} = \int \chi_p(\mathbf{r})\left[-\frac{1}{2}\nabla^2\right]\chi_q(\mathbf{r})d\mathbf{r} \tag{1.54}$$

and nuclear attraction elements

$$V_{pq} = \int \chi_p(\mathbf{r}) \left[-\sum_A \frac{Z_A}{|\mathbf{R}_A - \mathbf{r}|} \right] \chi_q(\mathbf{r}) d\mathbf{r} \tag{1.55}$$

The Coulomb and exchange elements are given by

$$J_{pq} = \sum_{rs} P_{rs}(pq|rs) \tag{1.56}$$

$$K_{pq} = \frac{1}{2} \sum_{rs} P_{rs}(pr|qs) \tag{1.57}$$

where the density matrix elements are

$$P_{pq} = 2 \sum_{k=1}^{n/2} C_{pk} C_{qk} \tag{1.58}$$

and the two electron integrals are

$$(pq|rs) = \int \int \chi_p(\mathbf{r}_1) \chi_q(\mathbf{r}_1) \left[\frac{1}{r_{12}} \right] \chi_r(\mathbf{r}_2) \chi_s(\mathbf{r}_2) d\mathbf{r}_1 d\mathbf{r}_2 \tag{1.59}$$

Subtituting the matrix element of the equation 1.52 back into the Roothaan-Hall equation and solving until self-consistency is achieved will yield the restricted Hartree-Fock (RHF) energy and wavefunction. Alternatively, one could have adopted the unrestricted form of the wavefunction by defining an

alpha and beta density matrix

$$P_{pq}^{\alpha} = \sum_{k=1}^{n_\alpha} C_{pk}^{\alpha} C_{qk}^{\alpha}$$
$$P_{pq}^{\beta} = \sum_{k=1}^{n_\beta} C_{pk}^{\beta} C_{qk}^{\beta} \tag{1.60}$$

and the total electron density matrix P^T is simply the sum of the alpha and beta density matrices. The unrestricted alpha Fock matrix

$$\hat{F}_{pq}^{\alpha} = H_{pq}^{core} + J_{pq} - K_{pq}^{\alpha} \tag{1.61}$$

differs from the restricted one only in the exchange contributions where the alpha exchange matrix elements are given

$$K_{pq}^{\alpha} = \sum_{r,s}^{n} P_{rs}^{\alpha} (pr|qs) \tag{1.62}$$

The Hartree–Fock–Roothaan algorithm is implemented by the following steps:

1. Specify the nuclear position, the type of nuclei, the number of electrons, and multiplicity.

2. Choose a basis set.

3. Calculate all of the integrals necessary to describe the core Hamiltonian, the Coulomb and exchange terms, and the overlap matrix.

4. Diagonalize the overlap matrix **S** to obtain the transformation matrix **X**.

5. Make a guess at the coefficient matrix $\mathbf{C}$ and obtain the density matrix $\mathbf{P}$.

6. Calculate the Fock matrix and then the transformed Fock matrix $\mathbf{F}'$.

7. Diagonalize $\mathbf{F}'$ to obtain $\mathbf{C}$ and ε.

8. Obtain the new coefficient matrix with the expression $\mathbf{C}=\mathbf{X}\mathbf{C}'$ and the corresponding new density matrix.

9. Decide if the procedure has converged. There are typically two criteria for convergence, one based on the energy and the other on the orbital coefficients. The energy convergence criterion is met when the difference in the energies of the last two iterations is less than some preset value. Convergence of the coefficients is obtained when the standard deviation of the density matrix elements in successive iterations is also below some preset value. If convergence has not been met, return to Step 6 and repeat until the convergence criteria are satisfied.

The molecular orbitals that are produced in this procedure are such that the energy matrix ε will be diagonal, with the diagonal elements being interpreted as the molecular orbital energies.

1.2.1 Restricted and Unrestricted Hartree-Fock

Most polyatomic molecules have a closed-shell ground state. This closed-shell state is occupied by two electron with opposite spins in each occupied molecular orbital. For an open-shell state, in contrast, there are molecular

orbitals containing one electron. If the number of electrons is even, the system does not necessary have to be closed-shell. If the number of electrons is odd, the system will always be open-shell.

A molecular orbital is a product of a spatial orbital and a spin function, α or β. For a closed-shell system, each orbital is occupied of two electrons with opposite α and β spin. These systems can be treated using a restricted Hartree-Fock (RHF) formalism, whereby each orbital is doubly occupied with electrons of opposite spin. For open-shell systems, restricted open-shell or unrestricted (UHF) Hartree-Fock formalism can be adopted. In ROHF the spatial parts of the doubly occupied orbitals for the electrons of different spin are the same, and in UHF this constraint is lifted. This is illustrated in Figure 1.1. Variationally, the UHF wavefunctions is better since it will give a lower energy. However, UHF wavefunctions are no longer eigenfunction of the total spin operator (S^2).

1.2.2 Basis sets

As described above, solution of the Hartree-Fock-Roothaan equations requires the introduction of a basis set. If the set of basis functions is infinite, then the variational principle tells us that we will obtain the lowest possible energy within the Hartree-Fock Self-consistent field (HF–SCF) method. This is called the Hartree–Fock limit. This is not the actual energy of the molecule. Because an infinite set of atomic orbitals is impractical, a choice must be made on how to truncate the expansion and the type of basis functions to use. This

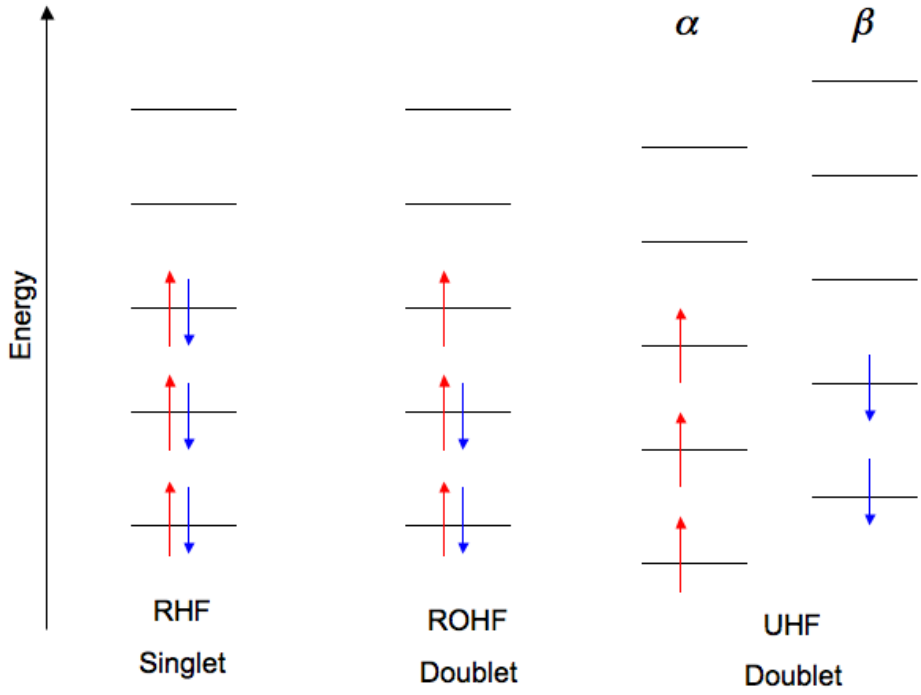

Figure 1.1: Illustrating an RHF singlet, and ROHF and UHF doublets states

choice of atomic orbitals defines the basis set.

A natural starting point is to use functions from the exact solution of the Schrödinger equation for the hydrogen atom. These orbitals have the form

$$\chi = Cx^i y^j z^k e^{-\zeta(\mathbf{r}-\mathbf{R})} Y_{l,m}(\theta, \phi) \tag{1.63}$$

where $\mathbf{R}$ is the position vector of the nucleus upon which the function is centred and C is normalization constant. $Y_{l,m}(\theta, \phi)$ are spherical harmonic functions and describe the angular part of the function. Basis functions of this type are called Slater-type orbitals (STOs). The value of ζ for every STO for a given element is determined by minimizing the atomic energy with respect to ζ. These values are used for every atom of that element, regardless of the molecular environment. STOs are primarily used for atomic and diatomic systems where high accuracy is required, and in semi-empirical methods where all three and four centre integrals are neglected. They can also be used with density functional methods that do not include exact exchange and where the Coulomb energy is calculated by fitting the density into a set of auxiliary functions. Conceptually, the STO basis is straightforward as it mimics the exact solution for the single electron atom. Unfortunately, with STOs many of the integrals that need to be evaluated to construct the Fock matrix can only be solved using an infinite series. Truncation of this infinite series results in errors, which can be significant.[17]

In 1950, Boys[18] proposed an alternative to the use of STOs. That is the radial decay of the STOs can be changed from e^{-r} to e^{-r^2}, in which the atomic orbital-like functions are chosen to have form of a Gaussian function. The

advantage of the Gaussian-type orbitals (GTOs) is that with this function, the integrals required to build the Fock matrix can be evaluated exactly. The form of GTO as shown in equation 1.64.

$$\chi = Cx^i y^j z^k e^{-\alpha(\mathbf{r}-\mathbf{R})^2} Y_{l,m}(\theta, \phi) \tag{1.64}$$

The r^2 dependence in the exponential makes the GTO inferior to the STOs in two aspects. At the nucleus the GTO has zero slope, in contrast to the STO which has a "cusp" or discontinuous derivative, and GTOs have problems representing the proper behaviour near the nucleus. This can be seen in Figure 1.2. The other problem is that the GTO falls off too rapidly far from the nucleus compared with an STO, and the "tail" of the wavefunction is consequently represented poorly.

In order to address these problems, the first basis sets developed with GTOs used them as building blocks to approximate STOs. This leads to the basis function χ used for calculations being not individual GTOs, but a linear combination of GTOs fitted to reproduce as accurately as possible a STO. The basis functions generated as a linear combination of GTOs are called contracted basis functions. Whereas the individual Gaussians from which it is formed are called primitive Gaussian functions. The degree of contraction refers to the total number of primitives used to make all of the contracted functions. Hehre, Stewart and Pople[19] were the first to systematically determine optimal contraction coefficients and exponents for mimicking STOs with contracted GTOs for a large number of atoms in the periodic table.

The minimum basis set is usually inadequate, failing to allow the core elec-

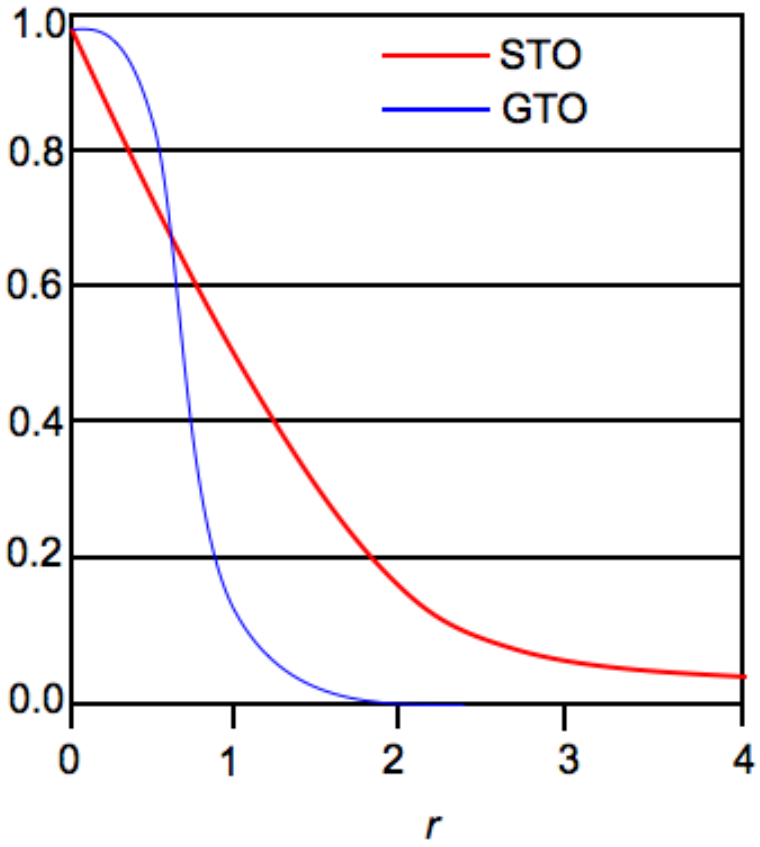

Figure 1.2: Plot of radial component of a Slater-type orbital (red line) and a Gaussian-type orbital (blue line).

trons to get close enough to the nucleus and valence electrons to delocalize. An obvious solution is to double the size of the basis set, creating a double-zeta (DZ) basis. Thus for carbon, for example, the DZ basis set has four s basis functions and two sets of p basis functions, for a total of ten basis functions. Further improvement has made by choosing a triple zeta (TZ) or even larger basis sets.

As most of chemistry focuses on the action of the valence electrons, Pople et al[20,21] developed the split-valence basis sets, single zeta in the core and

double zeta in the valence region. A double-zeta split-valence basis set for carbon has three s basis functions and two p basis functions for a total of nine functions, a triple-zeta split valence basis set has four s basis functions and three p functions for a total of thirteen functions, and so on. One concern is that even large multi-zeta basis sets will not provide sufficient flexibility to adequately describe the electron distribution. An example of this deficiency is the inability to describe bent bonds of small rings. Extending the basis set to include a set of functions that mimic the atomic orbitals with angular momentum one greater than in the valence space greatly improves the basis flexibility. These added basis functions are called polarization functions. Thus for carbon atom, adding polarization means adding a set of d GTOs, whereas for hydrogen, polarization functions are a set of p functions. Addition of polarization functions is labelled with $+P$. $DZ+P$ indicates a double-zeta basis set with one set of polarization functions. 6-31G* is an example of a split-valence basis sets, where the asterix denotes adding a set of polarization functions to all atoms but hydrogen and helium.

Chemistry also focuses on ionic systems. For anions, the basis set must be augmented with diffuse functions to allow the electron density to expand into a larger volume. It is designated as +, such as 6-31+G(d) for split-valence basis sets. The diffuse functions added are a full set of functions of the same type as are present in the valence space. So, for carbon, the diffuse function would be an added s function and a set of p basis functions . The correlation-consistent basis sets developed by Dunning are popular alternatives.[22–24] The correlation-consistent were constructed to extract the maximum electron correlation energy for each atom. They are designated as $cc-pV\xi Z$, read as

correlation-consistent polarized split-valence ξ-zeta, where ξ indicates the degree to which the valence space is split. As ξ increases, the number of polarization functions are also increased. The addition of diffuse functions to the correlation-consistent basis sets is designated with the prefix *aug*, as in aug-cc-pVDZ.

Hartree-Fock theory is the most prominent approximation because it provides an exact treatment of exchange functional. The cost of a Hartree-Fock calculation formally scales as the fourth order of molecular size[16] (or basis set size) and depending on implementation, the scaling can be reduced. However, it is insufficiently accurate for quantitative predictions of the properties of many compounds, although, it is useful for determining information such as trends in structural parameters with system size.

Hartree-Fock theory treats each electron independently moving in an average field of all other electrons and the nuclei. This leads to an uncoupling of the many-body Schrödinger equation to many single particle equations, and subsequently mimics single-particle picture of molecular orbitals. However, the HF scheme does not cover electron correlation caused by instantaneous repulsion between the electrons. The error of the Hartree-Fock model due to neglecting electron correlation is defined as correlation energy

$$E_{corr} = E_{exact} - E_{HF} \tag{1.65}$$

where E_{exact} is the exact energy within the given basis set. The correlation energy tends to remain constant for atomic and molecular changes that conserve the numbers and types of chemical bonds, but it can change drastically and

become determinative when bonds change. There are two contributions to the E_{corr}, dynamical and non-dynamical electron correlation. The dynamical electron correlation means that the E_{corr} is affected by the proportion of the electron-electron repulsion term $1/r_{12}$ in the Hamiltonian. The non-dynamical electron correlation is related to the fact that in certain circumstances the ground-state Slater determinant is not a good approximation. The electron correlation in a helium atom is almost purely dynamic, while the correlation in the hydrogen molecule at the dissociation limit is purely non-dynamic.[25]

Much efforts have been undertaken to recover the missing electron correlation, and a profusion of quantum chemical ab initio methods called wavefunction-based methods have emerged. Examples of these methods are Moller-Plesset (MP),[10,11] configuration interactions[12,13] and coupled-cluster approaches.[14,15] Even though powerful in describing electron-electron corelations, these methods are expensive for the sake of computational calculations. Density functional theory, on the other hand, is able to capture correlation energy. However, the cost of the computational calculations using this method is inexpensive compared to the correlated wavefunction-based methods.

Chapter 2

Density Functional Theory

It is well known that HF theory neglects electron correlation. The disregard of electron correlation can result in computed properties that are inaccurate or predictions that are qualitatively incorrect. The most computationally efficient method of incorporating electron correlation is density functional theory (DFT). It has practical utility and is highly valuable to most electronic structure calculations in quantum chemistry and condensed matter physics. Consequently, DFT has become the most popular quantum chemical method.

DFT is a quantum mechanical method used in physics and chemistry to investigate the electronic structure of many-body systems, in particular molecules and condensed phases. It describes an interacting system of fermions,[26] via its density and not by its many-body wavefunction. In other words, there exists a one-to-one correspondence between the electron density of a system and the energy. Therefore, a functional can be designed to connect the electron density with the energy. Instead of the dependence on $3n$ variables of the many-body electronic wavefunctions, i.e. three spatial variables for each of the n electrons, the density is merely a function of three variables, and is a simpler quantity to deal with both conceptually and practically. In short, DFT is a remarkable theory that allows one to replace the complicated n-electron wavefunction $\Psi(\mathbf{x}_1, \mathbf{x}_2, \ldots, \mathbf{x}_n)$ by the much simpler electron density

$\rho(\mathbf{r})$.

2.1 The Hohenberg-Kohn Theorem

In 1964, Hohenberg and Kohn declared an appropriate theorem of DFT in a seminal publication.[26] They proved that every observable of stationary quantum mechanics system (including energy), can be calculated, in principle exactly, from the ground-state density alone, i.e., every observable can be written as a functional of the ground state density. They also established that the ground state density can be calculated, in principle exactly, using the variational method involving only the density. The simplification of the proof of the Hohenberg-Kohn theorem is as follows. Since the electronic Schrödinger equation in equation 1.6 is solved for fixed location of the nuclei, the nuclear coordinates are not variables for the electronic Schrödinger equation. Once the external potential $v(\mathbf{r}_i)$ and the number of electrons n are specified, the electronic wavefunctions and allowed energies of the molecule are determined as the solution of the electronic Schrödinger equation. Hohenberg and Kohn proved that for systems with a nondegenerate ground state, the ground-state electron probability density $\rho_0(\mathbf{r})$ determines the external potential and the number of electrons. Hence, the ground-state wavefunction and energy are determined by the ground-state electron density.

The ground-state electronic energy E_0 is thus a functional of $\rho_0(\mathbf{r})$, which can be written as

$$E_0 = E_v[\rho_0] \tag{2.1}$$

Each term of the equation 1.7 can be written as a functional of ρ_0:

$$E_0 = E_v[\rho_0] = \hat{T}_e[\rho_0] + \hat{V}_{n,e}[\rho_0] + \hat{V}_{e,e}[\rho_0] \tag{2.2}$$

where

$$\hat{V}_{n,e} = \langle\psi_0| \sum_{i=1}^{n} v(\mathbf{r}_i)|\psi_0\rangle = \int \rho_0(\mathbf{r})v(\mathbf{r})d\mathbf{r} \tag{2.3}$$

and

$$\hat{V}_{e,e} = \frac{1}{2}\int\int \frac{\rho_0(\mathbf{r}_1, \mathbf{r}_2)}{r_{12}} d\mathbf{r}_1\mathbf{r}_2 \tag{2.4}$$

Hohenberg and Kohn also introduced the **variational principle** to change the equation 2.2 from a formal relation to a practical tool which gave birth to the second theorem of Hohenberg-Kohn. They proved that for every trial density function $\rho_{tr}(\mathbf{r})$ that satisfies

$$\int \rho_{tr}(\mathbf{r})d\mathbf{r} = n \tag{2.5}$$

with $\rho_{tr}(\mathbf{r}) \geq 0$ for all $\mathbf{r}$, the following inequality holds

$$E_0 \leq E_v[\rho_0] \tag{2.6}$$

where ρ_0 is the true ground-state electron density obtained from minimizing the energy functional $E_v[\rho_{tr}]$. This is very similar to the usual variational principle for wavefunctions. From here, the expectation value of a Hamiltonian with a trial wavefunction ψ_{tr} that corresponds to a ρ_{tr} for a molecule can be

written as

$$\langle\psi_{tr}|\hat{H}|\psi_{tr}\rangle = \langle\psi_{tr}|\hat{T}_e + \hat{V}_{e,e} + \sum_{i=1}^{n} v(\mathbf{r}_i)|\psi_{tr}\rangle \geq E_0 = E_v[\rho_0] \tag{2.7}$$

where this energy can never below the true ground state energy. Using the fact that the average kinetic and potential energies are functionals of the electron density, and using equation 2.3 with ψ_0 replaced by ψ_{tr}, the last equation becomes

$$\hat{T}_e[\rho_{tr}] + \hat{V}_{e,e}[\rho_{tr}] + \int \rho_{tr} v(\mathbf{r}) d\mathbf{r} \geq E_v[\rho_0] \tag{2.8}$$

Hohenberg and Kohn proved their theorems only for nondegenerate ground states. However, the theorem does not tell us how to calculate E_0 from ρ_0, nor does it tell us how to find ρ_0 without first finding the wavefunction. This leads us to the discussion of the Kohn-Sham method.[27,28]

2.2 The Kohn-Sham Method and Exchange-Correlation Functionals

Additional progress was made by Kohn and Sham when they suggested the use of an auxiliary non-interacting system, the Kohn-Sham (KS) system, to assay the use of the interacting system. They suggested a brilliant method of combining of wavefunction and density approaches. They re-separated the total energy functional into following parts[27]

$$E[\rho] = T[\rho] + \int [\upsilon_{ext}(\mathbf{r}) + \upsilon_{cl}(\mathbf{r})]\rho(\mathbf{r}) dr + E_{xc}[\rho] \tag{2.9}$$

where $T[\rho]$ is the kinetic energy of the electron in a system which has the same density, ρ, as the real system with no electron-electron interactions. $\upsilon_{cl}(\mathbf{r})$ is the pure Coulomb interaction between the electrons or classical electron interactions.

$$\upsilon_{cl}(\mathbf{r}) = \int \frac{\rho(\mathbf{r}')}{|\mathbf{r}' - \mathbf{r}|} d\mathbf{r}' \tag{2.10}$$

$\upsilon_{ext}(\mathbf{r})$ is the external potential, i.e, the potential that arises from nuclei:

$$\upsilon_{ext} = \sum_{\alpha} \frac{-q_a}{|\mathbf{R}_\alpha - \mathbf{r}|} \tag{2.11}$$

The last term, $E_{xc}[\rho]$ is called exchange-correlation energy. All the energy contributions that are not accounted for are incorporated in $E_{xc}[\rho]$.

Derivation of the KS equation, which is not discussed in detail here, was done by assuming that energy functional is reasonable. Applying the variational principle, one can be found

$$\frac{\delta E[\rho(\mathbf{r})]}{\delta \rho(\mathbf{r})} = \frac{\delta T[\rho(\mathbf{r})]}{\delta \rho(\mathbf{r})} + \upsilon_{eff}(\mathbf{r}) \tag{2.12}$$

in which

$$\upsilon_{eff}(\mathbf{r}) = \upsilon_{ext}(\mathbf{r}) + \upsilon_{cl}(\mathbf{r}) + \upsilon_{xc}(\mathbf{r}) \tag{2.13}$$

From here, the exchange correlation potential $\upsilon_{xc}(\mathbf{r})$ is defined as the functional derivative of the exchange correlation energy:

$$\upsilon_{xc}(\mathbf{r}) = \frac{\delta E_{xc}[\rho(\mathbf{r})]}{\delta \rho(\mathbf{r})} \tag{2.14}$$

The form of the equation 2.12 allows for a solution as a Schrödinger equation for non-interacting particles

$$[-\frac{1}{2}\nabla_i + \upsilon_{eff}(\mathbf{r})]\phi_i^{KS}(\mathbf{r}) = \varepsilon_i\phi_i(\mathbf{r})^{KS} \tag{2.15}$$

This equation is similar to the eigenequation of the HF method. The KS orbitals can be used to compute the total density

$$\rho(\mathbf{r}) = \sum_i^n |\phi_i^{KS}(\mathbf{r})|^2 \tag{2.16}$$

where this equation is then used to calculate an improved potential $\upsilon_{eff}(\mathbf{r})$, and leads to a new cycle in the self-consistent field process.

The total energy can be calculated economically using orbital energies as

$$E[\rho] = \sum_{i=1}^n \varepsilon_i - \frac{1}{2}\int d\mathbf{r}d\mathbf{r}'\frac{\rho(\mathbf{r})\rho(\mathbf{r}')}{|\mathbf{r}-\mathbf{r}'|} - \int \upsilon_{xc}(\mathbf{r})\rho(\mathbf{r})d\mathbf{r} + E_{xc}[\rho] \tag{2.17}$$

in which

$$\sum_{i=1}^n \varepsilon_i = T_s[\rho] + \int d\mathbf{r}\rho(\mathbf{r})\upsilon_{eff}(\mathbf{r}) \tag{2.18}$$

Even though in an artificial way, equation 2.15 shows that the electron interaction is included into $\upsilon_{eff}(\mathbf{r})$. It is possible to prove that the exchange-correlation potential is a unique functional, valid for all systems, but an explicit functional form of this potential has been elusive, except for special cases such as a uniform electron gas. Kohn and Sham also proposed a simple approximation to υ_{xc}, the local density approximation (LDA). This functional uses the knowledge of the exchange-correlation energy of the homogeneous

electron gas. The form of LDA in atomic units is[29]

$$E_x^{LDA} = -C_x \sum_\sigma \int \rho_\sigma^{4/3}(\mathbf{r}) d\mathbf{r}, \tag{2.19}$$

$$C_x = \tfrac{3}{2}[\tfrac{3}{4\pi}]^{1/3}$$

where σ denotes either up or down electron spin, and the integrand is essentially the volume exchange-energy density of a uniform spin-polarized electron gas of spin density ρ_σ.

In the case for which α and β spins are not equal, LDA has been virtually abandoned and replaced by the Local Spin Density Approximation (LSDA). The simplest form of the LSDA is[30]

$$E_{xc}^{LSDA} = \int \varepsilon_{xc}[\rho_\alpha(\mathbf{r}), \rho_\beta(\mathbf{r})] d\mathbf{r} \tag{2.20}$$

where the integrand ε_{xc} is the exchange-correlation energy density of a uniform electron gas with spin densities $\rho_\alpha(\mathbf{r})$ and $\rho_\beta(\mathbf{r})$ equal to their local atomic or molecular values. For closed-shell systems LSDA is equal to LDA. Of course, an atomic or molecular density is not homogeneous and the improvement of the LSDA has to be considered.

Improvements over the LSDA approach that considers a non-uniform electron gas have been made. This includes making exchange correlation energies dependent not only on the value of the electron density, but also on derivatives of the density. Such methods are known as Gradient Corrected or Generalized Gradient Approximation (GGA) methods. Perdew and Wang (PW86)[31] proposed modifying the LSDA exchange expression to that shown in equa-

tion 2.21, where x is a dimensionless gradient variable, and a, b, and c being suitable constants and summation over equivalent expression for the α and β densities implicitly assumed.

$$E_x = E_x^{LDA}(1 + ax^2 + bx^4 + cx^6)^{1/5}, \tag{2.21}$$

$$x = \frac{|\nabla\rho|}{\rho^{4/3}}$$

Becke proposed a widely used correction,[32] B or B88, to the LSDA exchange energy, which has the correct $-r^{-1}$ asymptotic behaviour for the energy density

$$E_x^{B88} = E_x^{LDA} + \Delta E_x^{B88}, \tag{2.22}$$

$$\Delta_x^{B88} = -\beta\rho^{1/3}\frac{x^2}{1+6\beta x sinh^{-1}x}$$

In which the β parameter is determined by fitting to known atomic data and x defined in equation 2.21.

Handy and Cohen[33] have also investigated several forms related to equation 2.21 where the parameters were optimized with respect to exchange energies calculated at the Hartree-Fock level. The best resulting model had two parameters and was labelled $OPTX$ (OPTimized eXchange). It was also found that no significant improvement could be made by including higher order derivatives. Hamprecht, Cohen, Tozer and Handy[34] have further extended the B97 model using only the pure density components, i.e. no exact exchange, to a functional containing 15 parameters which were fitted to experimental and *ab initio* data, known as the acronyms of $HCTH93$, $HCTH14$, and $HCTH407$.

The most successful class of functional is hybrid functionals , where Hartree-

Fock exchange is introduced. The exact definition of B3LYP exchange correlation functional is[35]

$$E_{xc} = aE_x^{DS} + (1-a)E_x^{HF} + bE_x^{B88} + cE_c^{LYP} + (1-c)E_c^{VWN} \tag{2.23}$$

where[30] $a = 0.8$, $b = 0.72$, $c = 0.81$, and the superscript DS, HF, B88, LYP, and VWN refer to the Dirac-Slater,[29] Hartree-Fock, Becke,[32] Lee-Yang-Parr,[36] and Vosko-Wilk-Nusair[37] exchange correlation functionals.

Further extensions to the GGA methods were also introduced. The exchange and correlation functionals were allowed to depend on the higher order derivatives of the electron density, with the Laplacian ($\nabla^2\rho$) being the second-order term. Alternatively, it can be taken to depend on the orbital kinetic energy density τ, for single orbital

$$\tau(\mathbf{r}) = \frac{1}{2}\sum_i^{occ} |\nabla\phi_i(\mathbf{r})|^2 \tag{2.24}$$

$$\tau_w(\mathbf{r}) = \frac{|\nabla\rho(\mathbf{r})|^2}{8\rho(\mathbf{r})}$$

where τ_w is the von Weizsäker[39] kinetic energy. The orbital kinetic energy density and the Laplacian of the density essentially carry the same information, since they are related via the orbitals and the effective potential can be written as

$$\tau(\mathbf{r}) = \frac{1}{2}\sum_i^{occ} \varepsilon_i|\phi_i(\mathbf{r})|^2 - \nu_{eff}(\mathbf{r})\rho(\mathbf{r}) + \nabla^2\rho(\mathbf{r}) \tag{2.25}$$

Inclusion of either the Laplacian or kinetic energy density as a variable leads to the so-called *meta-GGA* functionals and the two functions in equation 2.24 are the common components of *meta-GGA* functionals.

DFT is accurate, if we know how to derive necessary relations between density and energy. Unfortunately, energy functionals relating electronic density to energy are unknown, and there is no general way to improve them beside trying new ones and judging their quality by the results. However, DFT provides a hope for an accurate method which scales with fourth power of molecular size in the worst case, and possibly linearly for larger molecules.[40]

Chapter 3

Excited State Calculations

The development of HF and DFT in the previous chapters has focused on the electronic ground state. As for ground state calculations, performing an adequate excited state calculation involves making an appropriate choice of method and basis set. In dealing with excited state, it always useful to distinguish two different cases. These are the dependency on the same or a different symmetry than the lower state(s). Excited states of different symmetry can be treated as the lowest energy state of a given symmetry may handled analogously to the ground state. However, excited states where there is a lower energy solution of the same symmetry are somewhat more difficult to treat. It will be difficult to generate a HF type wavefunction, for instance, for those states as a consequences of the variational collapse to the lowest energy solution of the given symmetry. This leads to a number of alternative methods for studying excited states.

It is a challenge to acquire a reliable description of the electronic excited states. This is because there is a great diversity of excited states—some involve one-electron valence excitations from the ground state, such as an $n \rightarrow \pi^*$ state in carbonyl groups, while others involve excitations into very diffuse Rydberg orbitals, such as lower excited state of atoms and saturated molecules, some involve charge transfer from on region to another, some involve significant

contributions from promotion of 2 (or even more) electrons, such as the so-called dark states of polyenes, etc. Thus it is difficult to build economical and yet accurate theoretical chemical models that can describe this diversity. Most popular at present are approaches based on time-dependent extensions to DFT, although this still suffers from significant limitations. Coupled cluster theory provides an alternative framework that is useful for smaller molecules. Complete active space-based methods are another alternative, although the selection of the active space is a tremendous challenge. The lowest level of theory for a qualitative description of excited state is a configuration interaction with singly excited determinants, CIS.

3.1 Configuration Interaction Singles, CIS

Configuration interaction singles (CIS)[41] is the computationally, as well as conceptually, simplest wavefunction based ab initio method for the calculation of electronic excitation energies and excited-state properties. The starting point of the derivation of the CIS equations is the Hartree–Fock ground state, Ψ_{HF}, which corresponds to the best single Slater determinant describing the electronic ground state of the system. This determinant is shown in equation 1.16 and represents only one of several possible determinants for an electronic wavefunction of the system. For the n number of electrons with η number of basis functions , there are $n(\eta - n)$ possible singly excited determinants made by replacing an occupied spin orbital with a virtual spin orbital. Such wavefunctions and associated energies can be written

$$\psi_{ia} = (n!)^{-1/2} det[\psi_1 \psi_2 \cdots \psi_a \psi_i \cdots \psi_n] \tag{3.1}$$

$$E_{ia} = E_{HF} + \varepsilon_a - \varepsilon_i - (ia||ia) \tag{3.2}$$

The following subscript notation will be used throughout; $\mu, \nu, \lambda, \sigma, ...$, denote atomic basis functions; $i, j, k, l, ...$ denote molecular orbitals which are occupied in the ground state; $a, b, c, d, ...$ denote virtual molecular orbitals, unoccupied in the ground state; $p, q, r, s, ...$ denote generic molecular spin orbitals. Introducing the antisymmetrized two-electron integrals in the molecular orbital basis

$$(pq||rs) = \sum_{\mu\nu\lambda\sigma} c_{\mu p} c_{\nu q} c_{\lambda r} c_{\sigma s} (\mu\nu||\lambda\sigma) \tag{3.3}$$

The singly excited wavefunction in equation 3.1 and energies can be considered first approximation to the molecular excited states of the system. However, there are several disadvantages in using equation 3.1 as a wavefunction:

1. It is not an eigenfunction of the S^2 operator and therefore does not yield pure spin states for closed-shell systems.

2. The spin orbitals involved in transition have been variationally determined for the ground state. Forcing the virtual orbital to be occupied is more closely related to ionization rather than excitation.

3. It is not at all appropriate for excitations into degenerate spin orbitals. For instance, the π to π^* excited states of benzene can be understood only as a mixture of four singly excited determinants.

These objections are partially overcome if the excited-state wavefunction is written as a linear combination of all possible singly excited determinants[41]

$$\Psi_{CIS} = \sum_{ia} C_{ia} \psi_{ia} \tag{3.4}$$

These configuration interaction (CI) coefficients can be deduced as normalized eigenvectors of the Hamiltonian matrix

$$< \psi_{ia}|H|\psi_{jb} >= [E_{HF} + \varepsilon_a - \varepsilon_i]\delta_{ij}\delta_{ab} - (ja||ib) \tag{3.5}$$

This procedure is known as full configuration interaction in the space of substitutions or "CI singles". Eigenvalues, E_{CIS}, of equation 3.4 are the CI-singles total energies for various excited states .

$$E_{CIS} = E_{HF} + \sum_{ia} a_{ia}^2(\varepsilon_a - \varepsilon_i) - \sum_{ijab} a_{ia}a_{jb}(ja||ib) \tag{3.6}$$

The Ψ_{CIS} is properly orthogonal to the ground-state Ψ_{HF} by virtue of Brillouin theorem, i.e, the matrix elements between HF reference and singly excited state are zero.[42]

$$\langle \Psi_{ia}|H|\Psi_{HF}\rangle = 0 \tag{3.7}$$

The variational determinant of the CIS coefficients allows the overall wavefunction to relax so that Ψ_{CIS} more properly represents an excited state rather than an ionized state. CIS leads to a well-defined wavefunction and differentiable energy, thus analytical gradient techniques to determine properties and optimized excited-state geometries are relatively straight to apply.

3.2 CIS(D)

CIS(D) is a second-order perturbative approximation to coupled cluster singles and doubles (CCSD) method. It is based on a single state excitation configuration interaction (CIS) reference,[43,44] and can be considered as an ex-

cited state analogue to MP2. CIS(D) is size-consistent and scales with the fifth power of molecular size in the canonical orbital basis. For vertical excitation energies of closed-shell molecules, CIS(D) typically reduces by a factor of two or so, the quite large error obtained at the CIS level.[43] A general views CIS(D) is as follows. When the Hartree-Fock ground state of a system is described by a single determinant ψ_0 and when its single substitution of any occupied spin orbital i to any unoccupied spin orbital a is denoted as ψ_i^a, the CIS excitation energy ω is obtained as the solution to an eigenvalue equation

$$\langle \psi_i^a | \hat{H} | U_1 \psi_0 \rangle = \omega b_i^a \tag{3.8}$$

where $\hat{H} = H - E_{HF}$ and U_1 is an operator that generates the CIS wavefunction from ψ_0

$$\Psi_{CIS} = U_1 \psi_0 = \sum_{ia} b_i^a \psi_i^a \tag{3.9}$$

The correlation energy of the excited state corrected through second-order perturbative theory is then given by

$$E^{CISD} = \langle \Psi_{CIS} | V | U_2 \psi_0 \rangle + \langle \Psi_{CIS} | V | T_2 U_1 \psi_0 \rangle \tag{3.10}$$

where V is the fluctuation potential due to electron correlation, and T_2 is the operator that generates the first-order Møller-Plesset wavefunction from ψ_0

$$T_2 \psi_0 = \frac{1}{4} \sum_{ijab} a_{ij}^{ab} \psi_{ij}^{ab} = -\frac{1}{4} \sum_{ijab} \frac{(ij||ab)}{\varepsilon_a + \varepsilon_b - \varepsilon_i - \varepsilon_j} \psi_{ij}^{ab} \tag{3.11}$$

U_2 is the operator that generates the first-order excited state pair correlations

$$U_2\psi_0 = \frac{1}{4}\sum_{ijab} b_{ij}^{ab}\psi_{ij}^{ab} = -\frac{1}{4}\sum_{ijab}\frac{\langle\psi_{ij}^{ab}|V|U_1\psi_0\rangle}{\varepsilon_a+\varepsilon_b-\varepsilon_i-\varepsilon_j}\psi_{ij}^{ab} \tag{3.12}$$

The first term in equation 3.10, accounts for electron correlation effects that involve one electron that is active in the CIS excitation plus a second electron, which thereby generates a double excitation. The second term accounts for the effect of electron correlation between pairs of the electron that are not directly involved in the CIS excitation. The first and second terms are called *direct* and *indirect*, respectively.

It can be shown that equation 3.10 can be transformed into[43]

$$E^{CIS(D)} - E^{MP2} = -\frac{1}{4}\sum_{ijab}\frac{(u_{ij}^{ab})^2}{\varepsilon_a+\varepsilon_b-\varepsilon_i-\varepsilon_j-\omega} + \sum_{iab} b_i^a b_i^b R_{ab} + \sum_{ijc} b_i^c b_j^c R_{ij} + \sum_{ia} b_i^a w_i^a \tag{3.13}$$

where

$$(u_{ij}^{ab}) = \sum_c [(ab||cj)b_i^c - (ab||ci)b_j^c] + \sum_k [(ka||ij)b_k^b - (kb||ij)b_k^a] \tag{3.14}$$

$$R_{ab} = -\sum_{jkbc}(jc|kb)a_{jk}^{ca} \tag{3.15}$$

$$R_{ij} = -\sum_{jkab}(ja|kb)a_{ik}^{ab} \tag{3.16}$$

$$w_i^a = \sum_{jkbc}(jk||bc)a_{ik}^{ac}b_j^b \tag{3.17}$$

Equation 3.13 defines the second-order correction to the CIS excitation energy, $\omega^{CIS(D)}$, leading a total excitation energy that is $\omega^{CIS} + \omega^{CIS(D)}$.

Recently, Rhee and Head-Gordon reported a resolution of the identity (RI) implementation of CIS(D) in addition to spin component scaled and scaled opposite spin versions of CIS(D), denoted SCS-CIS(D) and SOS-CIS(D), respectively.[45] SCS-CIS(D) is an extension of the SCS-MP2 method,[46,47] where the opposite and same spin components of the energy are scaled separately. Within SCS-CIS(D) the excitation energy can be considered as

$$\omega^{\mathrm{SCS-CIS(D)}} = c_U^{OS} w_U^{OS} + c_T^{OS} w_T^{OS} + c_U^{SS} w_U^{SS} + c_T^{SS} w_T^{SS} \tag{3.18}$$

where OS and SS denote opposite and same spin, and w_U and w_T are the direct and indirect terms of equation 3.10, respectively. For SOS-CIS(D), only the opposite spin components of equation 3.18 are considered.

3.3 Time-dependent Density Functional Theory

Time dependent density functional theory (TDDFT)[48,49] is an extension of DFT to study excited states. TDDFT calculates the poles in the response of the ground state density to a time-varying applied electric field. These poles are the Bohr frequencies or excitation energies. The advantage of this approach is that TDDFT provides an accurate prediction of excitation energies and oscillator strengths at relatively low computational cost. TDDFT, formally, is based on the Kohn-Sham formulation (KS-DFT). However, traditional KS-DFT is limited to time-independent systems. If one wants to

establish an analogous time-dependent theory, time-dependent versions of the first and second Hohenberg-Kohn theorems must be formulated and proven, and a time-dependent Kohn-Sham equation must be derived. The first task has been formulated by Runge and Gross, who proposed so the-called Runge-Gross Theorem.[48] This theorem serves as the time-dependent analogue of the first Hohenberg-Kohn theorem and constitutes the cornerstone of the formal foundation of the time-dependent Kohn-Sham formalism.

The formalism of the Runge-Gross theorem is

$$A[\rho] = B[\rho] - \int_{t_0}^{t_1} d\mathbf{t} \int d\mathbf{r}\rho(\mathbf{r},\mathbf{t})v(\mathbf{r},\mathbf{t}) \tag{3.19}$$

where $A[\rho]$ is the action density to obtain the exact density, $B[\rho]$ is the universal functional which is independent of the potential $v(\mathbf{r},\mathbf{t})$,

$$B[\rho] = \int_{t_0}^{t_1} d\mathbf{t} \left\langle \Psi[\rho](\mathbf{r},\mathbf{t}) \left| i\frac{\partial}{\partial t} - \hat{T}(\mathbf{r}) - \hat{V}_{e,e}(\mathbf{r}) \right| \Psi[\rho](\mathbf{r},\mathbf{t}) \right\rangle \tag{3.20}$$

and

$$\rho(\mathbf{r},\mathbf{t}) = \int |\Psi(\mathbf{r}_1,\mathbf{r}_2,\mathbf{r}_3,\ldots\mathbf{r}_n,\mathbf{t})|^2 d\mathbf{r}_2 d\mathbf{r}_3 \ldots d\mathbf{r}_n \tag{3.21}$$

$$v(\mathbf{r},\mathbf{t}) = V_{e,n}(\mathbf{r}) + V(\mathbf{r},\mathbf{t}) \tag{3.22}$$

Subsequently, the time-dependent Kohn-Sham equation can be derived as follows. If we assume that a time-dependent noninteracting reference system exists with external one-particle potential $v_s(\mathbf{r},\mathbf{t})$ of which the electron density $\rho_s(\mathbf{r},\mathbf{t})$ is equal to the exact electron density $\rho(\mathbf{r},\mathbf{t})$ of the real interacting system, then the existence of a time-dependent noninteracting reference system is usually ensured. Thus, the density, after applying single Slater determinant

is

$$\rho(\mathbf{r},\mathbf{t}) = \rho_s(\mathbf{r},\mathbf{t}) = \sum_{i}^{n} |\psi_i(\mathbf{r},\mathbf{t})|^2 \tag{3.23}$$

The details of this derivation has been examined elsewhere.[50] In short, the time-dependent Kohn-Sham equations can be conveniently expressed in matrix notation in a basis of η time-independent single-particle wavefunctions $\chi(\mathbf{r})$

$$\psi_p(\mathbf{r},\mathbf{t}) = \sum_{j}^{\eta} c_{pj}(\mathbf{t})\chi_j(\mathbf{r}) \tag{3.24}$$

Then, the time-dependent Kohn-Sham equation reads

$$i\frac{\partial}{\partial t}\mathbf{C} = \mathbf{F}^{KS}\mathbf{C} \tag{3.25}$$

where the ith column of the matrix $\mathbf{C}$ contains the time-dependent expansion coefficients of $\psi_i(\mathbf{r},\mathbf{t})$ and $\mathbf{F}^{KS}$ is the matrix representation of the time-dependent Kohn-Sham operator in the given basis. Thus, the Dirac form of the time-dependent Kohn-Sham equation in density matrix is

$$\sum_{q} \mathbf{F}_{pq}\mathbf{P}_{qr} - \mathbf{P}_{pq}\mathbf{F}_{qr} = i\frac{\partial}{\partial t}\mathbf{P}_{pr} \tag{3.26}$$

in which the density matrix P_{pr} is in general related to the electron density.

Pursuing the equation 3.26 is to obtain excitation energies and oscillator strengths. There are two different strategies can be followed. The first possibility is to propagate the time-dependent Kohn-Sham wavefunction in time, which is referred to as real-time TDDFT.[51,52] The second possibility is the so-called linear-response TDDFT equation. In principle, the excitation energies

can be obtained from linear time-independent ground-state electron density to a time-dependent external electric field. The condition is that before the time-dependent electric field is applied, the system is assumed to be in its electronic ground state, which is determined by the standard time-independent Kohn-Sham equation. The TDDFT equation can be written[50]

$$\begin{bmatrix} \mathbf{A} & \mathbf{B} \\ \mathbf{B}^* & \mathbf{A}^* \end{bmatrix} \begin{bmatrix} \mathbf{X} \\ \mathbf{Y} \end{bmatrix} = \omega \begin{bmatrix} \mathbf{1} & \mathbf{0} \\ \mathbf{0} & -\mathbf{1} \end{bmatrix} \begin{bmatrix} \mathbf{X} \\ \mathbf{Y} \end{bmatrix} \tag{3.27}$$

This is the non-Hermitian eigenvalue equation where the two-electron integrals are given in Mulliken notation. The element of the matrices $\mathbf{A}$ and $\mathbf{B}$ are given as

$$A_{ai\sigma,jb\tau} = \delta_{ij}\delta_{ab}\delta_{\sigma\tau}(\varepsilon_{a\sigma} - \varepsilon_{i\tau}) + (ia\sigma|jb\tau) + (ia\sigma|f_{XC}|jb\tau) - K^{HF}_{ia\sigma,jb\tau} \tag{3.28}$$

$$B_{ai\sigma,jb\tau} = K_{ai\sigma,jb\tau} + (ai\sigma|f_{XC}|jb\tau) \tag{3.29}$$

where

$$(ia\sigma|jb\tau) = \int\int \psi^*_{i\sigma}(\mathbf{r}_1)\psi^*_{a\sigma}(\mathbf{r}_1)\frac{1}{r_{12}}\psi_{j\tau}(\mathbf{r}_2)\psi_{b\tau}(\mathbf{r}_2)d\mathbf{r}_1 d\mathbf{r}_2 \tag{3.30}$$

$$(ia\sigma|f_{XC}|jb\tau) = \int \psi^*_{i\sigma}(\mathbf{r}_1)\psi_{a\sigma}(\mathbf{r}_1)\frac{\Delta^2 E_{XC}}{\Delta\rho_\sigma(\mathbf{r}_1)\Delta\rho_\tau(\mathbf{r}_2)}\psi_{j\tau}(\mathbf{r}_2)\psi^*_{b\tau}(\mathbf{r}_2)d\mathbf{r}_1 d\mathbf{r}_2 \tag{3.31}$$

TDDFT is well established for computing valence excited states. The advantage to use this approach is that it provides an accurate prediction of excitation

energies and oscillator strengths at relatively low computational cost. Within the Tamm-Damcoff approximation[53] (TDA) of TDDFT, B is assumed to be zero giving the simpler eigenvalue equation[50]

$$\mathbf{AX} = \omega\mathbf{X} \tag{3.32}$$

where the elements of $\mathbf{A}$ are the same as in equation 3.28 and ω_i are the excitation energies, E_{XC} is the exchange correlation functional and $K^{HF}_{ia\sigma,jb\tau}$ is the HF exchange term. TDDFT is becoming very popular as a method for studying excited states because the computational cost is roughly similar to the simple CIS method, but a description of a electron correlation effects is implicit in the method. The excitation energies for low-lying valence excited states of molecules (below ionization threshold) are often remarkably improved relative to CIS, with an accuracy of roughly 0.3 eV being observed with either gradient corrected or local density functional.[16]

However, standard density functionals do not yield a potential with the correct long-range Coulomb tail (due to the so-called self-interaction problem), and therefore excited states which sample this tail, Rydberg states for instance, are not described accurately.[54,55] Hence it is advisable to only employ TDDFT for low-lying valence excited state that are below the first ionization potential of the molecule.

3.4 Equation of Motion-Coupled Cluster Theory

Another tool for calculating electronic excitation energies of polyatomic molecules is the Equation-of-Motion Coupled Cluster method (EOM-CCSD). This approach was originally proposed by Monkhorst[56] and has been developed by many others[57–61] in the recent years. Most practical implementations of this method have been based on coupled cluster singles and double (CCSD) ground-state wavefunctions.[62–65] However, due to the high computational cost including triple excitations, their application is limited to systems with only few electrons. The EOM-CCSD procedure usually gives reasonable agreement with full configuration interaction (FCI) results for those states that are adequately described by the promotion of a single electron from ground state.

Since the EOM-CCSD method has been extensively described by many authors (see Refs.[61,63,66]), we give only short introduction to this approach. In the EOM-CCSD method the kth excited state is obtained by applying a linear wave operator $\hat{U}^k$ to the CC ground-state wavefunction,

$$\Psi^k = \hat{U}^k e^{\hat{T}} \psi_0, \tag{3.33}$$

where ψ_0 is usually the (normalized) closed-shell HF determinant for the ground state. After inserting the expression for Ψ^k into the time-independent Schrödinger equation one gets the following equation for the operator $\hat{U}^k$ and the excitation energy is

$$\omega^k = E^k - E^0 \tag{3.34}$$

where E^k and E^0 are the energies of the kth excited state in the EOM-CC approximation and of the ground-state energy in the CC approximation, respectively:

$$[\hat{\bar{H}}, \hat{U}^k]\Psi_0 = \omega^k \hat{U}^k \psi_0, \tag{3.35}$$

where $\hat{\bar{H}}$ is a similarity transformed Hamiltonian,

$$\hat{\bar{H}} = e^{-\hat{T}} \hat{H} e^{\hat{T}} \tag{3.36}$$

The equation 3.35 represents a generalized eigenvalue problem for ω^k and $\hat{U}^k$. Restricting operators $\hat{T}$ and $\hat{U}^k$ to at most double excitations,

$$\hat{T} = \hat{T}_1 + \hat{T}_2 \tag{3.37}$$

and

$$\hat{U}^k = \hat{U}_0^k + \hat{U}_1^k + \hat{U}_2^k \tag{3.38}$$

yield the EOM-CCSD method. The detailed expression for the elements of the $\bar{H}$ matrix in the spin-orbital form can be found in Refs.[61] and.[63]

3.5 Multireference Methods

The HF wavefunction often is a good starting point for correlated treatments of molecular electronic structure. However understanding the true nature of the chemical bond requires a more general mathematical formulation at the mean-field level. The insufficient account of static electron correlation is the

reason behind the failure of the HF reference wavefunction in many situations. Systems such as molecules with unfilled valencies in their electronic ground state e.g, radicals and diradicals or molecules containing atoms with low-lying excited states that possess a number of near degenerate electronic configurations and therefore exhibit strong static correlation effects. More generally, at the dissociation limit for chemical bonds, along reactions paths in chemical and photochemical reactions, and often for excited electronic states, a qualitatively correct description of the wavefunction is possible only if the most significant electronic configurations are included.

The natural way to extend the HF model to account for static correlation effects is therefore to construct the mean-field electronic wavefunction from multiple Slater determinants. This approach results in a multiconfigurational self-consistent field (MCSCF) wavefunction. The increased complexity of the MCSCF wavefunction is accompanied by a sizable increase in computational cost compared to the HF wavefunction. The computational cost can be kept at a reasonable level by selecting a small number of electrons and orbitals, the so-called active space, and include in the MCSCF wavefunction all possible electronic configurations obtained by distributing these active electrons into the active orbitals. This leads to the complete active space self-consistent field wavefunction (CASSCF).[67] Given a physically correct active space, the CASSCF wavefunction offers maximum flexibility for a qualitative description of the electronic structure of even the most exotic types of chemical bonds.[68] The dynamical correlation required for a quantitative description can be recovered by a subsequent second-order perturbative correction (CASPT2).[69] The success of this approach has been documented by a number of studies

on electronic ground[70,71] and excited states.[72–74] In addition, the CASSCF wavefunction has been instrumental for understanding photochemical processes.[75,76]

Chapter 4

Computation of NEXAFS and IR Spectra

The work in this thesis is concerned primarily with the calculation of the spectroscopy of core electrons, including near-edge X-ray absorption fine structure (NEXAFS) and X-ray emission spectroscopy (XES). This work incorporates improving the accuracy of NEXAFS calculations and application to study the NEXAFS of molecules adsorbed on surfaces. For these systems, we have also studied the infrared (IR) spectroscopy. In this chapter, quantum chemical calculations of NEXAFS and IR spectra are described. In the following chapters the NEXAFS spectroscopy of organic molecules adsorbed on metal and semiconductor surfaces is described. Subsequently, the calculations of NEXAFS spectra using the CIS(D) method and XES spectra are described.

Even though less familiar than the analogous techniques for valence electrons, studying and exploiting the spectroscopy of core electrons has a long history.[77] The spectroscopy of core electrons is attractive for several reasons. The spatially local nature of the core orbitals and large energy difference between core orbitals of different elements means that the spectroscopic techniques can provide an atom specific probe of electronic structure. A drawback of

these techniques is the high energy X-ray light source required and this has hindered the wide spread use of core-electron spectroscopic methods. However, in recent years there have been considerable advances in the quality and availability of X-ray sources.

There are a number of commonly used X-ray spectroscopic techniques. Figure 4.1 shows a schematic of an absorption spectrum in the X-ray region. The structure near the absorption edge is referred to as NEXAFS or X-ray absorption near edge structure (XANES) and corresponds to the excitation of a core excitation to give a bound state below the ionization continuum. This part of the X-ray absorption spectrum provides information on the unoccupied orbitals. At the higher energy, usually beyond 20-30 eV of the absorption edge, are weak oscillations which correspond to extended X-ray absorption fine structure (EXAFS) and arise from excitation to states above the ionization continuum and subsequent scattering of the photoelectron by its environment. For some systems, pre-edge features are observed that arise from excitation from the core orbitals to singly occupied orbitals. In addition to these absorption processes, X-ray emission can also occur. Excitation of a core electron creates a singly occupied core orbital, referred to as a core hole. XES results from the subsequent decay of a valence electron to the core orbital with the emission of a photon. XES is dependent on the nature of the occupied valence orbitals, and thus provides complementary information to NEXAFS.

Surface science is a field of research that has exploited X-ray spectroscopy extensively, providing information on the structure and orientation of the adsorbed molecules and the nature of their bonding to the surface.[77,78] In

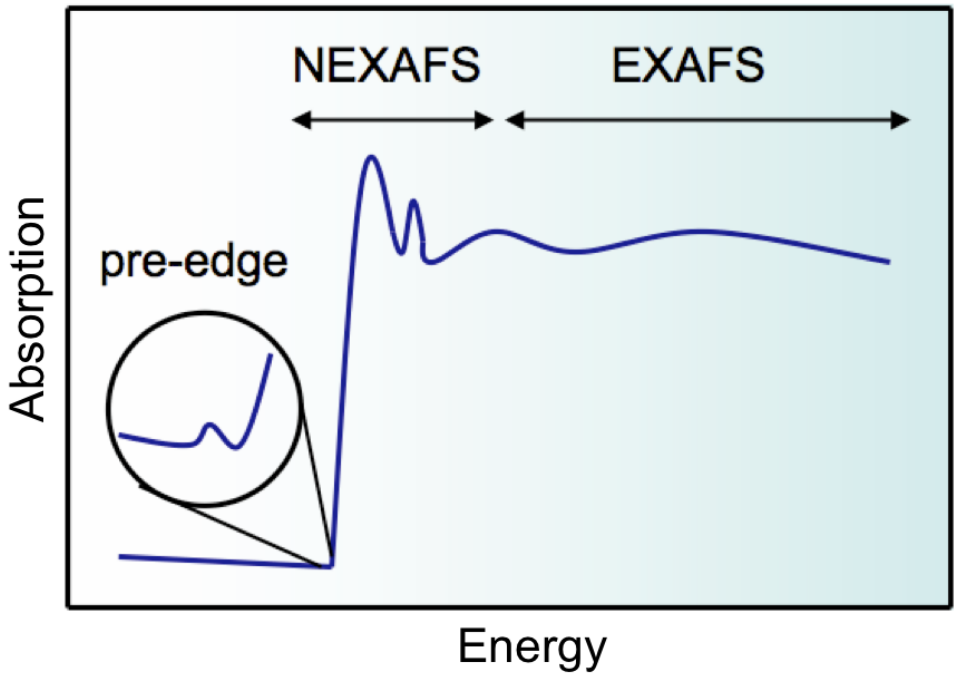

Figure 4.1: Schematic of a X-ray absorption spectrum.

comparison, the number of studies focusing on the calculation of core-excited states is modest. However, such calculations can play a crucial role in aiding the interpretation and understanding of experimental spectra, and the development of accurate calculations remain important to future progress in the application of X-ray spectroscopic methods.

4.1 Computation of NEXAFS Spectra

Experimental NEXAFS spectroscopy is used extensively in surface science to probe the bonding and orientation of molecules adsorbed on surfaces. Despite the experimental importance of NEXAFS, theoretical calculations of NEXAFS are relatively uncommon in comparison with the more familiar ultra-

violet spectroscopy. However, a small number of groups have addressed this problem.[89–94] Horsley *et al.*[90] studied the NEXAFS of ethene on the Pt(111) surface, and Petterson and co-workers have studied the X-ray absorption and x-ray emission spectra of small molecules on the Cu(110) surface using STEX and transition potential methods.[89,92,95–97]

Within density functional theory, core-excited states can be computed with a ΔKohn-Sham self-consistent field approach. In this method, the core-excited state is computed by imposing a constraint of a single occupancy of a core orbital within the self-consistent field calculation to prevent the variational collapse. For calculations of NEXAFS spectra comprising many core-excited states, this method is inefficient since it requires individual Kohn-Sham calculations for each excited state. The problem of optimizing individual states is avoided in the transition potential method.[89] In this approach the ground and excited states are determined within a single calculation in which the core level has half an electron removed, capturing a balance between final and initial states. Alternatively, NEXAFS spectra can be computed using TDDFT.[98,99] Recently, a resonant converged complex polarization propagator method has been implemented[100] and applied to study NEXAFS.[101,102]

Within standard implementations of TDDFT, the calculation of core excited states can become prohibitively expensive even for relatively small molecules. One solution is to restrict the single excitation space to include only excitations from the relevant core orbital(s). This makes the computation of core excited states of comparable expense as for computing valence excited states.

The nature of exchange-correlation functionals of TDDFT dictates the accu-

racy of the computed core excitation energies and NEXAFS spectra. Unfortunately, standard generalized gradient approximation and hybrid functionals fail dramatically for core excitations resulting in large underestimation of the excitation energy. Furthermore, the extent of this underestimation increases with the nuclear charge of the nuclei on which the core orbitals are localized.[103] This failure stems from the approximate exchange within the exchange-correlation functionals and is associated with the self interaction error,[99,105,105–108] and self-interaction corrections have been explored to correct for this error.[107,108] There is an analogy between the calculation of core-excited states and the calculation of charge transfer states. The failure of TDDFT to describe the charge transfer states is well understood,[109] and can be predicted by the Λ diagnostic.[110] This diagnostic is a measure of the overlap between donating and accepting orbitals, and given by

$$\Lambda = \frac{\sum_{i,a} \kappa_{ia}^2 o_{ia}}{\sum_{i,a} \kappa_{ia}^2} \tag{4.1}$$

where o_{ia} is a measure of the spatial overlap between occupied orbital ψ_i and virtual orbitals ψ_a

$$o_{ia} = \int |\psi_i(\mathbf{r})||\psi_a(\mathbf{r})| d\mathbf{r} \tag{4.2}$$

and within the Tamm-Dancoff approximation

$$\kappa_{ia} = \mathbf{X}_{ia}. \tag{4.3}$$

Table 4.1 shows computed values Λ for a range of core excitation energies. These values are automatically generated when one compute the excitation energies using QCHEM software package. The compactness of the core orbital

makes the value of Λ small, and comfortably in the regime where GGA or hybrid functionals fail.[110] For nuclei with higher nuclear charge, the core orbitals will be more compact and greater failure of the functional would be anticipated. In general, this underestimation is roughly constant of about 0.06 eV across different excitations from a given core orbital, and a pragmatic approach is to simply apply a constant shift to the computed spectra.[111,112] However, it remains desirable to compute accurate core excitations within TDDFT , and several groups have developed new exchange-correlation functionals designed for NEXAFS calculations.[99,104–106,113,114] Nakai and co-workers reported the

Table 4.1: Values of the Λ diagnostic for core excitations from BLYP/6-311(2+,2+)G(d,p) calculations.

Excitation	Λ
CO C(1s)→ $\pi*$	0.18
CO C(1s)→3s	0.04
CO O(1s)→ $\pi*$	0.14
CO O(1s)→3s	0.03
HF F(1s)→ $\sigma*$	0.08
SiH_4 Si(1s)→ $\sigma*$	0.03
H_2S S(1s)→ $\sigma*$	0.04
H_2S S(1s)→4p	0.01
HCl Cl(1s)→ $\sigma*$	0.02
HCl Cl(1s)→ $4p_\pi$	0.01

first attempts to improve the description of core-excited states within TDDFT. The BmLBLYP exchange-correlation functionals[113] was developed from the observation that the modified Leeuwen-Baerends (mLB) exchange functional performed better for core excitations and Becke88 (B) exchange was better for valence excitations. The resulting functional combined these two exchange functionals by adopting LB94 in the core and asymptotic regions and Becke88

in the valence regions, and gave an average error of about 1.5 eV for a set of core excitations compared to over 13 eV for B3LYP. Subsequently, the CV-B3LYP[105] and CVR-B3LYP[104,106] functionals were introduced. These functionals were designed to be accurate for all types of excitation, including core excitations, and worked by using an appropriate fraction of HF exchange depending on the type of excitation. These functionals were applied to core-excitations from first and second row nuclei and showed a substantial improvement in accuracy, yielding mean absolute errors below 1 eV.

Following this work, a hybrid functional was optimized for carbon K-edge excitations which was used to study the NEXAFS spectroscopy of hydrocarbon adsorbed on the Si(100)-2x1 surface.[99] In this functional, the fraction of HF exchange in B3LYP was increased to predict the 1s$\rightarrow \pi^*$ excitation energies in acetylene, ethylene and benzene correctly. This led to the following functionals with 57% HF exchange, with the fraction of Becke exchange reduced proportionately

$$BH^{0.57}LYP = 0.57HF + 0.35B + 0.08S + 0.81LYP + 0.19VWN \quad (4.4)$$

where HF, B and S are Hartree-Fock , Becke,[32] and Slater[29] exchange functionals, respectively, and LYP and VWN are Lee-Yang-Parr[36] and Vosko-Wilk-Nusair,[37] respectively. We have also tested this functional to the excitations from other nuclei with a significantly different nuclear charge, and it shows less satisfactory performances. From here, it can be assured that this functional is operated well only for carbon K-edge excitations.

4.2 Computation of Infra-red Spectra

Quantum chemical calculations of IR spectra are well established as useful tools that can aid the deciphering of experimental spectra. Due to computational expense, vibrational frequencies are usually computed within the harmonic approximations. In this approximation, vibrational modes and frequencies are obtained from the eigenvectors and eigenvalues of the Hessian matrix in the mass-weighted coordinates,[38] where the Hessian matrix contains the second derivatives of the electronic energy with respect to the nuclear coordinates. The harmonic frequencies are then determined by constructing and diagonalizing the full Hessian matrix. This produces all the normal modes of the molecule under consideration including modes that experimentally identified. Furthermore, the intensities are evaluated through the derivative of the dipole moment with respect to the normal coordinates.

The evaluation of harmonic frequencies through computation of energy second derivatives can be done either numerically or analytically. Q-CHEM[79] applies analytical evaluation of the energy second derivatives and then subsequently evaluates it efficiently via the coupled-perturbed Hartree-Fock (or coupled-perturbed Kohn-Sham) equations using the iterative procedure introduced by Pople *et al.*[80]

Application of a standard harmonic frequency calculation to the problem of studying the IR spectroscopy of large systems, such as a molecule on a surface, is computationally expensive. This is because the large number of atoms necessary to model the semiconductor makes the calculation too expensive. Strategies for reducing the cost of these calculations can arise from recognizing

that while standard harmonic frequency calculations compute all vibrational modes, often only a small fraction of these modes are of interest. Reiher and co-workers have developed a mode-tracking approach which allows a pre-selected vibration modes to be determined.[81] Using a suitable estimate of the normal mode, an iterative Davidson approach[82] is used to construct the exact normal modes and frequency. An advantage of this approach is the Hessian is not approximated. This approach has been applied to study a number of problems, and shown to reduce the computational cost significantly.[83–85]

Partial Hessian methods provide an alternative approach to this problem. If the vibrational modes of interest are localized within a distinct region of the system, the corresponding normal modes and frequencies can be evaluated by computing only the sub-block of the Hessian matrix comprising the derivatives of the energy with respect to the coordinates of the atoms within this region. Physically, this approximation corresponds to attributing an infinite mass to the atoms not included within the partial Hessian. This approximation is valid for normal modes in which the atoms excluded from the partial Hessian are stationary. Consequently, vibrational modes that are amenable to a partial Hessian approach can be identified from analysis of the normal modes. For such vibrational modes, the partial Hessian approximation introduces a small error in the computed frequencies and intensities whilst significantly reducing the computational cost.

A partial Hessian method that exploits the partial Hessian approximation has been implemented in the Q-CHEM program package. The partial Hessian approximation has been used to study a range of systems, from amide I band

in polypeptides to the IR spectroscopy of molecules on surfaces.[86–88]

4.3 Computation of XES Spectra using Maximum Overlap Method

Experimental observations using the X-ray emission technique provides another possibility for investigating reactions on surfaces and interfaces. The calculation of XES can be done in several ways including with TDDFT and equation of motion coupled cluster theory (EOM-CCSD).[63,66] Either TDDFT and EOM-CCSD can be applied to study XES by invoking the Maximum overlap method (MOM),[194,195] a simple protocol for choosing which orbitals to occupy at each iteration of an SCF calculation.

In SCF procedures with an Aufbau protocol, the occupancy of the orbitals are chosen with the lowest orbitals energies and tend to converge to the lowest SCF solution. However, MOM provides an alternative approach by selecting such that they have the largest projections into the space of orbitals occupied on the previous SCF cycle.

On each iteration of the SCF procedure, the current MO coefficient matrix $\mathbf{C}^{old}$ is used to build a Fock (or Kohn-Sham) matrix $\mathbf{F}$ and generalized eigenvalue problem

$$\mathbf{F}\mathbf{C}^{new} = \mathbf{S}\mathbf{C}^{new}\varepsilon \tag{4.5}$$

where **S** is the basis function overlap matrix. Equation 4.5 is then solved to obtain a new MO coefficient matrix $\mathbf{C}^{new}$ and orbitals energies ε. One usually follows the Aufbau protocol, which dictates that one simply occupies the n orbitals with the lowest orbitals energies ε_j.

MOM gives an alternative to the Aufbau protocol. It states that the new occupied orbitals should be those that overlap most with the span of the old occupied orbitals.[194] The orbital overlap matrix, then, can be defined as

$$\mathbf{O} = (\mathbf{C}^{old})^{\ddagger}\mathbf{S}\mathbf{C}^{new} \tag{4.6}$$

$$\tag{4.7}$$

then O_{ij} is the overlap between the ith old orbital and the jth new orbital, and the projection of the jth new orbital onto the old occupied space is

$$p_j = \sum_{i}^{n} O_{ij} = \sum_{\nu}^{N}[\sum_{\mu}^{N}(\sum_{i}^{n} C_{i\mu}^{old})S_{\mu\nu}]C_{\nu j}^{new} \tag{4.8}$$

In this way, the full set of p_j values can be found by three matrix-vector multiplications, at $O(N^2)$ cost, and this adds negligibly to the cost of each SCF cycle. One then occupies the orbitals with the largest projections p_j.

The MOM begins the SCF calculation with orbitals that lie within the area of attraction of the target excited solution. In the case of the guess is sufficient to perform a ground-state calculation, then simply promote an electron from an occupied to a virtual orbital. If it is sufficiently close to the target solution, the MOM will retain the excited configuration as the orbitals relax during the SCF. If, on the other hand, the guess lies outside of the area of

attraction, the SCF will converge to another solution of the same symmetry. In difficult cases, the quality of the guess may be improved by using orbitals that are optimal for the $(n-1)$-electron system, or by using orbitals from another excited-state calculation.

The advantage of using MOM over other excited-state methods is having the possibility to single out a particular state without computing all lower energy states of the same symmetry. In particular, when targeting excited states of molecules in the presence of explicit solvent or when adsorbed onto a surface. This approach is also applicable to both HF and DFT calculations.

For the calculation of XES spectrum, MOM can be used to obtain an SCF solution with an unoccupied core orbital which can then be used in a subsequent TDDFT or EOM-CCSD calculation.

Chapter 5

IR and NEXAFS Spectroscopy of Acetylene and Benzene on Group IV Semiconductor Surfaces

---

The study of hydrocarbon chemistry on semiconductor surfaces has been the focus of much interest in recent years. This interest is motivated by developments in the area of new semiconductor-based materials and devices.[115] Surface phenomena have always been a cornerstone of the microelectronic industry. Processes such as epitaxy,[116,117] chemical vapor deposition, etching, oxidation and passivation[118] have been routinely used in silicone-based manufacturing development. These processes involve chemical or physical action at the surface of the semiconductor wafer. However, with the rapid miniaturization of devices, understanding of the atomic-level phenomena underlying these processes becomes more critical. This importance of atomic-level is highlighted in the growing field of organic functionalization of semiconductor surfaces.

Problems that have been addressed include the reaction of organic molecules with the surface, and the structure of the resulting adsorbed molecule. Most

of this work has focused on the Si(100)-2x1 surface. This surface undergoes a characteristic (2×1) reconstruction in which adjacent atoms pair, and the resulting silicon dimers make the surface particularly amenable to organic functionalization. The Si=Si double bonds of the Si(100) surface are much weaker than molecular Si=Si double bonds and C=C double bonds. These weak bonds make the surface reactive toward the adsorption of molecules because stronger bonds are formed, resulting in an energetically favorable process.[119] Detailed studies have been reported for a wide range of molecules, from small molecules such as butadiene[120–122] to much larger systems such as C_{60}.[123–125]

In comparison to Si(100)-2x1, the related Ge(100)-2x1 and C(100)-2x1 surfaces have received less attention. However, several studies have been reported, and much of this work has been reviewed elsewhere.[115,126,127] Hydrocarbons adsorbed on Ge(100)-2x1 reveal similar chemistry to the reactions on Si(100)-2x1, but the products are less strongly bound due to the weaker C−Ge bond.[128,129] The structure of acetylene on Si(100)-2x1 has been studied by a number of groups.[130–132] Recent work has used multireference wavefunctions with dynamic correlation.[133] This work found the most stable binding site to correspond to acetylene bonded to a single surface dimer, with an acetylene carbon-carbon bond length of 1.36 Å. A comprehensive investigation of benzene adsorbed on the Si(100)-2x1 surface has been reported, and showed the favoured binding site to correspond to a butterfly structure arising from a 4 + 2 addition.[134] DFT calculations have been used to study the adsorption of acetylene and benzene on the Ge(100)-2x1 surface.[135] These calculations were consistent with the observation that there is weaker binding

to the Ge(100)-2x1 surface. Theoretical studies have also investigated the adsorption of several small molecules, such as acetylene, the methyl radical and carbon dimer on diamond surfaces.[136–140]

Investigation of the IR spectrum of benzene deposited on Si(100)-2x1 at 100 K has been reported.[141] Strong IR absorption peaks were observed at 3086, 3067, 3036 and 3030 cm^{-1} which correspond to the vibrational features of molecular benzene, and the adsorption product was subsequently identified as physisorbed benzene. For benzene chemisorbed on the surface, the hybridization of the carbon directly bonded to the surface change from sp^2 to sp^3. At room temperature, benzene is chemisorbed on the surface and two peaks at 3044 and 2945 cm^{-1} are observed, and assigned to the C-H stretching of the sp^2 and sp^3 hybridized carbons, respectively. This was consistent with earlier work.[142] Another study showed several C-H stretching bands in the frequency range 2899-3042 cm^{-1}, and determined the dominant adsorption product to correspond to a 1,4-cyclohexadiene like structure.[143] More recently, the vibrational spectroscopy of benzene was re-examined. Three different chemisorbed phases were indentified, which corresponded to the 1,4-cyclohexadiene structure but bonded to a single Si-Si dimer or bridging between two dimers.[144] Measurement of the IR spectrum of ethylene on Ge(100)-2x1 showed the symmetric and antisymmetric C-H stretching modes occurring at 2913 and 2961 cm^{-1}, respectively.[129]

A number of theoretical calculations of the vibrational frequencies of organic molecules on the Si(100)-2x1 surface have been reported.[120,121,145–149] These calculations usually use DFT and adopt small cluster models of the surface,

however, larger surface clusters have been using in conjunction with semi-empirical calculations.[143] The vibrational frequencies of acetylene on the Si(100)-2x1 surface have been computed at the MCSCF + MRMP2 level of theory.[133] Recently, a partial Hessian approach was employed to compute the IR spectroscopy of a range of organic molecules, including acetylene and benzene , on Si(100)-2x1 using DFT.[150] The use of the partial Hessian methodology reduced the cost of the calculations and allowed larger cluster models of the surface to be used.

In a NEXAFS study of acetylene on the Si(100)-2x1 surface, Matsui and coworkers observed peaks at 284.7, 286.0 and 287.6 eV, which were assigned to excitations from the carbon 1s orbitals to π^*_{C-C}, σ^*_{Si-C} and σ^*_{C-H} orbitals, respectively.[151,152] Above threshold, a broad peak at 300 eV was observed and assigned to the σ^*_{C-C} orbital. In a later study Pietzsch *et al.* reported a fully polarization resolved NEXAFS investigation of acetylene on the surface.[153] Acetylene adsorbed on the surface showed four resonances at 283.8, 286.7, 288.4 and 299 eV, in broad agreement with earlier work. Interestingly, the π^*_{C-C} feature was evident in spectra with the incident radiation parallel or perpendicular to surface silicon dimers, indicating that two adsorption products are present. NEXAFS spectra of benzene adsorbed on Si(100)-2x1 have been reported by Kong *et al.*[141] At 100 K benzene is predominantly physisorbed to the surface and the resulting spectra have two peaks at 285.0 and 288.8 eV due to C(1s)$\rightarrow \pi^*(e_{2u})$ and C(1s)$\rightarrow \pi^*(b_{2g})$ transitions. In contrast, at room temperature chemisorption is favoured. The π^* excitation was found at 285 eV, with weaker bands at 287.7 and 289.5 eV arising from excitation to σ^*_{C-H} and σ^*_{Si-C} orbitals. In polarized NEXAFS measurements for benzene,

the π^* feature was evident at more than one polarization, indicating that benzene is no longer flat on adsorption.[154]

The application of NEXAFS to study Ge(100)-2x1 and C(100)-2x1 is much less common. Studies of sulphur atoms adsorbed on Ge(100)-2x1,[155] and hydrogenated C(100)-2x1 surface[156] have been reported, but the NEXAFS of acetylene or benzene on these surfaces has not been measured. Time dependent density functional theory (TDDFT) calculations of the NEXAFS of acetylene and benzene have also been reported.[99] This calculation used a small cluster model and an optimized HF exchange of hybrid functional to give accurate $1s \rightarrow \pi^*$ excitation energies . They found that the spectra of acetylene on the surface is dominated by intense $1s \rightarrow \pi^*$ bands with weaker bands at higher energies arising from excitation to Rydberg states. For benzene adsorbed on the surface, an intense π^* bands that arose from core orbitals localized on the carbons not bonded to the surface was observed. Here, we report the calculation of the IR and NEXAFS of acetylene and benzene on the semiconductor surfaces.

5.1 Computational Details

Experimental measurements of the IR spectroscopy of organic molecules adsorbed on semiconductor surfaces focus on the C-H stretching region, and this work was also concentrated on these vibrational modes. C_9H_{12}, Si_9H_{12} and Ge_9H_{12} clusters are used to model the surfaces and are shown in Figure 5.1. The harmonic frequency calculations using the full Hessian can be performed for molecules on the C(100)-2x1 and Si(100)-2x1 surfaces.[150] However,

for the Ge(100)-2x1 surface, the calculation of the vibrational frequencies becomes computationally expensive. Therefore, it is quite useful to adopt a partial Hessian framework to reduce the cost of these calculations, and for consistency this approach is used for all three surfaces. For the vibrational frequency calculations the B3LYP functional was used in conjunction with the 6-311G** basis set. The exception was for the Ge(100)-2x1 surface, where to reduce the cost of the calculation, the 6-31G* basis set was used for the atoms of the surface cluster not bonded to the adsorbant. The structures were fully optimized at the same level of theory prior to the frequency calculations, and the resulting vibrational frequencies are scaled by the standard factor of 0.96.[157]

For NEXAFS calculations, a mixed basis set comprising the 6-311++G* basis set for the atoms of the adsorbed molecule and the 6-311G* basis set for the atoms of the surface cluster was used for the same semiconductor clusters. Molecules are treated as binding to one surface dimer, with the 'butterfly' binding configuration considered for benzene. These binding configurations are often referred to as the 'di-σ' structures and have been shown to be the favored binding site for acetylene and benzene on Si(100)-2x1 and Ge(100)-2x1.[87,135] Structures were optimized at the B3LYP/6-31G* level of theory, and Figure 5.1 shows acetylene and benzene bound to the Si(100)-2x1 surface cluster. Spectra are generated by representing each computed core excitation and associated intensity with a Gaussian function with full width at half maximum of 0.3 eV. The optimized hybrid exchange-correlation function in equation 4.4 was used. All calculations were performed with a development version of the QCHEM software package.[79]

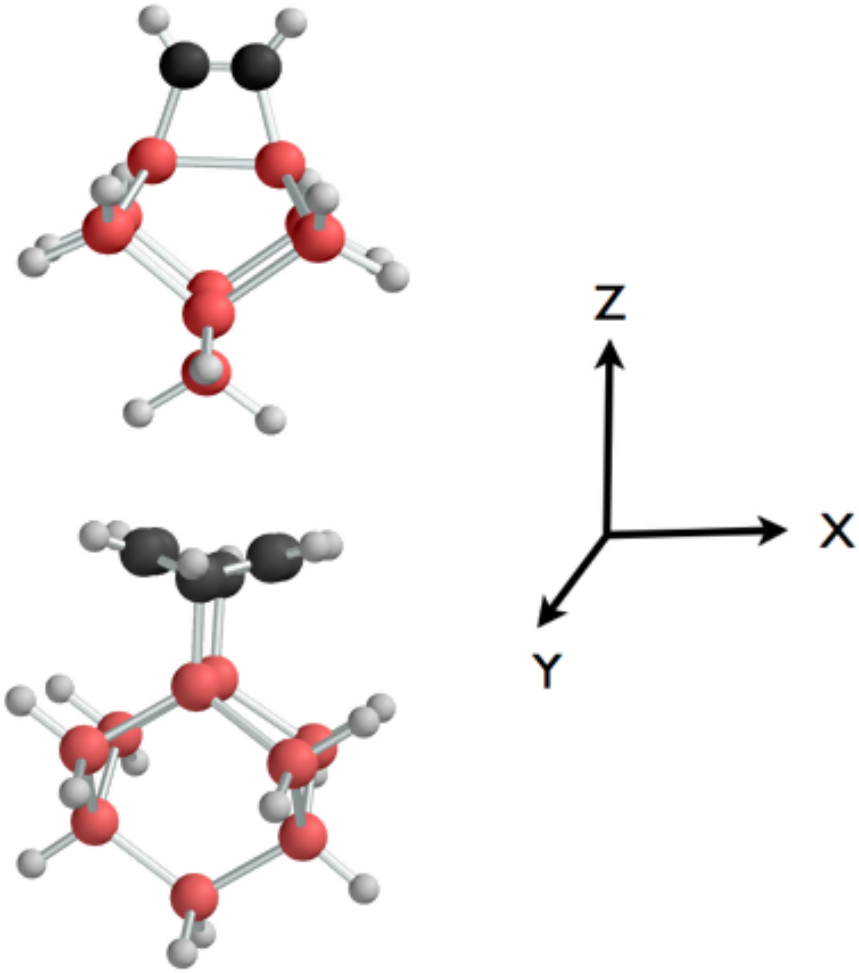

Figure 5.1: Models of acetylene and benzene adsorbed on Si(100)-2x1. Black and light-red colours represent carbon and silicon atoms, respectively.

5.2 Results and Discussion

5.2.1 Partial Hessian Harmonic Frequencies

Earlier work showed that the partial Hessian approximation introduced a very small error for the C-H stretching modes of organic molecules on the Si(100)-2x1 surface.[150] Since carbon is lighter than silicon, it is necessary to examine

this approximation for the adsorbants on the C(100)-2x1 surface. For acetylene on the C(100)-2x1 surface, a full Hessian calculation predicts the symmetric C-H and antisymmetric C-H stretching vibrations to have (unscaled) frequencies of 3183.7 cm^{-1} and 3152.3 cm^{-1} with associated intensities 49.0 km mol^{-1} and 18.4 km mol^{-1}, respectively. This compares with 3183.7 cm^{-1} and 3152.3 cm^{-1} with intensities 49.8 km mol^{-1} and 17.4 km mol^{-1} for the partial Hessian calculation. Thus, even for the C(100)-2x1 surface, the partial Hessian approximation introduces essentially no error for the computed frequencies and a very small change in the computed intensities. For the Si(100)-2x1 surface the unscaled vibrational frequencies for the symmetric C-H, antisymmetric C-H stretching and C-C stretching mode are 3128.6, 3105.6 and 1572.0 cm^{-1}. These can be compared to corresponding frequencies of 3324, 3302 and 1575 cm^{-1} computed at the MCSCF + MRMP2 level of theory.[133] This shows the C-H stretching frequencies to be significantly lower in the present calculations.

Table 5.1 shows the computed frequencies of the relevant vibrational modes. For acetylene, the C-H stretching region of the spectrum shows an intense band corresponding to the symmetric stretching mode and a weak band corresponding to the antisymmetric stretch. There is only a small difference of approximately 5 cm^{-1} between the computed frequencies on the Si(100)-2x1 and Ge(100)-2x1 surface, but for the C(100)-2x1 surface the predicted frequencies are significantly higher. This is consistent with experimental measurements of C-H stretching modes of butadiene, which found a difference of less that 15 cm^{-1} between Si(100)-2x1 and Ge(100)-2x1 surfaces.[128] Another mode of interest is the C-C stretch, the computed frequencies increase in

the order Si(100)-2x1<Ge(100)-2x1<C(100)-2x1. This is consistent with the analysis of the NEXAFS spectra (see later), and indicates that the C-C bond is strongest on the C(100)-2x1 surface, and weakest on Si(100)-2x1. The IR

Table 5.1: Computed vibrational frequencies (in cm^{-1}) and intensities in parenthesis (in km mol^{-1}) for the C-H stretching modes. Calculated frequencies have been scaled by 0.96. Experimental results from reference[141]
.

Mode	C(100)-2x1	Si(100)-2x1	Ge(100)-2x1	Exp. (Si(100)-2x1)
Acetylene				
Symmetric C-H	3056.3 (49.8)	3003.5 (65.4)	3009.8 (62.3)	
Antisymmetric C-H	3026.2 (17.4)	2981.4 (6.1)	2985.3 (3.5)	
C-C stretch	1606.6 (2.8)	1509.1 (0.5)	1520.8 (5.2)	
Benzene				
C-H stretch (sp^2)	3069.0 (16.2)	3065.1 (13.7)	3062.2 (16.3)	3044
C-H stretch (sp^2)	3066.3 (20.6)	3062.7 (16.2)	3059.6 (18.1)	
C-H stretch (sp^2)	3045.4 (14.4)	3044.0 (3.9)	3041.7 (5.2)	
C-H stretch (sp^2)	3044.0 (0.0)	3042.8 (0.0)	3040.2 (0.0)	
C-H stretch (sp^3)	2957.7 (0.6)	2971.9 (6.3)	2993.4 (7.4)	2945
C-H stretch (sp^3)	2958.0 (62.3)	2970.8 (11.1)	2992.1 (9.1)	

spectra of benzene adsorbed on the surface shows two C-H stretching bands arising from the sp^2 hybridized carbon atoms not bonded to the surface and sp^3 carbon atoms bonded directly to the surface. The vibrational frequencies for the C-H stretching modes of the sp^3 carbon atoms are computed to lie at approximately 2971 cm^{-1} compared to an experimental value of 2945 cm^{-1}.[141] For the sp^2 carbon atoms, the C-H stretching band is predicted to lie at approximately 3063 cm^{-1}, compared to an experimental value of 3044 cm^{-1}.[141] Both of the predicted frequencies are in good agreement with the experiment. For the sp^3 carbons that are bonded directly to the surface, the predicted frequencies increase in the order C(100)-2x1<Si(100)-2x1<Ge(100)-2x1. The

magnitude of the difference in frequencies between Si(100)-2x1 and Ge(100)-2x1 is approximately 20 cm^{-1}, which is a little greater than the 15 cm^{-1} observed for butadiene. The calculations indicate a decrease in frequency for the C(100)-2x1 surface compared with the Si(100)-2x1 surface, which contrasts with acetylene for which an increase in the C-H stretching frequencies is predicted.

5.2.2 NEXAFS Spectroscopy

Figure 5.2 shows the computed x,y and z-polarized NEXAFS spectra for acetylene adsorbed on the surfaces. The computed spectrum for acetylene on Si(100)-2x1 is similar to previous work,[99] although a different basis set is used here. The spectrum is dominated by an intense transition that appears with y polarization. This corresponds to excitation to the π^*_{C-C} orbital, which is shown in Figure 5.3. At higher energy, weaker bands are evident in the x and z polarized spectra. These correspond to excitation to σ^*_{Si-C} and σ^*_{C-H} orbitals, these orbitals are also shown in Figure 5.3. This is consistent with experiment, the π^*_{C-C}, σ^*_{Si-C} and σ^*_{C-H} bands are observed at 284.7, 286.0 and 287.6 eV, respectively,[151,152] which compare well with the computed values of 283.8, 286.7 and 288.2 eV, and indicates that the modified hybrid exchange-correlation functional used provides a good description of these excitations.

The predicted spectra for acetylene on the C(100)-2x1 and Ge(100)-2x1 surfaces appear similar, although there is variation in the position of the spectral bands. Table 5.2 summarizes the computed excitation energies on the three surfaces. The C(1s)$\rightarrow \pi^*_{C-C}$ excitation energy is dependent on the surface, and increases in the order Si(100)-2x1 < Ge(100)-2x1 < C(100)-2x1. This or-

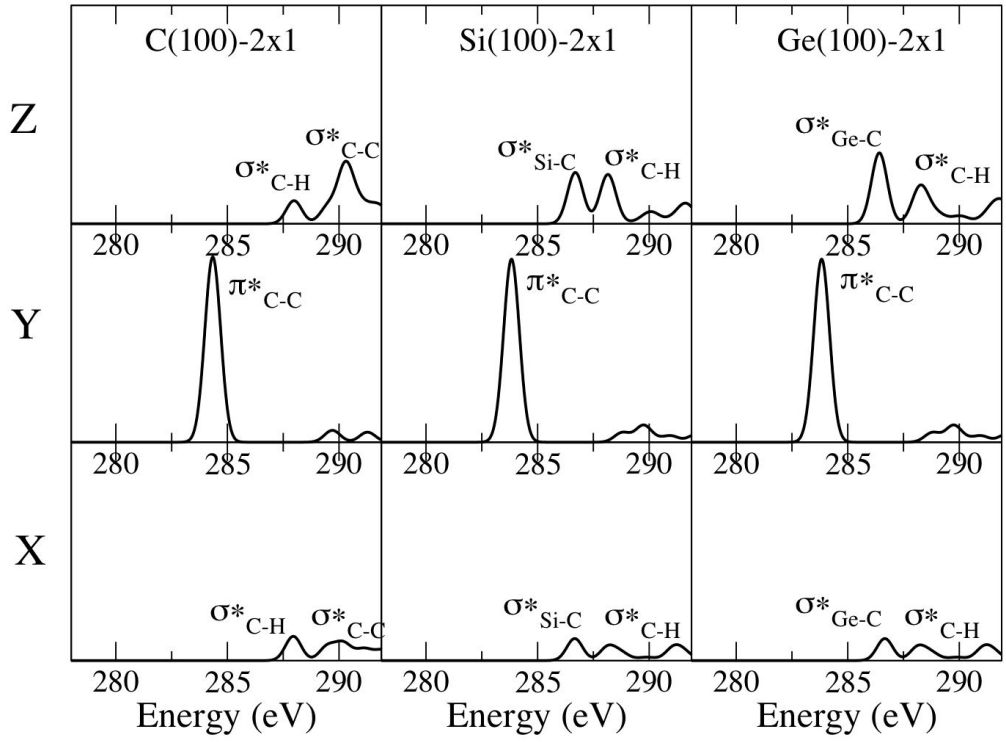

Figure 5.2: Computed $BH^{0.57}LYP$ x,y and z-polarized spectra for acetylene adsorbed on C(100)-2x1, Si(100)-2x1 and Ge(100)-2x1.

dering can be rationalized by the C-C bond length of the adsorbed acetylene molecule. This bond length is shortest on the C(100)-2x1 surface and longest on the Si(100)-2x1 surface. Shortening of the C-C bond length will lead to a destabilization of the π^*_{C-C} orbital, and result in an increase in the associated core excitation energy. There is little change in the computed excitation energy for the C(1s)$\rightarrow \sigma^*_{C-H}$ excitation. This is reasonable since the σ^*_{C-H} orbital is located on the carbon and hydrogen of the acetylene molecule, and has little interaction with the surface. The σ^*_{X-C} (where X denotes C, Si or Ge)

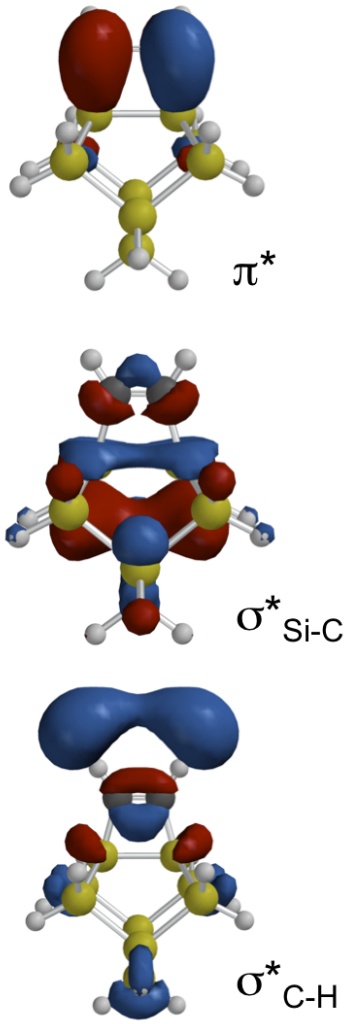

Figure 5.3: Virtual orbitals of acetylene adsorbed on Si(100)-2x1.

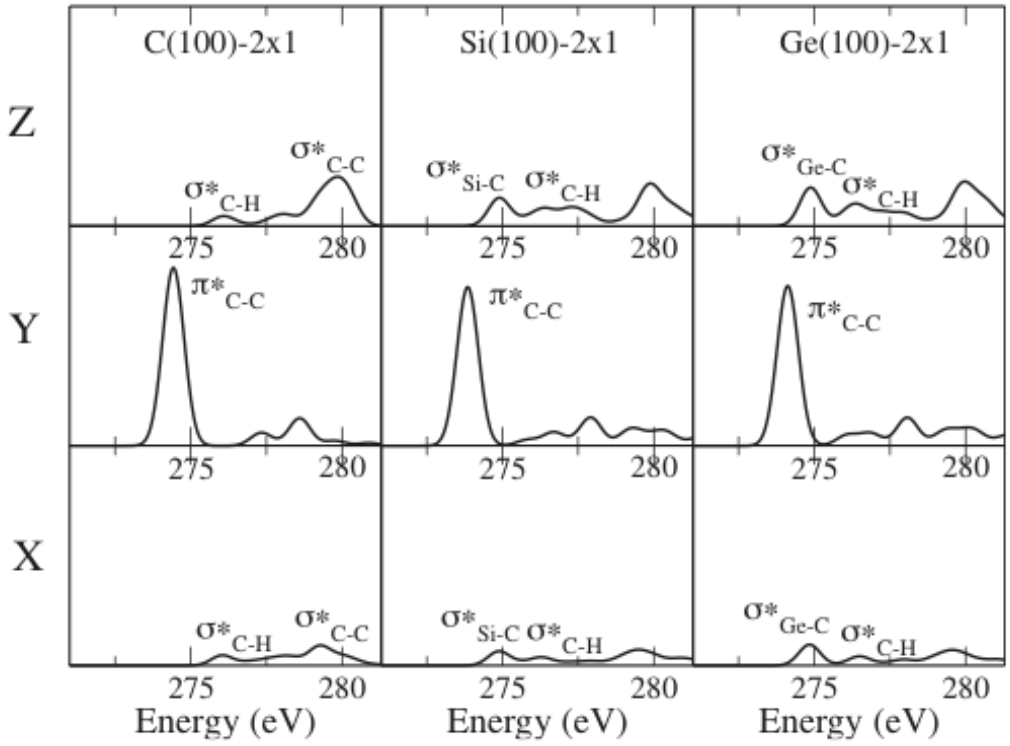

Figure 5.4: Computed B3LYP x,y and z-polarized spectra for acetylene adsorbed on C(100)-2x1, Si(100)-2x1 and Ge(100)-2x1.

orbital has a large contribution from the surface, and the associated excitation is the most sensitive to the surface. The excitation energy is much higher for the C(100)-2x1 surface, and results in a change in the order of the $\sigma^*_{\mathrm{C-H}}$ and $\sigma^*_{\mathrm{X-C}}$ bands. This is likely to be a consequence of the greater strength of the adsorbate-surface C-C bonds compared to Si-C and Ge-C bonds.

It is interesting to compare the spectra computed with the $\mathrm{BH}^{0.57}$LYP functional with the more standard B3LYP functional. Figure 5.4 shows NEXAFS spectra for acetylene on the three surfaces computed with the B3LYP functional and the computed excitation energies for the π^*_{C-C}, σ^*_{C-H} and σ^*_{X-C} excitations are shown in Table 5.2. It is well known that the B3LYP functional

underestimates core excitation energies for carbon 1s excitations by about 10 eV, and this is observed for the excitations considered here. However, figure

Table 5.2: Computed excitation energies and C-C bond lengths of acetylene adsorbed on the surfaces. Experimental results for the Si(100)-2x1 surface.[151,152]

Surface	π^*_{C-C} (eV)	σ^*_{C-H} (eV)	σ^*_{X-C} (eV)	r_{C-C} (Å)
$BH^{0.57}LYP$				
C(100)-2x1	284.3	288.0	289.5	1.340
Si(100)-2x1	283.8	288.2	286.7	1.352
Ge(100)-2x1	284.1	288.1	286.4	1.344
B3LYP				
C(100)-2x1	274.4	276.1	279.3	1.340
Si(100)-2x1	273.8	276.5	274.9	1.352
Ge(100)-2x1	274.1	276.4	274.9	1.344
Experiment	284.7	287.6	286.0	

5.5 shows the computed spectra for benzene adsorbed on the three surfaces. Several bands are observed in the spectra, which correspond to excitation to π^*, σ^*_{C-H} and σ^*_{X-C} orbitals. These orbitals are shown for the Si(100)-2x1 surface in Figure 5.6. For the Si(100)-2x1 surface excitation to the π^* orbitals results in an intense band in the z-polarised spectrum. A weaker π^* band is also observed in the y-polarized spectrum indicating that benzene is no longer planar on adsorption. The π^* band is computed to lie at 284.6 eV, which agrees well with the value of 284.8 eV measured in experiment.[154] An additional feature at 286.9 eV was also observed in experiment. The calculations show two further bands at higher energies corresponding to excitation to σ^*_{Si-C} and σ^*_{C-H} orbitals, and are computed to lie at 286.8 eV and 287.9 eV. Based on these results, the additional band observed in experiment corresponds to the σ^*_{Si-C} excitation, although this does not agree with assignments

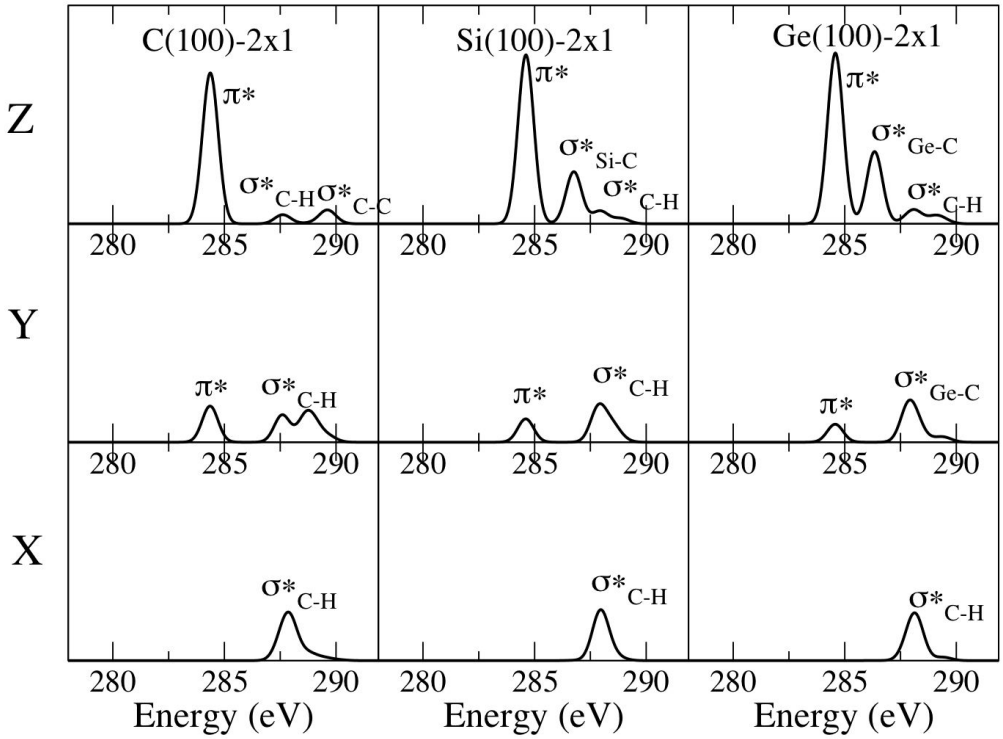

Figure 5.5: Computed BH$^{0.57}$LYP x,y and z-polarized spectra for benzene adsorbed on C(100)-2x1, Si(100)-2x1 and Ge(100)-2x1.

made in earlier experimental work,[141] where it was assigned as to additional π^* excitation. The excitation energies for benzene on the three surfaces are summarized in Table 5.3. Unlike acetylene, the π^* excitation energies do not show a dependence on the surface. This is physically intuitive since the π^* orbitals are associated with the sp^2 carbons that are not bonded directly to the surface, and as a result will not be affected by the change of surface to the same extent. The $\sigma^*_{\mathrm{C-H}}$ and $\sigma^*_{\mathrm{X-C}}$ excitations show a similar behaviour to that observed for acetylene. The $\sigma^*_{\mathrm{C-H}}$ excitation is localized on the benzene

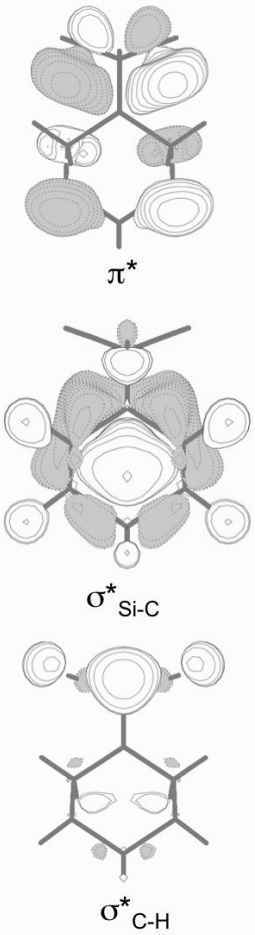

Figure 5.6: Virtual orbitals of benzene adsorbed on Si(100)-2x1.

molecule, and the corresponding excitation energy does not vary significantly between the three surfaces. The $\sigma^*_{\mathrm{X-C}}$ excitation is significantly higher for the C(100)-2x1 surface, and results in a change in the order of the $\sigma^*_{\mathrm{C-H}}$ and $\sigma^*_{\mathrm{X-C}}$ bands.

Table 5.3: Computed excitation energies of benzene adsorbed on the surfaces.

Surface	π^*_{C-C} (eV)	σ^*_{C-H} (eV)	σ^*_{X-C} (eV)
C(100)-2x1	284.4	287.6	289.6
Si(100)-2x1	284.6	287.9	286.8
Ge(100)-2x1	284.6	287.8	286.3

5.3 Conclusions

DFT calculations of the NEXAFS and IR spectroscopy of acetylene and benzene have been described. Within TDDFT, core-excitation energies computed with a modified hybrid exchange-correlation functional with an increased fraction of HF exchange are in good agreement with values measured in experiment. Although it should be noted that this functional has been optimized for carbon 1s excitations, and a different fraction of HF exchange would be optimal for other types of core excitation. For acetylene, the π^* excitation energy is dependent on the nature of the underlying surface, and correlates with the length of the C-C bond length of the adsorbed molecule, with a shorter bond leading to a higher excitation energy. For benzene, π^* orbitals are associated with carbon atoms that are not bonded directly to the surface, and no significant variation of the excitation energy between the surfaces is predicted. Weaker features at higher energy arising for σ^*_{C-H} and σ^*_{X-C} excitations are also predicted. These bands show a similar behaviour for acetylene and benzene. The σ^*_{C-H} band shows little dependence on the surface, while the σ^*_{X-C} band is much higher for the C(100)-2x1 surface than both Si(100)-2x1 and Ge(100)-2x1 surfaces, reflecting the greater strength of the adsorbate-surface bond.

Calculations of the IR spectra using partial Hessian approach show the C-H stretching frequencies for carbon atoms bonded directly to the surface have significant variation between the three surfaces. The frequencies are predicted to be 4 to 20 cm^{-1} higher on the Ge(100)-2x1 surface compared to the Si(100)-2x1 surface. For acetylene, an increase in frequency is predicted, while for benzene a decrease in frequency is predicted for the C(100)-2x1 surface compared to the Si(100)-2x1 surface. Overall, DFT calculations can provide an accurate description of the NEXAFS and IR spectra of these systems, and can be a useful tool to aid the interpretation of experiment.

Chapter 6

NEXAFS Calculations of Benzene in Gas Phase and on Metallic Surfaces

---

The adsorption of benzene on metal surfaces is a prototypical problem in surface science that has been studied extensively, and NEXAFS spectra have been reported for benzene adsorbed on several metal surfaces.[158–162] The NEXAFS spectroscopy of benzene is dominated by an intense π^* resonance. From measurements with the polarization of the incident radiation orthogonal and parallel to the surface, it has been established that benzene lies parallel to the surface. However, the measured spectra vary between different surfaces. For example, the NEXAFS spectra of benzene adsorbed on Pt(111) and Au(111) differ significantly, reflecting the different natures of the bonding to the surface.[161,162]

Benzene is physisorbed on the Au(111) surface, and the spectrum for benzene adsorbed on Au(111) is similar to the spectrum for a benzene multilayer. The π^* resonance occurs at 285.1 eV and is intense at grazing photon incidence and absent at normal photon incidence. A second weaker band at 289.3 eV is

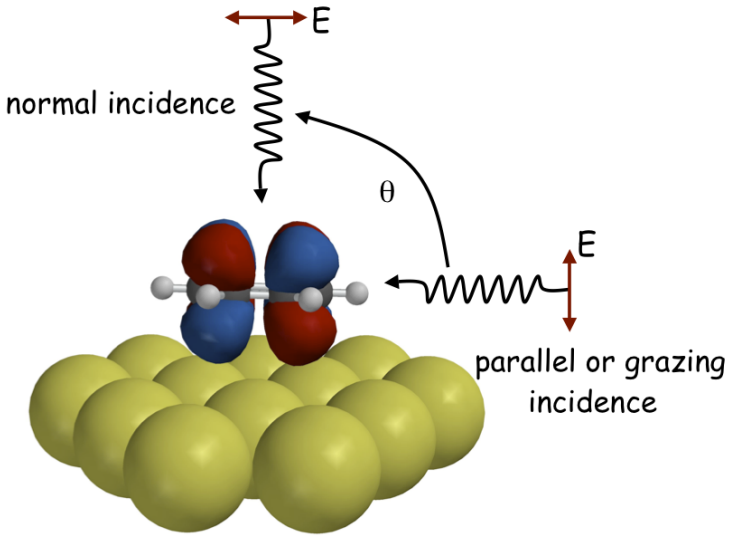

Figure 6.1: Variation in the angle of incident radiation.

also evident. At normal photon incidence, as shown in Figure 6.1, weak features at 287 eV can be distinguished. Benzene is chemisorbed on the Pt(111) surface, and the resulting spectrum shows a broad, less intense feature with two distinct peaks. This change has been attributed to the hybridization of the π^* orbitals with the metal electronic states.[161] The variation in intensity of this feature with the photon angle of incidence indicated a bending of the C-H bonds out of the plane of the benzene ring. For normal photon incidence, a weak broad feature centred at approximately 287 eV can be distinguished. In a study of *n*-octane, it was shown that resonances arising from excitation to Rydberg states were strongly quenched and there is significant hybridization of molecular valence states with the metal bands.[96] In this chapter, we investigate the calculation of the NEXAFS spectra of benzene in the gas phase and adsorbed on Au(111) and Pt(111) surfaces with TDDFT.

6.1 Computational Details

In this study, two types of small surface cluster of metal atoms, comprising one and three layers, were modeled. The simple one layer cluster has 12 atoms, and the three layer cluster has 22 atoms. While relatively small, the calculation of NEXAFS spectra for molecules adsorbed on the 22 atom cluster is computationally demanding because of the very large number of excited states required. However, earlier work has shown that NEXAFS spectra are less sensitive to cluster size than other properties such as binding energy.[163] Bilic *et al.*[164] have reported a detailed study of the adsorption of benzene on a range of metal surfaces, including Au(111). For the calculations presented here, the most stable structure predicted for benzene on Au(111) by Bilic *et al.* corresponding to benzene in a threefold hollow site is used. When physisorbed on Au(111), benzene retains its planar structure. On Pt(111), benzene can occupy a three-fold hollow or bridge. Structures for benzene in both threefold and bridge sites were adapted from the work of Morin *et al.*[165] For both binding sites, the surface atoms are fixed in position and benzene is strongly chemisorbed to the surface with six metal-carbon bonds formed. In both threefold hollow and bridges sites the hydrogens are distorted upwards from the plane of the carbon ring. For the threefold site, the adsorbed benzene retains its sixfold rotational symmetry. For the bridge site, the hydrogens bonded to the "end" carbons are distorted upwards to a greater extent than the other hydrogen atoms, and the sixfold rotational symmetry is lost. All of these structures are illustrated in Figure 6.2.

All calculations were performed with the Q-Chem software package,[79] except

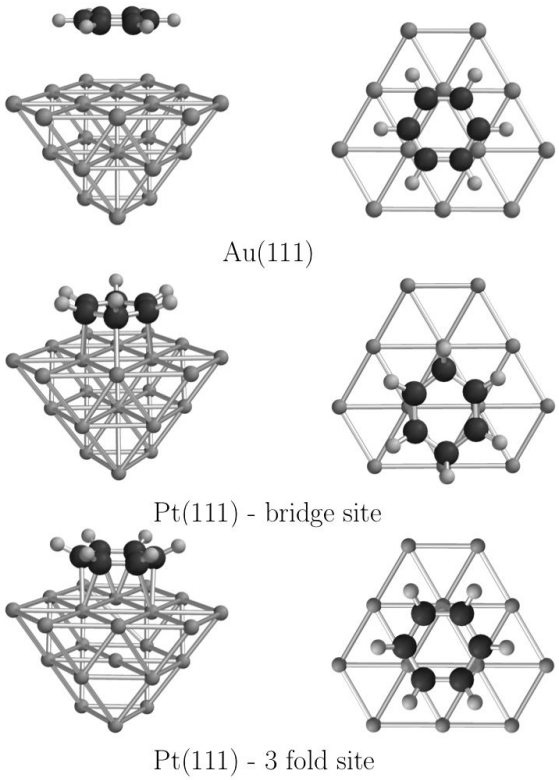

Figure 6.2: Cluster models of benzene adsorbed on Au(111) and Pt(111) surfaces.

the calculations with the CS00 functional,[54,166] which used the NWChem software.[167] The 6-311G* basis set was used for benzene, which was augmented with a set of Rydberg basis functions[168] placed at the centre of the ring for some calculations. For the NEXAFS calculations of adsorbed benzene, the LANL2DZ basis set[169,170] was used for the gold and platinum atoms. Theoretical spectra are generated by representing the computed excitation energy and intensity of each electronic transition by a Gaussian function, a full width at half maximum of 0.4 eV was used for the spectra of gas phase benzene. Spectra for benzene adsorbed on the surfaces used a full width at half maximum of 1 eV.

6.2 Results and Discussions

6.2.1 Benzene - gas phase

Before considering benzene, the effect of restricting the excitation space to include only excitations from core orbitals is examined. Table 6.1 shows the effect of introducing this restriction compared to the full excitation space for the 10 lowest core excited states for a range of molecules at the B3LYP/6-31+G* level of theory. The results show that this restriction introduces a very small error in the computed excitation energies and oscillator strengths. The average error is very small and is negligible relative to other errors inherent in the calculations. The largest error observed is for excitation from the 2s orbital of phosphorous in PH_3. In general, larger errors are observed for excitations from core 2s orbitals compared to the corresponding core 1s orbitals. This is expected since there is likely to be more mixing between excitations

from this orbital and those from other occupied orbitals. However, even the largest errors are relatively small. For benzene the excitations from the carbon 1s orbitals do not appear in the lowest 1000 roots. Therefore it is difficult to assess directly the effect of restricting the excitation space, however, it would be expected that a similarly small error would be observed. Thus, imposing the restriction of only including excitations from the relevant core orbitals represents a practical and efficient method for computing NEXAFS spectra that can be incorporated easily into standard TDDFT codes.

In the experiment four prominent bands are observed below the ionization threshold.[171] These are referred to as A, B, C and D, and occur at 285.2, 287.2, 287.9 and 289.2 eV, respectively in Figure 6.3. Peak A is the most intense peak and is assigned to excitation to e_{2u} orbitals, which correspond to the lowest π^* orbitals. However, there is less consensus in the literature over the assignment of the remaining peaks. Peak B has been assigned to Rydberg 3s[171] or σ^* orbitals.[172,173] Similarly, peak C has been assigned to Rydberg 3p or 3d[171,174] or σ^* orbitals.[172,173] Furthermore, peak D has been assigned to $b_{2g}(\pi^*)$ or Rydberg 3d, 4s or 4p excitations.[171–174] That said, most authors acknowledge these orbitals are of mixed character, and the assignment of the nature of these excitations will depend on the details of the calculation and on the precise definition of a Rydberg orbital adhered to.

TDDFT spectra computed with a range of basis sets and exchange-correlation functionals are shown in Figure 6.3. The experimental spectrum adapted from reference[171] is also shown. It has been observed previously that core-excitation energies computed with TDDFT with conventional functionals are

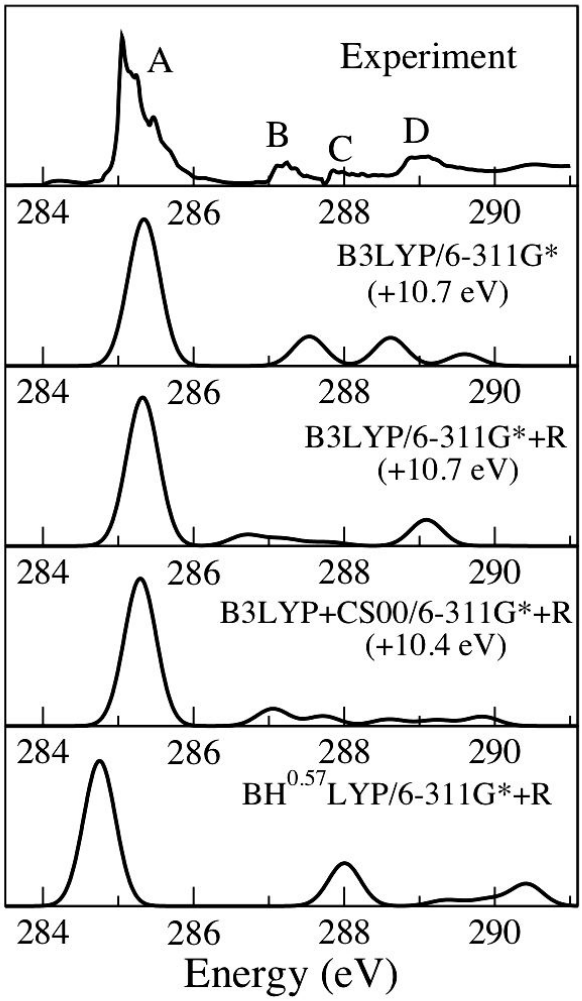

Figure 6.3: Experimental and computed NEXAFS spectra of benzene in the gas-phase. Experimental spectrum adapted from reference.[171]

Table 6.1: The largest and average error in the excitation energies in eV and oscillator strengths (in parenthesis) of the 10 lowest core excited states resulting from the truncation of the single excitation space.

Molecule	Largest Error	Average Error
N_2	0.01 (0.013)	0.00 (0.003)
$\underline{C}_2H_2$	0.01 (0.009)	0.00 (0.002)
$\underline{C}_2H_4$	0.02 (0.011)	0.01 (0.002)
$H_2\underline{C}O$	0.01 (0.009)	0.00 (0.002)
$H_2C\underline{O}$	0.01 (0.004)	0.00 (0.001)
H$\underline{\text{Cl}}$ - 1s	0.00 (0.000)	0.00 (0.000)
H$\underline{\text{Cl}}$ - 2s	0.05 (0.004)	0.01 (0.004)
$\underline{\text{Si}}H_4$ - 1s	0.00 (0.000)	0.00 (0.000)
$\underline{\text{Si}}H_4$ - 2s	0.04 (0.001)	0.01 (0.000)
$\underline{\text{P}}H_3$ - 1s	0.01 (0.000)	0.01 (0.000)
$\underline{\text{P}}H_3$ - 2s	0.07 (0.001)	0.02 (0.000)

too low.[104,106] For the B3LYP/6-311G* calculation, all excitation energies have been shifted by +10.7 eV to match experiment. The shifted spectrum is in good agreement with experiment, with an intense π^* band with three weaker bands predicted at higher energies. The 6-311G* basis set does not contain diffuse basis functions , and is not designed for describing Rydberg states. Inclusion of a set of *s,p* and *d* Rydberg basis functions located at the centre of the benzene ring, denoted 6-311G*+R, does not affect the intense π^* band. However, the energies and intensities of the weaker bands are changed significantly, indicating some Rydberg character of these bands. For the B3LYP/6-311G*+R calculation, three weaker bands occur at 286.7, 287.2 and 289.1 eV (shifted by +10.7 eV). Orbitals derived from the B3LYP/6-311G*+R calculation are shown in Figure 6.4. The intense band at 285.3 eV (shifted by +10.7 eV) corresponds to excitation to the e_{2u} orbitals, which are clearly π^* orbitals. The next band in the spectrum is much weaker and arises

from an excitation to the a_{1g} orbital and corresponds to peak B. Previous work has assigned this orbital as 3s,[171] σ(C−C) bonding with antibonding C−H character[172] and σ^*(C−C).[173] Overall, we find this orbital is most appropriately labelled a 3s orbital. The orbital has the correct symmetry and Figure 6.4 shows that it looks like a 3s orbital, although it is perhaps not as diffuse as one might expect for a Rydberg orbital. The 3s orbital has two spherical nodal surfaces (not shown in Figure 6.4). One of these surfaces does occur between the carbon and hydrogen atoms, which would reflect σ^*(C−H) character. However, there is no σ^*(C−C) character since there is no node between the carbon atoms. Peak C is weaker than peak B, and is calculated to arise from excitations to the e_{1u} orbitals. These orbitals are also shown in Figure 6.4, and are best described as the in-plane Rydberg 3p orbitals. Again the orbitals also have a nodal surface along the C−H bonds, which reflects some σ^*(C−H) character. Above peak C a weak band arising from excitation to e_{2g} orbitals and a more intense band corresponding to excitation to an a_{2u} orbital. The e_{2g} orbitals are best described as Rydberg 3d orbitals, while the transition to the a_{2u} orbital corresponds to peak D and is best described as an out-of-plane Rydberg p orbital. Previous work has assigned peak D to the $b_{2g}(\pi^*)$ orbital. However, in our calculations this orbital is found at a significantly higher energy. For the B3LYP/6-311G*+R calculation, the weak (Rydberg) bands are too low in energy with respect to the π^* band. It is well known for valence excited states that functionals such as B3LYP underestimate the excitation energies of Rydberg states. This can be corrected by the use of the CS00 asymptotically corrected (AC) functional.[166] The NEXAFS spectrum computed with B3LYP with an asymptotic correction is also shown

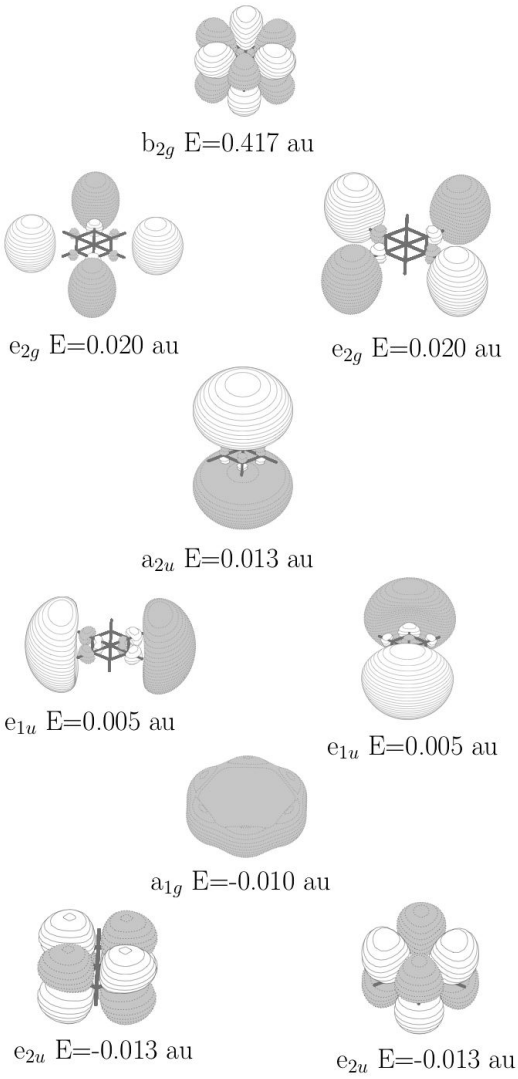

Figure 6.4: Virtual orbitals of benzene in the gas-phase with the computed orbital energies (in a.u.).

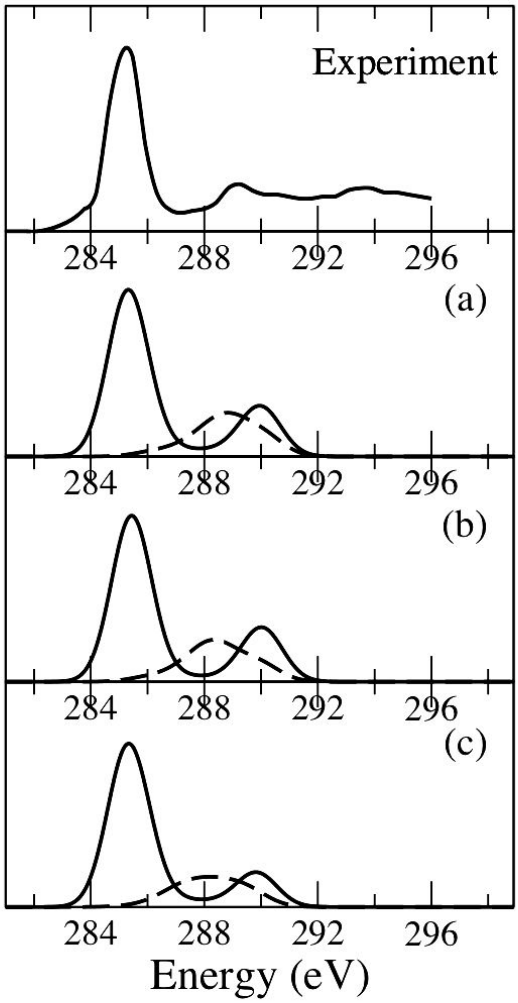

Figure 6.5: Experimental and computed NEXAFS spectra of benzene adsorbed on Au(111)
(a) B3LYP/6-311G*+R calculation with a one-layer surface cluster. (b) B3LYP/6-311G*calculation with a one-layer surface cluster. (c) B3LYP/6-311G*calculation with a three-layer surface cluster. Solid lines: grazing photon incidence, broken lines: normal photon incidence. All calculated spectra have been shifted by +10.7 eV. Experimental spectrum for grazing photon incidence adapted from reference.[161]

in Figure 6.3. The AC functional does not correct the large underestimation of the excitation energies, but does shift the Rydberg bands to higher energies relative to the π^* band. Once shifted by +10.4 eV, the resultant spectrum is in reasonable agreement with experiment. The peaks at B, C and D are computed to lie at 287.1, 287.7 and 288.6 eV, respectively. This compares to experimental values of 287.2, 287.9 and 288.9 eV. The largest deviation from experiment is the intensity of band D is underestimated.

The origin of the error that results in the large underestimation of the computed core excitation energies is analogous to the error observed for charge transfer states, and is not corrected by a AC functional. This error has been discussed extensively in the literature, and has been termed the electron transfer self-interaction error[175] and arises when there is little spatial overlap between the occupied and virtual orbitals involved in the excitation. Since core orbitals are compact and localized on the nuclei, there is little overlap between these orbitals and typical valence orbitals, such as π^*. Consistent with this analysis, greater accuracy can be achieved by increasing the proportion of Hartree-Fock exchange in the functional. A spectrum was computed with the $BH^{0.57}LYP$ functional.[99] This functional was developed to reproduce the 1s$\rightarrow$ π^* excitations in acetylene , ethylene and benzene . The calculation predicts the π^* band to lie at 284.7 eV, which is in good agreement with experiment and it is no longer necessary to shift the spectrum. However, the weaker bands at higher energy are not described less well by this functional, and are predicted to lie at energies that are too high relative to the π^* band.

6.2.2 Benzene on Au(111) and Pt(111)

Figure 6.5 shows experimental and computed spectra for benzene adsorbed on the Au(111) surface. The experimental spectrum for incident radiation parallel to the surface shows an intense peak at 285.3 eV with a weaker band at 289.2 eV. For this system, the lowest lying virtual orbitals correspond to the orbitals of the metal cluster. To reduce the cost of the calculation, the excitation space is reduced further, and excitation to the lowest ten virtual orbitals are excluded. This has a negligible effect on the position and intensity of the lowest π^* band. In order to aid comparison with experiment, the computed spectra are shifted by +10.7 eV, the value derived from the gas phase calculations. Computed spectra are shown for incident radiation parallel and perpendicular to the surface.

All calculations use the B3LYP exchange-correlation functional and the LANL2DZ basis set for the gold atoms. The 6-311G*+R basis set for benzene in conjunction with the one layer surface calculation, predicts an intense band arising from excitations to the $e_{2u}(\pi^*)$ orbitals of benzene at 285.4 eV (when shifted by +10.7 eV) with a weaker band arising from excitation to the $b_{2g}(\pi^*)$ orbitals of benzene at 290 eV. The relative positions and intensities of these bands are in good agreement with experiment. In comparison with the spectra of benzene in the gas phase there is no evidence of excitation to Rydberg states in the spectrum for grazing photon incidence. The absence of Rydberg states in the spectrum is likely to be a result of the presence of the surface, resulting in the Rydberg states being destabilized relative to the valence states as, observed for molecules in solution.[176,177] Removing the Rydberg basis functions from

the basis set and using the larger cluster surface model has little effect on the computed spectra, although there is a little reduction in the intensity of the $b_{2g}(\pi^*)$ band. For incident radiation normal to the surface, the calculations predict a weak band at about 288.5 eV. For the three layer cluster, this band occurs at a slight lower energy of 285.1 eV. In the experiment, there is some evidence for a weak feature in this region for normal incidence. In terms of gas phase benzene, this band arises from excitation to the a_{1g} orbital, which is best described as the Rydberg 3s orbital, although it does have some σ^*_{C-H} character. The relative compactness of this Rydberg state results in its continued presence in the NEXAFS region on adsorption. Figure 6.6 shows the experimental and calculated spectra for benzene adsorbed on the Pt(111) surface. Spectra have been calculated for both bridge and 3-fold binding sites. All calculations use the B3LYP exchange-correlation functional in conjunction with the 6-311G* basis set for benzene and LANL2DZ basis set for the platinum atoms. For grazing photon incidence, the calculations predict a broad band centered at 285.8 eV (shifted by +10.7 eV). For the one-layer surface cluster, two distinct peaks can be distinguished in this band. A further band at higher energy is also evident in the computed spectra. Overall, the predicted spectra between the bridge and 3-fold sites are similar. Some small differences are predicted, in particular, the higher energy band occurs at a slightly higher energy for the 3-fold site. The broad band arises from excitation to a number of low lying virtual orbitals, the predominant contributions involve excitation to the orbitals shown in Figure 6.7. The orbitals are clearly mixed between the benzene and surface, consistent with previous work on this system.[161] For ethene chemisorbed on Pt(111), the features observed in the

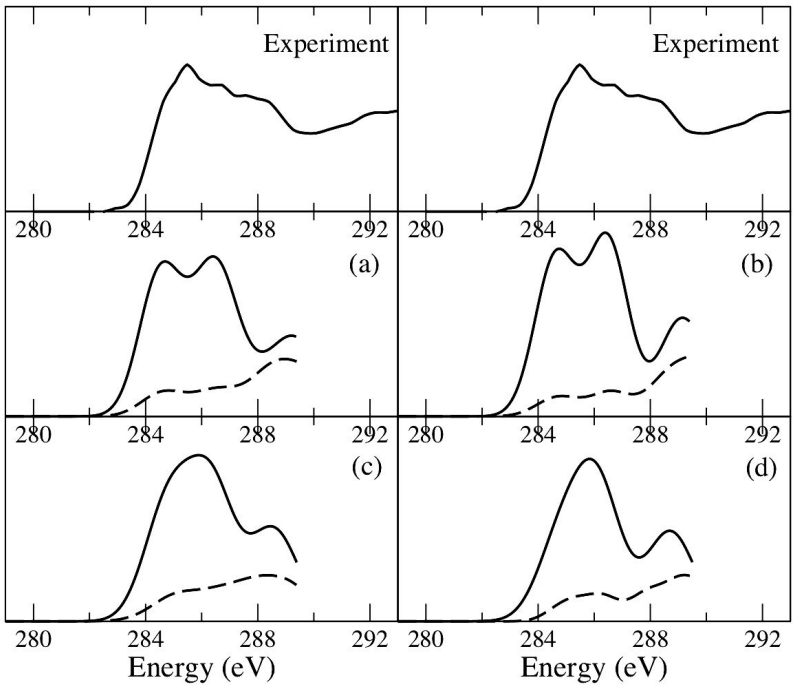

Figure 6.6: Experimental and computed NEXAFS spectra of benzene adsorbed on Pt(111) .
(a) bridge site on a one-layer surface cluster. (b) 3-fold site on a one-layer surface cluster (c) bridge site on a three-layer surface cluster. (d) 3-fold site on a three-layer surface cluster. Solid lines: grazing photon incidence, broken lines: normal photon incidence. All calculated spectra have been shifted by +10.7 eV.Experimental spectrum for grazing photon incidence adapted from reference.[161]

NEXAFS spectra and underlying molecular orbitals have been discussed in detail.[90] Surprisingly, it was found that despite being bonded to the surface, the π^* orbital retained its identity. The resulting orbital was described as an antibonding combination of the ethene π^* orbital and the Pt d orbitals. Providing definitive labels for these orbitals is difficult, but chemically $\sigma^*_{\mathrm{Pt-C}}$ orbitals would be expected. The orbitals would lie along the Pt-C bonds and should be observed for grazing photon incidence. The upper orbital in Figure 6.7 is consistent with this. However, in terms of the benzene molecule, the lower two orbitals do have π^* character. So similar to ethene, some π^* orbital characters is retained. At normal photon incidence, experiment predicts a weak feature at 286.5 eV.[161] All the computed spectra show a weak feature at this energy. Overall, the agreement with experiment is not as good as for benzene on the Au(111) surface. This reflects the much more complex bonding to the surface that occurs on the Pt(111) surface. However, the general features of the experimental spectrum are reproduced.

6.3 Conclusions

The adsorption of benzene on metal surfaces is a prototypical problem in surface science, and high quality NEXAFS spectra have been reported in the literature.[161] Consequently, it provides a useful system to assess the performance of TDDFT for the calculation of NEXAFS spectra of molecules adsorbed on metal surfaces. For gas phase benzene, the excitation energies computed with TDDFT with hybrid functionals are too low compared to experiment. However, applying a constant shift to all excitation energies results in spectra that are in good agreement with experiment. The source of this discrepancy is not

corrected by the use of an asymptotically corrected functional and is associated with the approximate local exchange in the hybrid functional. The use of a functional that has an increased fraction of Hartree-Fock exchange, results in a spectrum for which the application of a shift is not required, however, the agreement for the higher lying Rydberg bands is less good.

The NEXAFS spectra of benzene adsorbed on the Au(111) and Pt(111) surfaces has been computed with cluster models of the surface. For benzene adsorbed on the Au(111) surface, the computed spectra are in good agreement with experiment. For grazing photon incidence, the spectrum show two bands that arise from excitation to the π^* orbitals of benzene and an absence of Rydberg bands. For normal photon incidence, a weaker band at 285.8 eV, which corresponds to excitation to the 3s orbital of benzene. Benzene adsorbed on the Pt(111) is a much more complex system, and the agreement between experiment and theory is less good. For grazing photon incidence, the computed spectra show a broad band that is less intense than the π^* band observed on Au(111). These bands arise from excitation to virtual orbitals of benzene that are mixed extensively with the orbitals of the surface, and have both $\sigma^*_{\mathrm{Pt-C}}$ and π^* character. Overall, while the accurate calculation of NEXAFS spectra for adsorbed molecules remains a challenge, TDFFT can provide a useful tool for understanding and interpreting NEXAFS spectra.

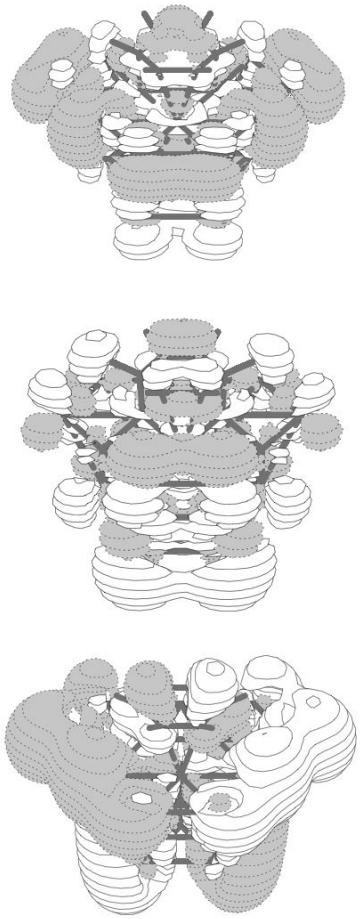

Figure 6.7: Virtual orbitals of benzene adsorbed on Pt(111) in the 3-fold bonding site.

Chapter 7

CIS(D) Calculation of NEXAFS

As demonstrated in the previous chapters NEXAFS spectra can be computed using TDDFT. While the computed spectral profile is often in good agreement with experiment, the predicted excitation energies are much too low compared with experiment. The amount by which the excitation energies are underestimated increases with the nuclear charge of the atomic centres on which the core orbitals are localised. The source of this error is associated with the approximate exchange within the exchange-correlation functionals. The CIS(D) approximation, on the other hand, comprises exact exchange HF and often provides similar spectral profile of valence excited state to TDDFT. Since CIS(D) is based on exact exchange, it would expected to provide accurate core excitation energies. In this chapter, the performance of the CIS(D) method for the calculation of core-excitation energies and NEXAFS spectra is investigated.

7.1 Computational Details

We have calculated core excitation energies of 54 core excited states. These states are drawn from the following molecules CO, H_2CO, CO_2, CH_4, C_2H_2, C_2H_4, N_2, N_2O, SiH_4, H_2S, SO_2, PH_3, HCl and Cl_2, and a list of the excita-

Table 7.1: Core excited states studied.

Molecule	Excitation
CO	C(1s)→ π^*, C(1s)→ $3s$, C(1s)→ $3p_\pi$, C(1s)→ $3p_\sigma$ O(1s)→ π^*, O(1s)→ $3s$, O(1s)→ $3p_\pi$
H_2CO	C(1s)→ π^*, C(1s)→ $3sa_1$, C(1s)→ $3pb_2$, C(1s)→ $3pb_1$ O(1s)→ π^*, O(1s)→ $3sa_1$, O(1s)→ $3pa_1$
CO_2	C(1s)→ π^*, C(1s)→ $3s$, C(1s)→ $3p$
CH_4	C(1s)→ $3s$, C(1s)→ $3p$
C_2H_2	C(1s)→ π^*, C(1s)→ $3s_\sigma$, C(1s)→ $3p_\pi$, C(1s)→ $3p_\sigma$
C_2H_4	C(1s)→ π^*, C(1s)→ $3s_\sigma$
N_2	N(1s)→ π^* , N(1s)→ $3s$, N(1s)→ $3p_\pi$, N(1s)→ $3p_\sigma$
N_2O	N_t(1s) → π^*, N_t(1s)→ $3s$, N_t(1s)→ $3p$, N_c(1s)→ π^* , N_c(1s)→ $3s$, N_c(1s)→ $3p$
SiH_4	Si(1s)→ σ^* , Si(2p)→ σ^*
H_2S	S(1s)→ σ^* , S(1s)→ $4p$, S(1p)→ σ^*, S(1p)→ $4s$
SO_2	S(1s)→ π^*, S(1s)→ $4p$, S(2p)→ π^*, S(2p)→ $4s$
PH_3	P(1s)→ σ^*, P(2p)→ σ^*
HCl	Cl(1s)→ σ^* , Cl(1s)→ $4p_\pi$, Cl(2p)→ σ^* , Cl(2p)→ $4p_\pi$
Cl_2	Cl(1s)→ σ_u^*, Cl(1s)→ $4p$, Cl(2p)→ σ_u^*

tions is shown in Table 7.1. We considered excitation from 1s and 2p orbitals for SiH_4, H_2S, SO_2, PH_3, HCl and Cl_2 molecules. Whereas for others, only excitation from 1s orbitals are included. All structures were optimized at the MP2/cc-pVTZ level of theory. The RI-CIS(D) implementation of CIS(D) was used, and excitation energies were computed for a range of basis sets together with the auxiliary basis set of aug-cc-pVTZ.[178] All these calculations were performed with the Q-Chem software package.[79] Relativity has the effect of lowering the energy of core orbitals. In the calculation of core excitation energies, these effects are significant particularly for second row nuclei. In this work, the effect of relativity was estimated from the lowering of the core orbital energy between non-relativistic and relativistic HF/cc-pCVTZ calcu-

lations, with the relativistic effects computed with the Douglas-Kroll-Hess Hamiltonian.[179] For these calculations, the MOLPRO software package[180] was used.

7.2 Results and Discussion

The lowering in energy of the core orbital due to relativistic effects is found to be 0.10 eV for the carbon 1s orbital in CO, H_2CO, C_2H_2 and C_2H_4, and 0.11 eV in CO_2 and CH_4. For the nitrogen 1s orbital, values of 0.20, 0.19 and 0.22 eV are found for N_2, and the end (N_t) and central (N_c) nitrogen atoms in N_2O. For the oxygen 1s orbital, a value of 0.37 eV for CO and H_2CO is obtained. For the 1s orbitals of the second row elements, values of 3.44, 4.60, 5.90, 5.90, 7.88 and 7.99 eV are found for SiH_4, PH_3, H_2S, SO_2, Cl_2 and HCl, respectively. Similarly, for the 2p orbitals, values of 0.63, 0.88, 1.18, 1.18, 1.58 and 1.60 eV are found. As expected, this effect increases with the nuclear charge of the atom on which the core orbital is localised. Furthermore, this effect shows a weak dependence on the molecule in which the atom is located. Table 7.2

Table 7.2: MAE (in eV) in the computed core excitation energies .

Method	MAE
CIS(D)/aug-cc-pCVQZ	2.6
CIS(D)/aug-cc-pCVTZ	2.5
CIS(D)/aug-cc-pCVDZ	2.7
cSOS-CIS(D)/aug-cc-pCVQZ	1.2
cSOS-CIS(D)/aug-cc-pCVTZ	1.2
cSOS-CIS(D)/aug-cc-pCVDZ	2.3

shows the mean absolute error (MAE) in the computed CIS(D) core excitation

energies with a range of augmented core/valence basis sets[181,182] for the full set of 54 core excited states, and incorporating the correction due to relativity. MAE is taken as an average of the absolute errors of core excitation energies of the computed and experiment. For the largest basis set, aug-cc-pCVQZ, the MAE in the computed excitation energies is found to be 2.6 eV. This error is similar for the first and second row molecules, and does not change significantly with the smaller basis sets aug-cc-pCVTZ and aug-cc-pCVDZ. The magnitude of this error shows that CIS(D) does not have the systematic large underestimation of the excitation energy observed with TDFFT,[99,104,106] and an average error of about 2.5 eV is relatively good. However, closer inspection of the computed core excitation energies reveals severe problems with the predicted spectra. For a number of molecules, the Rydberg bands are computed to lie below a low-lying valence band, which is qualitatively incorrect compared to experiment. This is illustrated in Table 7.3, which shows the computed excitation energies for H_2CO, C_2H_2 and H_2S. More generally, for most molecules studied the Rydberg state excitation energies are underestimated. Hence, while TDDFT predicts "correct spectra in the wrong place", CIS(D) gives "incorrect spectra in the right place". The underestimation of Rydberg state excitation energies has been noted to be a generic problem, and was addressed by adopting SCS-CIS(D) and SOS-CIS(D) approaches.[45] Optimizing the coefficients in equation 3.18 to reproduce excitation energies from experiment resulted in an improved performance. The application of this parameterization to core excited states is not successful since a damping factor was also introduced. This results in the omission of the CIS excitation energy from the denominator of the direct term in equation 3.18. Core ex-

Table 7.3: Computed excitation energies with error in parenthesis with the aug-cc-pCVQZ basis set (in eV).

Molecule	Excitation	Expt.[1]	(Δ R)[2]	CIS(D)	cSOS-CIS(D)
C_2H_2	C(1s)$\rightarrow \pi^*$	285.8	0.10	288.5 (+2.7)	286.8 (+1.0)
	C(1s)$\rightarrow 3s_\sigma$	287.7	0.10	290.3 (+2.6)	289.9 (+2.2)
	C(1s)$\rightarrow 3p_\pi$	288.7	0.10	287.9 (-0.8)	289.1(+0.4)
	C(1s)$\rightarrow 3p_\sigma$	288.8	0.10	287.5 (-1.3)	288.7 (-0.1)
H_2CO	O(1s)$\rightarrow \pi^*$	530.8	0.37	531.8 (+ 1.0)	529.6 (-1.2)
	O(1s)$\rightarrow 3sa_1$	535.4	0.37	530.5 (-4.9)	533.6 (-1.8)
	O(1s)$\rightarrow 3pa_1$	536.3	0.37	531.7 (-4.6)	534.4 (-1.9)
H_2S	S(1s)$\rightarrow \sigma^*$	2473.1	5.90	2470.4 (-2.7)	2472.5 (-0.6)
	S(1s)$\rightarrow 4p$	2476.3	5.90	2469.9 (-6.4)	2474.9 (-1.4)

[1]References[183–186] [2]Relativistic correction at HF/cc-pCVTZ level, and the values taken from the previous page

citation energies are much larger than valence excitation energies, and their absence leads to a large error in the computed value. To find a version of CIS(D) that is applicable to core-excited states, we have adopted an opposite spin only formalism.

$$\omega^{\text{SOS-CIS(D)}} = c_U^{OS} w_U^{OS} + c_T^{OS} w_T^{OS} \tag{7.1}$$

For the core-excited states studied, the direct term is negative, leading to a lowering of the CIS excitation energy, while the indirect term is positive. Focus on improvement of the parameters in the direct term is crucial, and would expect to increase the CIS excitation energy. We have observed that including only the direct term can lead to a significant correction the calculated core excitation energies. This is denoted cSOS-CIS(D), and can be expressed as

$$\omega^{\text{cSOS-CIS(D)}} = c_U^{OS} w_U^{OS} \tag{7.2}$$

with the parameter c_U^{OS} determined to be 1.42 from optimization of the core excitation energies with aug-cc-pCVTZ and aug-cc-pCVQZ basis sets.

Mean absolute errors computed with cSOS-CIS(D) with augmented core/valence basis sets are also shown in Table 7.2. The mean absolute error for the aug-cc-pCVQZ and aug-cc-pCVTZ basis sets are reduced to 1.2 eV. For the aug-cc-pCVQZ basis set this corresponds to errors of 1.5 eV and 0.7 eV for first and second row molecules, respectively. This represents a significant reduction in the error compared to standard CIS(D) calculations. For cSOS-CIS(D) with the aug-cc-pCVDZ basis set, there is a significant increase in the observed error. However, the error remains lower than for CIS(D). In general, sSOS-CIS(D)/aug-cc-pCVDZ are too high and can be improved by a larger c_U^{OS} coefficient. However, it is not desirable to have many parameterizations that are dependent on the basis set. It would also be possible to optimize the method by reintroducing the indirect term and optimizing both c_U^{OS} and c_T^{OS} coefficients. However, our preliminary studies indicate that this would not lead to a large increase in accuracy, and including only the direct term leads to a reduction in the computational cost.[45] There is a considerable improvement in the predicted excitation energies for the Rydberg states. This is illustrated in Figure 7.1, which shows the distribution of errors in the computed excitation energies. For CIS(D), there is a broad distribution of errors, with some large negative errors corresponding to Rydberg states. For cSOS-CIS(D), the error distribution is much narrower and is peaked at an error of less that 0.5 eV. The cSOS-CIS(D) excitation energies for H_2CO, C_2H_2 and H_2S are also included in Table 7.3 and show the resulting spectra to be in much better agreement with experiment. Figure 7.2 shows experimental and

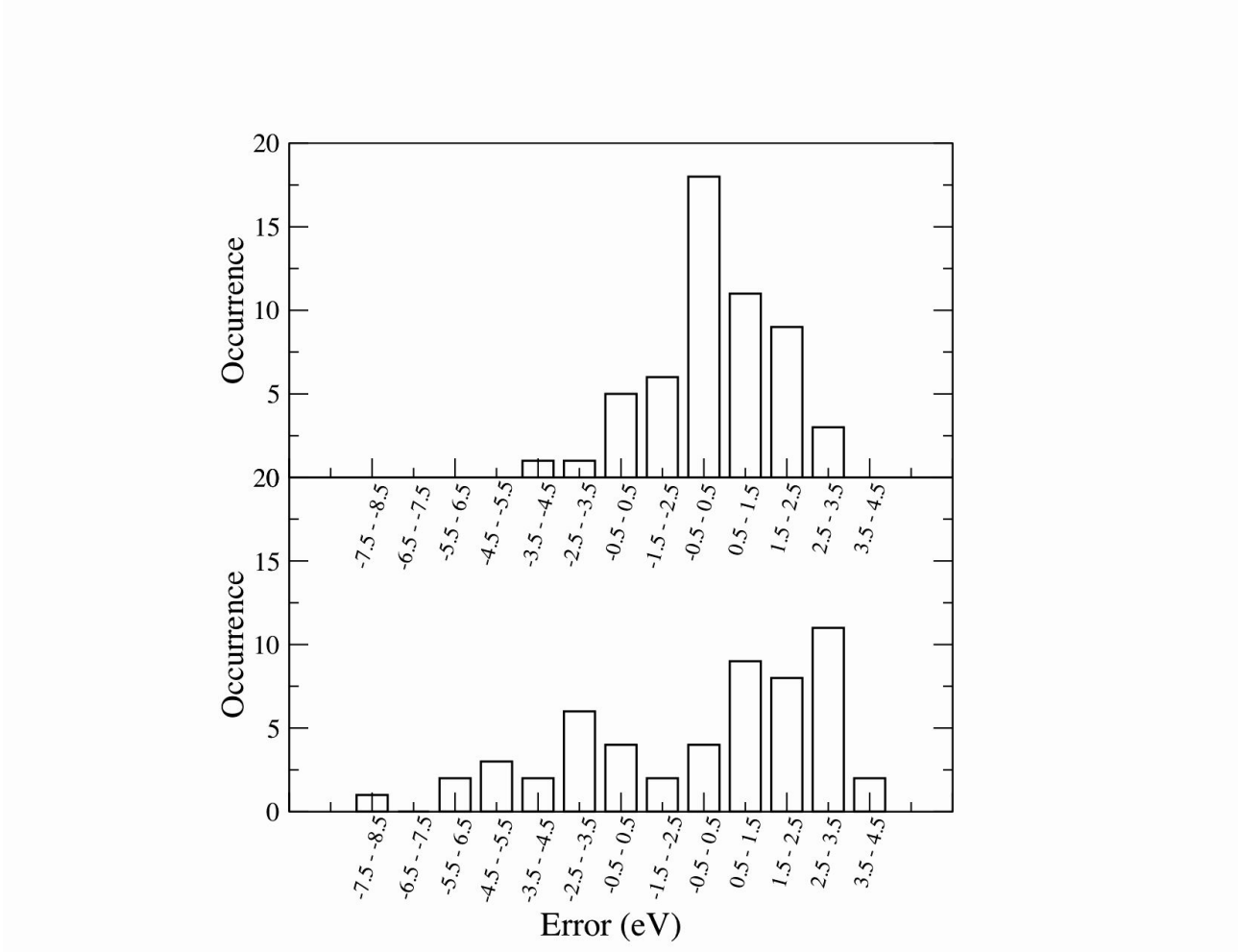

Figure 7.1: Distribution of errors in the computed core excitation energies . Lower panel - CIS(D), top panel - cSOS-CIS(D)

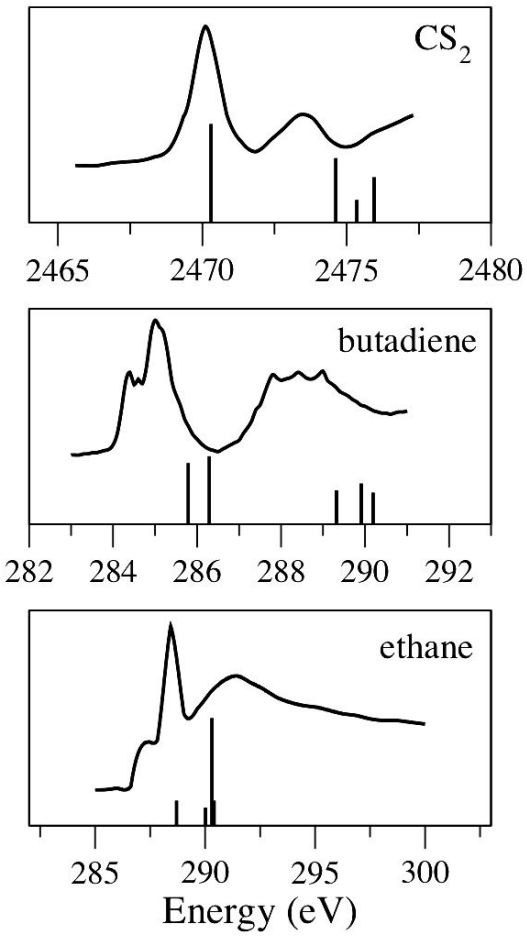

Figure 7.2: Experimental (bold line) and computed cSOS-CIS(D) (stick representation) NEXAFS spectra.
Experimental data adapted from references[187] for ethane,[188] for butadiene and[189] for CS_2.

computed cSOS-CIS(D) NEXAFS spectra for three molecules not included in the original data set. In general, the theoretical spectra do reproduce the experimental features. For butadiene, the calculations predicts the pattern of the experimental bands well, but are a little too high in energy. For ethane, the low energy features are reproduced, but again are a little too high in energy. The discrepancy in these computed core excitation energies is consistent with the average error of approximately 1 eV. For CS_2, the broad band at 2470 eV is predicted well, with the weaker band at higher energy found to be a little too high.

7.3 Conclusions

Core excitation energies computed with TDDFT show a large underestimation, which increases with the nuclear charge of the relevant atoms. Consequently, while the spectra are often correct, they need to be shifted in energy to match experiment. The origin of this error is associated with the approximate local exchange used in most exchange-correlation functionals. CIS(D) provides a natural alternative approach that avoids this problem. Core excitation energies computed with CIS(D) do not show a systematic underestimation, but the predicted spectra are often qualitatively incorrect with the Rydberg states predicted to lie too low in energy. Adopting a scaled spin only formalism, denoted cSOS-CIS(D), in which only the direct contribution to the excitation energy is retained, results in a much improved agreement with experiment.

Overall, the computed NEXAFS spectra represent an improvement over stan-

dard CIS(D) calculations, and provide a reliable basis for interpreting experimental spectra. However, there remains an average error of over 1 eV in the computed core excitation energies. This is larger than level of accuracy achieved with calculations of valence excited states. Ultimately, it is desirable for a similar level of accuracy to be obtained for core excited states. Errors in CIS(D) are corrected by the EOM-CCSD approach, and it is likely that this approach would provide accurate core-excitation energies. However, there is currently no implementation that can compute core-excitations efficiently using EOM-CCSD.

Chapter 8

XES Calculation with MOM

A large number of surface sensitive spectroscopic techniques are available for studying of the electronic structure of adsorbed molecules on the surfaces.[190] However, it is often important to enhance the local information around the adsorbed entity. XES provides a method to locally study the electronic properties centered around one atomic site. This is particularly important when investigating complex systems such as molecular adsorbates with many different atomic sites.

The investigation of reactions on the surfaces and interfaces aims to establish fundamental knowledge of how atoms and molecules interact with the surfaces. With a third-generation synchrotron radiation source, in combination with high-resolution photon spectroscopy, has emerged information about electronic structure and excitation dynamics including interaction of the molecules on the surfaces.

Fortunately, one of the applications of the quantum chemistry is to describe the electronic behaviour of atoms or molecules. Theoretical calculations of XES were reported by Mukoyama *et al.*[191] They simulated XES by computing the transition energy and intensity, which is evaluated through the transition dipole moment. The simplest approach to computing the intensity

is to evaluate the transition dipole moment using the ground state orbitals, and this has been shown to give a surprisingly good agreement with experiment.[78,192] A physically more realistic approach is to use orbitals that account for the relaxation in the core-excited state. These can be obtained through ΔKohn-Sham or transition potential approach. An illustration of this type of approach is a recent study of the XES of manganese coordination complexes.[193]

The calculation of the XES can be done in several ways, including with TDDFT and equation of motion coupled cluster theory (EOM-CCSD).[63,66] Either TDDFT and EOM-CCSD is applied to a Kohn-Sham determinant with a core hole, which is obtained using the Maximum overlap method (MOM)[194,195] procedure.

A brief outline for the protocol for these calculations is summarized as follows:

1. Perform calculation on the neutral ground state molecule.

2. Use the resulting molecular orbitals as the starting point for a further Kohn-Sham SCF calculation on the cation with a core hole in the relevant orbital, invoking MOM to prevent the collapse of the core hole during the SCF process.

3. Perform a TDDFT calculation.

In this work, we report the calculations of XES of a set of small molecules with TDDFT and EOM-CCSD using the MOM scheme.

8.1 Computational Details

The calculation of XES was performed in two efforts. First, we computed the X-ray emission energies using CIS, CIS(D), EOM-CCSD, ΔSCF with the B3LYP exchange-correlation functional and TDDFT with the BLYP and B3LYP functionals. Secondly, we used these methods to predict the accuracy of intensity by comparing to the experimental spectra of methanol and ethanol. For the first task, the 6-311G** basis set was used, and the calculations were performed using the ground state structure optimized at the MP2/cc-pVTZ level. For the second task, X-ray emission spectra are computed with CIS, TDDFT using B3LYP functional and EOM-CCSD in conjunction with the 6-311G** basis set for methanol and ethanol. For EOM-CCSD spectra, excitation energies computed with EOM-CCSD have been combined with intensities from the TDDFT calculations. Spectra were generated by representing the transitions with gaussian functionals with a full-width at half maximum of 1 eV.

8.2 Results and Discussion

Table 8.1 shows computed X-ray emission energies. The Mean absolute error is defined in the previous chapter. The orbital labels describing the transition refer to the ground state of the molecule and not those of the cation with a core hole. The ΔKohn-Sham approach with the B3LYP functional has a MAE of 0.6 eV, which represents a satisfactory level of accuracy that is comparable to the accuracy achieved with ΔKohn-Sham calculations of core excitations.[195] Turning to the methods based on response theory, the MAEs

for CIS and TDDFT are much higher, with errors of many electron volts. The emission energies computed with CIS are systematically underestimated, while those for TDDFT with BLYP and B3LYP functionals are systematically too large. The errors for TDDFT with the B3LYP functional are closer to the experiment than with the BLYP functional, but remain too large. These results illustrate that X-ray emission energies computed with TDDFT are also sensitive to the fraction of HF exchange in the functional and indicate that the large errors observed are associated with the self-interaction error. However, in contrast to the NEXAFS calculations, increasing the fraction of HF exchange results in an increase in the emission energies. Also shown are results for correlated ab initio methods CIS(D) and EOM-CCSD. The CIS(D) emission energies are improved significantly with respect to CIS. The MAE of 7.3 eV for CIS reduced to 1.1 eV. The most accurate emission energies are predicted by EOM-CCSD with a MAE of 0.5 eV. However, for this approach we have found within our implementation of EOM-CCSD that it can be problematic to converge the CCSD calculation for a wavefunction with a core hole. The origin of this convergence problem has been discussed elsewhere.[202] Despite this current limitation, EOM-CCSD does provide accurate X-ray emission energies where it can be applied. Figure 8.1 shows a test of these methods against experimental spectra of methanol and ethanol in order to predict the intensity accurately. High quality carbon-K and oxygen-K experimental spectra which have been reported elsewhere,[196] are shown in figure 8.2. The assignment of the bands in these spectra has been discussed in detail in the earlier theoretical work of Larkins and co-workers who studied X-ray emission of methanol and ethanol molecules using transition energies

Table 8.1: Computed X-ray Emission energies (in eV). Experimental data from references.[196–201] [a]Mean absolute Error.

Excitation	Exp.	CIS	CIS(D)	EOM-CCSD	ΔB3LYP	TD-BLYP	TD-B3LYP
CH_4 $1t_2 \rightarrow 1a_1$	276.3	269.8	275.6	276.2	276.8	286.4	283.3
C_2H_2 $1\pi_u \rightarrow 1\sigma_g$	278.9	272.6	280.5	279.7	280.4	289.5	286.2
C_2H_2 $3\sigma_g \rightarrow 1\sigma_g$	274.1	267.0	273.8	273.7	275.5	284.1	280.8
CO $5\sigma \rightarrow 2\sigma$	282.0	279.6	281.4	282.7	282.9	292.9	290.3
CO $1\pi \rightarrow 2\sigma$	278.4	271.9	281.7	278.6	280.0	288.9	285.3
CH_3OH 2a"$\rightarrow$2a′	281.2	271.6	278.9	280.0	282.0	291.7	287.4
CH_3OH 7a"$\rightarrow$2a′	279.5	271.5	278.1	278.7	280.4	290.1	286.1
CH_3OH 6a'$\rightarrow$2a′	277.4	268.5	277.8	276.6	278.0	287.5	284.1
NH_3 1e$\rightarrow 1a_1$	388.8	380.3	387.1	388.0	388.2	399.5	395.8
NH_3 $2a_1 \rightarrow 1a_1$	395.1	389.7	394.6	395.6	395.3	406.3	403.0
H_2O $1b_1 \rightarrow 1a_1$	521.0	512.5	519.4	521.0	520.9	534.3	530.0
H_2O $3a_1 \rightarrow 1a_1$	525.1	518.2	524.2	525.4	525.0	538.2	534.3
H_2O $1b_2 \rightarrow 1a_1$	527.0	521.1	526.6	527.8	527.2	540.0	536.2
CH_3OH 2a"$\rightarrow$1a′	527.8	521.0	527.4	528.0	528.2	541.3	536.7
CH_3OH 7a"$\rightarrow$1a′	526.1	518.3	525.4	526.0	526.6	540.3	535.1
CH_3OH 6a'$\rightarrow$1a′	523.9	513.0	522.3	522.7	524.1	537.9	532.4
CH_3F $5a_1 \rightarrow 1a_1$	675.6	667.1	675.4	674.9	675.5	691.7	686.1
CH_3F $2e_1 \rightarrow 1a_1$	678.6	671.1	678.0	678.4	679.5	696.1	689.5
MAE[a]	-	7.3	1.1	0.5	0.6	12.2	8.1

and orbitals from HF calculations.[203,204] The X-ray emission of methanol has also been studied using optimized multiconfigurational wavefunctions.[205] Initially, we will discuss the results for the O-K spectrum. For methanol the experimental spectrum has four distinct peaks at 527.8 eV, 526.1 eV, 523.9 eV and 521.5 eV which are assigned to 2a", 7a′, 6a′ and 5a′, respectively. The 1a" band is weaker and lies at 522.4 eV. The EOM-CCSD based spectrum reproduces the experiment well, with computed excitation energies of 528.0 eV, 526.0 eV, 522.7 eV, 521.2 eV 520.4 eV for the 2a", 7a′, 6a′, 1a" and 5a′ orbitals. The spectra based on CIS and B3LYP are shifted from the experi-

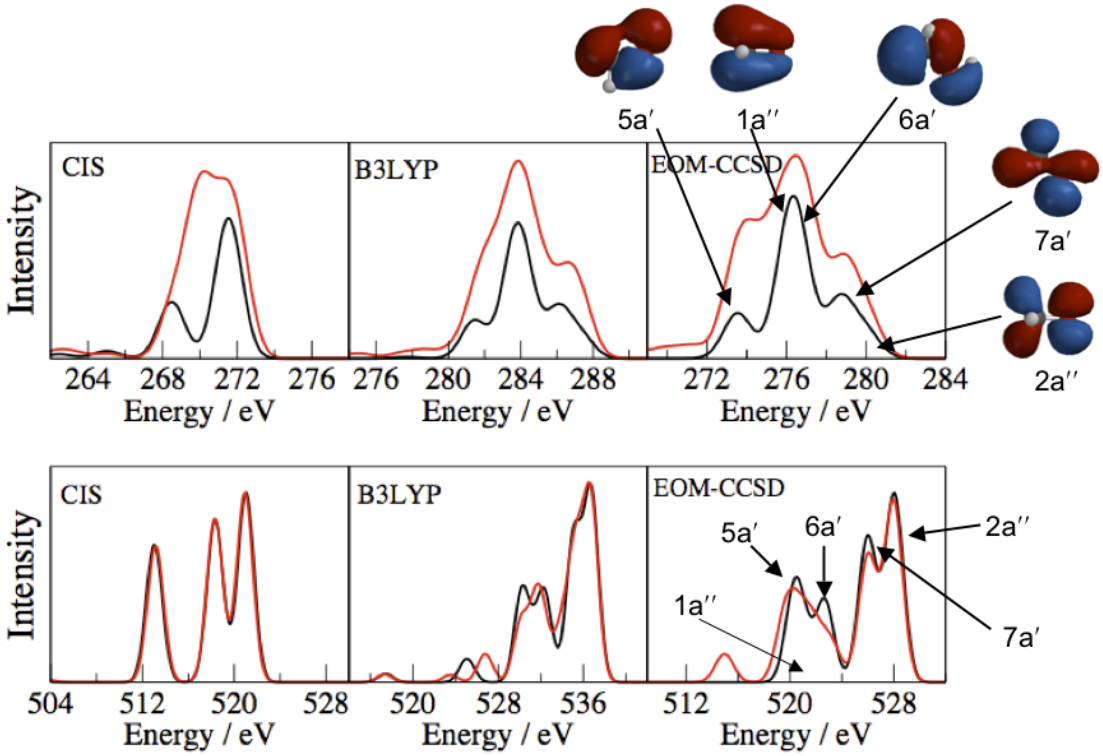

Figure 8.1: Computed C-K (top panels) and O-K (lower panels) X-ray emission spectra for methanol (black line) and ethanol (red line).

mental spectra. More significantly the CIS method provides a spectral profile that is close to the experiment. Similar to experiment, the predicted spectra for ethanol show only small deviations from methanol. In experiment the C-K spectrum shows four distinct peaks at 282.9 eV, 281.2 eV, 279.5 eV and 276.6 eV. The computed EOM-CCSD spectra has only three peaks and differs significantly from experiment. However, the computed spectrum does agree well with the computed spectrum of Larkins and Senn,[203] and in this work it was suggested that deviation from experiment is most likely due to satellite contributions and the presence of impurities.

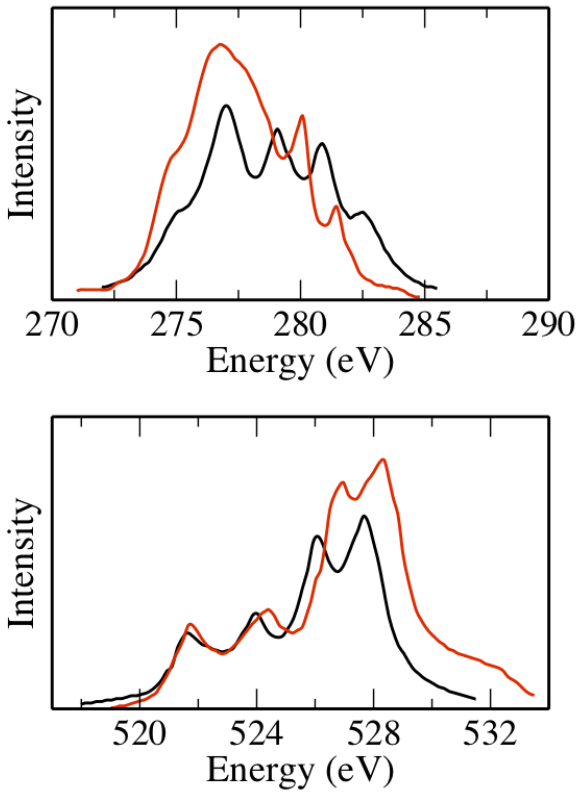

Figure 8.2: Experimental C-K (top panel) and O-K (lower panel) X-ray emission spectra for methanol (black line) and ethanol (red line). Adapted from reference.[196]

8.3 Conclusions

We have shown that the MOM scheme can be used to perform XES calculations. This can be achieved by applying CIS, TDDFT or EOM-CCSD methods to the wavefunction or a Kohn-Sham determinant with a core hole. Within TDDFT, standard exchange-correlation functionals predict emission energies that are significantly different from experiment. The EOM-CCSD method does provide accurate X-ray emission energies and when applied to the X-ray emission spectra of methanol and ethanol, good agreement with experiment and previous theoretical work is obtained.

Concluding Remarks

Quantum chemical calculations of X-ray absorption and X-ray emission spectra over many years have been a great challenge. We have shown that, in principle, these spectra can be computed using the current quantum chemical packages. We have also highlight deficiencies and areas for further development, such as new development in functionals of TDDFT to predict correct emission energies which are required. In the future, we would like to bring our concern to broaden TDDFT functionals to achieve an accurate prediction of the emission energies. We would also like to study core excitation using EOM-CCSD, and deal with problematic of converging of CCSD for the wavefunction with core hole.

Bibliography

[1] M. Mueller, *Fundamentals of Quantum Chemistry*, Kluwer Academic/Plenum Publisher: New York (2001).

[2] E. Schrödinger, *Phys. Review* 28 (1926) 1049.

[3] M. Born and R. Oppenheimer, *Ann. Phys. Leipzig* 84 (1927) 457.

[4] D. R. Hartee, *Proc. Cambridge Phil. Soc.* 111 (1928) 24.

[5] V. Fock, *Z. Phys.* 126 (1930) 61.

[6] T. Koopmans, *Physica* 104 (1933) 1.

[7] J. Kobus, *Adv. Quant. Chem.* 28 (1997) 1.

[8] C. C. J. Roothaan, *Revs. Modern Phys.* 32 (1960) 179.

[9] J. A. Pople and R. K. Nesbet, *J. Chem. Phys.* 22 (1954) 571.

[10] C. Møller, M. S. Plesset, *Phys. Rev.* 46 (1934) 618.

[11] R. J. Bartlett, *Annu. Rev. Phys. Chem.* 32 (1982) 359.

[12] P. Carsky, *In Encyclopedia of Computational Chemistry*; P. V. R. Schleyer, N. L. Clark, J. Gasteiger, III. H. F. S., P. R. Schreiner, Eds. Wiley, Chichester, U.K., p 485 (1998).

[13] W.J. Kutzelnigg, *J. Mol. Struct. (THEOCHEM)*, 181 (1988) 33.

[14] J. Gauss, *In Encyclopedia of Computational Chemistry*; P. v. R. Schleyer, N. L. Clark, J. Gasteiger, III. H. F. S, P. R. Schreiner, Eds. Wiley, Chichester, U.K., p 615 (1998) .

[15] R. J. Bartlett, *Ed. Modern Ideas in Coupled-Cluster Methods*; World Scientific: Singapore (1997).

[16] J. Dombroski, M. Head-Gordon and A. Gilbert, *Q-Chem User's Guide Ver. 3.0*, Edited by A. Gilbert (2006).

[17] R. Ditchfield, W. J. Hehre and J. A. Pople, *J. Chem. Phys.* 54 (1971) 724.

[18] S. F. Boys, *Proc. R. Soc. London Ser. A* 200 (1950) 542.

[19] W. J. Hehre, R. F. Stewart and J. A. Pople, *J. Chem. Phys.* 51 (1969) 2657.

[20] R. Ditchfield, W. J. Hehre and J. A. Pople, *J. Chem. Phys.* 54 (1971) 724.

[21] J. W. Hehre, R. Ditchfield and J. A. Pople, *J. Chem. Phys.* 56 (1972) 2257.

[22] T. H. Dunning, Jr., *J. Chem. Phys.* 90 (1989) 1007.

[23] D. E. Woon and T. H. Dunning, Jr., *J. Chem. Phys.* 98 (1993) 1358.

[24] D. E. Woon and T. H. Dunning, Jr., *J. Chem. Phys.* 103 (1995) 4572.

[25] W. Koch and M. C. Holthausen, *A Chemist's Guide to Density Functional Theory*, 2nd Ed., Wiley-VCH, p 15 (2001).

[26] P. Hohenberg and W. Kohn, *Phys. Rev.* 136 (1964) B864.

[27] W. Kohn and L. J. Sham, *Phys. Rev.A* 140 (1965) 1133.

[28] R. G. Parr and W. Yang, *Density-Functional Theory of Atoms and Molecules*, Oxford University Press, New York (1989).

[29] P. A. M. Dirac, *Proc. Cam. Phil. Soc.* 26 (1930) 376.

[30] A. D. Becke, *J. Chem. Phys.* 96 (1992) 2155.

[31] J. P. Perdew and Y. Wang, *Phys. Rev. B* 33 (1986) 8800.

[32] A. D. Becke, *Phys. Rev. A.* 38 (1988) 3098.

[33] N. C. Handy, and A. J. Cohen, *Mol. Phys.* 99 (2001) 403.

[34] F. A. Hamprecht, A. J. Cohen, D. J. Tozer and N. C. Handy, *J. Chem. Phys.* 109 (1998) 6264.

[35] G. Rauhut and P. Pulay, *J. Phys. Chem.* 99 (1995) 3093.

[36] C. Lee, W. Yang, and R. G. Parr, *Phys. Rev. B* 41 (1988) 785.

[37] S. H. Vosko, L. Wilk and M. Nusair, *Can. J. Phys.* 58 (1980) 1200.

[38] F. Jensen, *Introduction to Computational Chemistry*, 2nd Ed., John Wiley & Sons Inc., NJ, USA (2007).

[39] R. M. Dreizler and E. K. U. Gross, *Density Functional Theory* Springer, Berlin, (1990).

[40] W. Yang, *Phys. Rev. Lett.* 1438 (1991) 66.

[41] J. B. Foresman, M. Head-Gordon and J. A. Pople, *J. Phys. Chem.* 96 (1992) 135.

[42] R. Manne, *Mol. Phys.* 24 (1972) 935.

[43] M. Head-Gordon, R. J. Rico, M. Oumi and T. J. Lee, *Chem. Phys. Lett.* 219 (1994) 21.

[44] M. Head-Gordon, D. Maurice and M. Oumi, *Chem. Phys. Lett.* 246 (1995) 114.

[45] Y. M. Rhee and M. Head-Gordon, *J. Phys. Chem. A* 111 (2007) 5314.

[46] S. Grimme, *J. Chem. Phys.* 118 (2003) 9095.

[47] S. Grimme and E. Izgorodina, *Chem. Phys.* 305 (2004) 223.

[48] E. Runge and E.K.U. Gross, *Phys. Rev. Lett.* 52 (1984) 997.

[49] M. E. Casida, in *Recent Advances in Density Functional Methods,* Part I, Edited by D. P. Chong (World Scientific, Singapore, 1995), p 155.

[50] A. Dreuw and M. Head-Gordon, *Chem. Rev.* 105 (2005) 4009.

[51] K. Yabana and G. F. Bertsch, *Phys. Rev. B* 54 (1996) 4484.

[52] M. A. L. Marques, A. Castro, G. F. Bertsch and A. Rubio,. *Comput. Phys. Commun.* 151 (2003) 60.

[53] S. Hirata and M. Head-Gordon, *Chem. Phys. Lett.* 314 (1999) 291.

[54] M. E. Casida, C. Jamorski, K. C. Casida and D.R. Salahub, *J. Chem. Phys.* 108 (1998) 4439.

[55] D. J. Tozer and N. C. Handy, *J. Chem. Phys.* 109 (1998) 10180.

[56] H. J. Monkhorst, *Int. J. Quantum Chem. Symp.* 11 (1977) 421.

[57] D. Mukherjee and P. K. Mukherjee, *Chem. Phys.* 39 (1979) 325.

[58] K. Emrich, *Nucl. Phys. A* 351 (1981) 379.

[59] E. Dalgaard and H. J. Monkhorst, *Phys. Rev. A* 28 (1983) 1217.

[60] H. Koch and P. Jørgensen, *J. Chem. Phys.* 93 (1990) 3333.

[61] S. R. Gwaltney, M. Nooijen and R. J. Bartlett, *Chem. Phys. Lett.* 248 (1996) 189.

[62] H. Koch, H. J. A. Jensen, P. Jørgensen and T. Helgaker, *J. Chem. Phys.* 93 (1990) 3345.

[63] J. F. Stanton and R. J. Bartlett, *J. Chem. Phys.* 98 (1993) 7029.

[64] D. C. Comeau and R. J. Bartlett, *Chem. Phys. Lett.* 297 (1993) 414.

[65] R. J. Rico, T. J. Lee and M. Head-Gordon, *Chem. Phys. Lett.* 218 (1994) 139.

[66] H. Sekino and R. J. Bartlett, *Int. J. Quantum Chem., Symp.* 18 (1984) 255.

[67] B. O. Roos, *Adv. Chem. Phys.* 69 (1987) 399.

[68] L. Gagliardi and B. O. Roos, *Nature (London)* 433 (2005) 848.

[69] K. Andersson, P. -A. Malmqvist, B. O. Roos, A. J. Sadlej and K. Wolinski, *J. Phys. Chem.* 94, (1990) 5483.

[70] P. -A. Malmqvist, R. Lindh, B. O. Roos and S. Ross, *Theor. Chim. Acta* 73, (1988) 155.

[71] B. O. Roos, P. -A. Malmqvist and L. Gagliardi, *J. Am. Chem. Soc.* 128, (2006) 17000.

[72] L. Serrano-Andrés and M. P. Fülscher, *J. Am. Chem. Soc.* 120, (1998) 10912.

[73] F. Aquilante, K. P. Jensen and B. O. Roos, *Chem. Phys. Lett.* 380, (2003) 689.

[74] F. Aquilante, V. Barone and B. O. Roos, *J. Chem. Phys.* 119, (2003) 12323.

[75] L. Blancafort, D. Gonzalez, M. Olivucci and M. A. Robb, *J. Am. Chem. Soc.* 124, (2002) 6398.

[76] A. Migani, M. J. Bearpark, M. Olivucci and M. A. Robb, *J. Am. Chem. Soc.* 129, (2007) 3703.

[77] J. Stöhr, *NEXAFS Spectroscopy* Springer Series in Surface Science; Springer: Heidelberg (1996).

[78] A. Nilsson and L. G. M. Pettersson, *Surf. Sci. Rep.* 55 (2004) 49.

[79] Y. Shao, L. Fusti-Molnar, Y. Jung, J. Kussman, C. Ochsenfeld, S. T. Brown, A. T. B. Gilbert, L. V. Slipchenko, S. V. Levchenko, D. P. O'Neill, R. A. Distasio Jr., R. C. Lochan, T. Wang, G. J. O. Beran, N. A. Besley, J. M. Herbert, Y. L. Lin, T. Van Voorhis, S. H. Chien, A. Sodt, R. P. Steele, V. A. Rassolov, P. E. Maslen, P. P. Korambath, R. D. Adamson, B. Austin, J. Baker, E. F. C. Byrd, H. Daschle, R. J. Doerksen, A. Dreuw, B. D. Dunietz, A. D. Dutoi, T. R. Furlani, S. R. Gwaltney, A. Heyden, S. Hirata, C. -P. Hsu, G. Kedziora, R. Z. Khalliulin, P. Klunzinger, A. M. Lee, M. S. Lee, W. Lian, I. Lotan, N. Nair, B. Peters, E. I. Proynov,

P. A. Pieniazek, Y. M. Rhee, J. Ritchie, E. Rosta, C. D. Sherrill, A. C. Simmonett, J. E. Subotnik, H. L. Woodcock III, W. Zhang, A. T. Bell, A. K. Chakraborty, D. M. Chipman, W. J. Hehre, A. Warshel, H. F. Schaefer III, J. Kong, A. I. Krilov, P. M. W. Gill and M. Head-Gordon, *Phys. Chem. Chem. Phys.* 8 (2006) 3172.

[80] J. A. Pople, R. Krishnan, H. B. Schlegel and J. S. Binkley, *Int. J. Quantum Chem., Quantum Chem. Symp.* 13, (1979) 225.

[81] M. Reiher and J. Neugebauer, *J. Chem. Phys.* 118 (2003) 1634.

[82] E. R. Davidson, *J. Comput. Phys.* 17 (1975) 87.

[83] J. Neugebauer and M. Reiher, *J. Comput. Chem.* 25 (2004) 587.

[84] C. Hermann and M. Reiher, *Surf. Sci.* 600 (2006) 1891.

[85] C. Hermann, J. Neugebauer and M. Reiher, *New J. Chem.* 31 (2007) 818.

[86] X. Zhou, C. J. M. Wheeless and R. Liu, *Vibrational Spectroscopy* 12 (1996) 53.

[87] N. A. Besley and K. A. Metcalf, *J. Chem. Phys.* 126 (2007) 035101.

[88] N. A. Besley, *Phil. Trans. R. Soc. A* 365 (2007) 2799.

[89] L. Triguero, L. G. M. Pettersson and H. Ågren, *Phys. Rev. B* 58, (1998) 8097.

[90] J. A. Horsley, J. Stöhr, R. J. Koestner, *J. Chem. Phys.* 83 (1995) 3146.

[91] L. G. M. Pettersson, H.Ågren, O. Vahtras and V. Carravetta, *J. Chem.Phys.* 103, (1995) 8713.

[92] T. Triguero and L. G. M. Pettersson, *Surf. Sci.* 398 (1998) 70.

[93] L. G. M. Pettersson, H.Ågren, Y. Luo and L. Triguero, *Surf. Sci.* 408 (1998) 1.

[94] M. Nyberg, J. Hasselström, O. Karis, N. Wassdahl, M. Weinelt and L. G. M. Pettersson, *J. Chem. Phys.* 112 (2000) 5420.

[95] L. G. M. Pettersson, H.Ågren, Y. Luo and L.Triguero, *Surf. Sci.* 408 (1998) 1.

[96] K. Weiss, H. Öström, T. Triguero, H. Ogasawara, M. G. Garnier, L. G. M. Pettersson and A. Nilsson, *J. Electron Spectrosc. Relat. Phenom.* 128 (2003) 179.

[97] H. Öström, D. Nordlund, H. Ogasawara, K. Weiss, T. Triguero, L. G. M. Pettersson and A. Nilsson, *Surf. Sci.* 565 (2004) 206.

[98] M. Stener, G. Fronzoni and M. de Simone, *Chem. Phys. Lett.* 373 (2003) 115.

[99] N. A. Besley and A. Noble, *J. Phys. Chem. C* 111 (2007) 3333.

[100] P. Norman, D. M. Bishop, H. J. A. Jensen and J. Oddershede, *J. Chem. Phys.* 123 (2005) 194103.

[101] U. Elkström and P. Norman, *Phys. Rev. A* 74 (2006) 042722.

[102] U. Elkström and P. Norman, *Phys. Rev. Lett.* 97 (2006) 143001.

[103] Y. Imamura, T. Osuka and H. Nakai, *J. Comp. Chem.* 28 (2006) 2067.

[104] A. Nakata, Y. Imamura and H. Nakai, *J. Chem. Phys.* 125 (2006) 064109.

[105] A. Nakata, Y. Imamura, T. Otsuka and H. Nakai, *J. Chem. Phys.* 124 (2006) 094105.

[106] A. Nakata, Y. Imamura and H. Nakai, *J. Chem. Theory Comput.* 3 (2007) 1295.

[107] G. Tu, Z. Rinkevicius, O. Vahtras, H. Ågren, U. Elkström, P. Norman and V. Carravetta, *Phys. Rev. A* 76 (2008) 022506.

[108] Y. Imamura and H. Nakai, *Int. J. Quantum Chem.* 107 (2007) 23.

[109] A. Dreuw, J. Weisman and M. Head-Gordon, *J. Chem. Phys.* 119 (2003) 2943.

[110] M. J. G. Peach, P. Benfield, T. Helgaker and D. J. Tozer, *J. Chem. Phys.* 128 (2008) 044118.

[111] G. Fronzoni, R. De Francesco and M. Stener, *J. Phys. Chem. B* 109 (2005) 10332.

[112] G. Fronzoni, R. De Francesco and M. Stener, *J. Phys. Chem. B* 110 (2006) 9899.

[113] Y. Imamura and H. Nakai, *Chem. Phys. Lett.* 419 (2006) 297.

[114] N. A. Besley, M. J. G. Peach and D. J. Tozer, *Phys. Chem. Chem. Phys* 11 (2009) 10350.

[115] S. F. Bent, *Surf. Sci.* 500 (2002) 879.

[116] J.R. Arthur, *Surf. Sci.* 500 (2002) 189.

[117] P. Finnie and Y. Homma, *Surf. Sci.* 500 (2002) 437.

[118] M. K. Weldon, K. T. Queeney, J. Eng. Jr., K. Raghavachari and Y. J. Chabal, *Surf. Sci.* 500 (2002) 859.

[119] R. J. Hamers, P. Avouris and F. Bozso, *Phys. Rev. Lett.* 59 (1987) 2071.

[120] R. Konecny and D. J. Doren, *J. Am. Chem. Soc.* 119 (1997) 11098.

[121] R. Konecny and D. J. Doren, *Surf. Sci.* 417 (1998) 169.

[122] A. V. Teplyakov, M. J. Kong and S. F. Bent, *J. Chem. Phys.* 108 (1998) 4599.

[123] P. Moriarty, M. D. Upward, A. W. Dunn, Y. -R. Ma, P. H. Benton and D. Teehan, *Phys. Rev. B* 57 (1998) 362.

[124] K. Sakamoto, D. Kondo, M. Hirada, A. Kimura, A. Kakizaki and S. Suto, *Surf. Sci.* 642 (1999) 433.

[125] D. Kondo, K. Sakamoto, H. Takeda, F. Matsui, K. Amemiya, T. Ohta, W. Uchida and A. Kasuya, *Surf. Sci.* 514 (2002) 337.

[126] R. J. Hamers, S. K. Coulter, M. D. Ellison, J. S. Hovis, D. F. Padowitz, M. P. Schartz, C. M. Greenlief and J. N. Russell Jr., *Acc. Chem. Res.* 33 (2000) 617.

[127] L. A. Curtiss and M. S. Gordon (Eds.), *Computational Materials Chemistry-Methods and Applications*, Kluwer Academic Publishers, Dordrecht, Boston, London (2004).

[128] A. V. Teplyakov, P. Lal, Y. Noah and S.F. Bent, *J. Am. Chem. Soc.* 120 (1998) 7377.

[129] P. Lal, A. V. Teplyakov, Y. Noah, M. J. Kong, G. T. Wang and S. F. Bent, *J. Chem. Phys.* 110 (1999) 10545.

[130] Q. Liu and R. Hoffmann, *J. Am. Chem. Soc.* 117 (1995) 4082.

[131] Y. Imamura, Y. Morikawa, T. Yamasaki and H. Nakatsuji, *Surf. Sci.* 341 (1995) L1091.

[132] D. Sorescu and K. D. Jordan, *J. Phys. Chem. B* 104 (2000) 8259.

[133] J. M. Rintelman and M. S. Gordon, *J. Phys. Chem. B* 108 (2004) 7820.

[134] Y. Jung and M. S. Gordon, *J. Am. Chem. Soc.* 127 (2005) 3131.

[135] J.-H. Cho, K. S. Kim and Y. Morikawa, *J. Chem. Phys.* 124 (2006) 024716.

[136] M. Sternberg, P. Zapol and L. A. Curtiss, *Phys. Rev. B* 68 (2003) 205330.

[137] P. Zapol, L. A. Curtiss, H. Tamura and M. S. Gordon, in: L.A. Curtiss, M. S. Gordon (Eds.), *Computational Materials Chemistry-Methods and Applications*, Kluwer Academic Publishers, Dordrecht, Boston, London (2004) p. 266.

[138] M. Sternberg, P. Zapol and L. A. Curtiss, *Mol. Phys.* 103 (2005) 1017.

[139] M. Sternberg, D. A. Horner, P. C. Redfern, P. Zapol and L. A. Curtiss, *J. Comput. Theor. Nanosci.* 2 (2005) 207.

[140] H. Tamura and M. S. Gordon, *Chem. Phys. Lett.* 406 (2005) 197.

[141] M. J. Kong, A. V. Teplyakov, J. G. Lyubovitsky and S. F. Bent, *Surf. Sci.* 411 (1998) 286.

[142] Y. Taguchi, M. Fujisawa, T. Takoka, T. Okada and M. Nishijima, *J. Chem. Phys.* 95 (1991) 6870.

[143] G. P. Lopinski, T. M. Fortier, D. J. Moffatt and R. A. Wolkow, *J. Vac. Sci. Technol.* 16 (1998) 1037.

[144] B. Naydenov and W. Widdra, *J. Chem. Phys.* 127 (2007) 154711.

[145] G .T. Wang, C. Mui, C. B. Musgrave and S. F. Bent, *J. Phys. Chem. B* 103 (1999) 6803.

[146] C. Mui, G. T. Wang, S. F. Bent and C. B. Musgrave, *J. Chem. Phys.* 114 (2001) 10170.

[147] K. T. Nicholson and M. M. Banaszak Holl, *Phys. Rev. B* 64 (2001) 155317.

[148] M. A. Phillips, N. A. Besley, P. M. W. Gill and P. Moriarty, *Phys. Rev. B* 67 (2003) 035309.

[149] K. Okamura, H. Ishii, Y. Kimuar and M. Niwano, *Surf. Sci.* 576 (2005) 45.

[150] N. A. Besley and J. A. Bryan, *J. Phys. Chem. C* 112 (2008) 4308.

[151] F. Matsui, H.W. Yeom, A. Imanishi, K. Isawa, I. Matsuda and T. Ohta, *Surf. Sci. Lett.* 401 (1998) L413.

[152] F. Matsui, H.W. Yeom, I. Matsuda and T. Ohta, *Phys. Rev. B* 62 (2000) 5036.

[153] A. Pietzsch, F. Hennies, A. Föhlisch, W. Wurth, M. Nagasono, N. Witkowski and M. N. Piancastelli, *Surf. Sci.* 562 (2004) 65.

[154] N. Witkowski, F. Hennies, A. Pietzsch, S. Mattsson, A. Föhlisch, W. Wurth, M. Nagasono and M. N. Piancastelli, *Phys. Rev. B* 68 (2003) 115408.

[155] K. Newstead, A. W. Robinson, S. d,Addato, A. Patchett, N. P. Prince, R. McGrath, R. Whittle, E. Dudzik and I. T. McGovern, *Surf. Sci.* 287fl288 (1993) 317.

[156] A. Hoffmann, G. Comtet, L. Hellner, G. Dujardin and M. Petravic, *Appl. Phys. Lett.* 73 (1998) 1152.

[157] A. P. Scott and L. Radom, *J. Phys. Chem.* 100 (1996) 16502.

[158] J. A. Horsley, J. Stoöhr, A. P. Hitchcock, D. A. Newbury, A. L. Johnson and F. Sette, *J. Chem. Phys.* 83 (1985) 6099.

[159] A. C. Liu, J. Stöhr, C. M. Friend and R. J. Madix, *Surf Sci.* 235 (1988) 107.

[160] A. C. Liu, C. M. Friend and J. Stöhr, *Surf Sci.* 236 (1990) L439.

[161] K. Weiss, S. Gerbert, M. Wühn, H. Wadepohl and Ch. Wöll, *J. Vac. Sci. Technol.* 16 (1998) 1017.

[162] Ch. Wöll, *J. Synchrotron Radiat* 8 (2001) 129.

[163] L. G. M. Pettersson, H. Ågren, O. Vahtras and V. Carravetta, *J. Chem. Phys.* 103 (1995) 8713.

[164] A. Bilic, J. R. Reimers, N. S. Hush, R. C. Hoft and M. J. Ford, *J. Chem. Theory Comput.* 2 (1006) 1093.

[165] C. Morin, D. Simon and P.Sautet, *J. Phys. Chem. B* 108 (2004) 12084.

[166] M. E. Casida and D.R. Salahub, *J. Chem. Phys.* 113 (2000) 8918.

[167] E. Apr, T. L. Windus, T. P. Straatsma, E. J. Bylaska, W. de Jong, S. Hirata, M. Valiev, M. Hackler, L. Pollack, K. Kowalski, R. Harrison, M. Dupuis, D. M. A. Smith, J. Nieplocha, V. Tipparaju, M. Krishnan, A. A. Auer, E. Brown, G. Cisneros, G. Fann, H. Früchtl, J. Garza, K. Hirao, R. Kendall, J. Nichols, K. Tsemekhman, K. Wolinski, J. Anchell, D. Bernholdt, P. Borowski, T. Clark, D. Clerc, H. Dachsel, M. Deegan, K. Dyall, D. Elwood, E. Glendening, M. Gutowski, A. Hess, J. Jaffe, B. Johnson, J. Ju, R. Kobayashi, R. Kutteh, Z. Lin, R. Littlefield, X. Long, B.

Meng, T. Nakajima, S. Niu, M. Rosing, G. Sandrone, M. Stave, H. Taylor, G. Thomas, J. van Lenthe, A. Wong, and Z. Zhang, *NWChem, A Computational Chemistry Package for Parallel Computers*, Version 4.6, 2004, Pacific Northwest National Laboratory, Richland, Washington 99352-0999, USA.

[168] J. Lorentzon, P. -A. Malmqvist, M. Fülscher and B.O. Roos, *Theor. Chim. Acta* 91 (1995) 91.

[169] P. J. Hay and W. R. Wadt, *J. Chem. Phys.* 82 (1985) 270.

[170] P. J. Hay and W. R. Wadt, *J. Chem. Phys.* (1985) 299.

[171] E. E. Rennie, B. Kempgens, H. M. Köppe, U. Hergenhahn, J. Feldhaus, B. S. Itchkawitz, A. L. D. Kilcoyne, A. Kivimäki, K. Maier, M. N. Piancastelli, M. Polcik, A. Rüdel and A. M. Bradshaw, *J. Chem. Phys.* 113 (2000) 7362.

[172] R. Püttner, C. Kolczewski, M. Martins, A. S. Schlacter, G. Snell. M. Sant'Anna, J. Viefhaus, K. Hermann and G. Kaindl, *Chem. Phys. Lett.* 393 (2004) 361.

[173] C. Kolczewski, R. Püttner, M. Martins, A. S. Schlacter, G. Snell. M. Sant'Anna, K. Hermann and G. Kaindl, *J. Chem. Phys.* 124 (2006) 034302.

[174] W. H. E. Schwarz, T. C. Chang, U. Seeger and K. H. Hwang, *Chem. Phys.* 117 (1987) 73.

[175] A. Dreuw and M. Head-Gordon, *J. Am. Chem. Soc.* 126 (2004) 4007.

[176] N. A. Besley and J. D. Hirst, *J. Phys. Chem. A* 102 (1998) 10791.

[177] N. A. Besley and J. D. Hirst, *J. Am. Chem. Soc.* 121 (1999) 8559.

[178] R. A. Kendall, T. H. Dunning, R. J. Harrison, *J. Chem. Phys.* 96 (1992) 6796.

[179] M. Reiher and A. Wolf, *J. Chem. Phys.* 121 (2004) 2037.

[180] MOLPRO, version 2006.1, a package of ab initio programs, H. -J. Werner, P. J. Knowles, R. Lindh, F. R. Manby, M. Schütz, P. Celani, T. Korona, G. Rauhut, R. D. Amos, A. Bernhardsson, A. Berning, D. L. Cooper, M. J. O. Deegan, A. J. Dobbyn, F. Eckert, C. Hampel, G. Hetzer, A. W. Lloyd, S. J. McNicholas, W. Meyer, M. E. Mura, A. Nicklass, P. Palmieri, R. Pitzer, U. Schumann, H. Stoll, A. J. Stone, R. Tarroni and T. Thorsteinsson.

[181] D. E. Woon and T. H. Dunning Jr., *J. Chem. Phys.* 103 (1995) 4572.

[182] K. A. Peterson and T. H. Dunning Jr., *J. Chem. Phys.* 117 (2002) 10548.

[183] M. Tronc, G. C. King and F. H. Read, *J. Phys. B: Atom. Molec. Phys.* 12 (1979) 137.

[184] S. Bodeur and J.M. Esteva, *Chem. Phys.* 100 (1985) 415.

[185] G. Remmers, M. Domke, A. Puschmann, T. Mandel, C. Xue, G. Kaindl, E. Hudson and D. A. Shirley, *Phys. Rev. A* 46 (1992) 3935.

[186] J. Adachi, N. Kosugi, E. Shigemasa and A. Yagishita, *Chem. Phys. Lett.* 309 (1999) 427.

[187] A. P. Hitchcock and C.E. Brion, *J. Electron Spectrosc. Relat. Phenom.* 10 (1997) 317.

[188] A. Naves de Brito, S. Svensson, N. Correia, M. P. Keane, H. Ågren, O. P. Sarinen, A. Kivimäki and S. Aksela, *J. Electron Spectrosc. Relat. Phenom.* 59 (1992) 293.

[189] K. Yoshii, Y. Baba and T. A. Sasaki, *J. Electron Spectrosc. Relat. Phenom.* 93 (1998) 105.

[190] D. P. Woodruff and T. A. Delchar, *Modern Techniques of Surface Science* Cambridge University Press, New York (1986).

[191] T. Mukoyama, *Spectrochimica Acta B* 59 (2004) 1107.

[192] L. Triguero, L. G. M. Pettersson and H. Ågren, *J. Phys. Chem.* 102 (1998) 10599.

[193] G. Smolentsev, A. V. Soldatov, J. Messinger, K. Merz, Weyhermüller, U. Bergmann, Y. Pushkar, J. Yani, V. K.

Yachandra and P. Glatzel, *J. Am. Chem. Soc.* 131 (2009) 13161.

[194] Andrew T. B. Gilbert, N. A. Besley and Peter M. W. Gill, *J. Phys. Chem.* 112 (2008) 13164.

[195] N. A. Besley, Andrew T. B. Gilbert and Peter M. W. Gill, *J. Chem. Phys.* 130 (2009) 124308.

[196] J. E. Rubensson, N. Wassdahl, R. Brammer and J. Nordgren, *J. Electron Spectros. Relat. Phenom.* 47 (1988) 131.

[197] P. Glans, R. E. La Villa, Y. Luo, H. Ågren and J. Nordgren, *J. Phys. B* 27 (1994) 3399.

[198] J. Nordgren, H. Ågren, L. O. Werne, C. Nordling and K. Siegbahn, *J. Phys. B* 9 (1976) 295.

[199] R. Brammer, J. E. Rubensson, N. Wassdahl and J. Nordgren, *J. Physica Scripta* 36 (1987) 262.

[200] P. Skytt, P. Glans, K. Gunnelin, J. Guo, J. Nordgren, Y. Luo and H. Ågren, *Phys. Rev. A* 55 (1997) 134.

[201] S. Kashtanov, A. Augustsson, Y. Luo, J. Guo, C. Sathe, J. E. Rubensson, H. Siegbahn, J. Nordgren and H. Ågren, *Phys. Rev. B* 69 (2004) 024201.

[202] M. Nooijen and R. J. Bartlett, *J. chem. Phys.* 102 (1995) 6735.

[203] F. P. Larkins and A. J. Seen, *Phys. Scr.* 41 (1990) 827.

[204] A. J. Seen and F. P. Larkins, *J. Phys. B* 25 (1992) 1992.

[205] H. Ågren and A. Flores-Riveros, *J. Electron Spectros. relat. Phenom.* 56 (1991) 259.

Appendix A

Conferences/Meetings Attended

---

1. *RSC Theoretical Chemistry Group Meeting*, Cardiff, April 2009 (Poster Presented).

2. *UoN HPC Conference*, Nottingham, January 2008.

3. *QCHEM Workshop*, Pittsburgh, March 2009 (An online broadcast of the workshop).

Index